AD_____

AWARD NUMBER: W81XWH-08-1-0468

TITLE: Neural Stem Cell Delivery of Therapeutic Antibodies to Treat Breast Cancer Brain Metastases

PRINCIPAL INVESTIGATOR: Brunhilde Felding-Habermann, Ph.D.

CONTRACTING ORGANIZATION: The Scripps Research Institute
La Jolla, CA 92037

REPORT DATE: October 2009

TYPE OF REPORT: Annual

PREPARED FOR: U.S. Army Medical Research and Materiel Command
Fort Detrick, Maryland 21702-5012

REPORT DOCUMENTATION PAGE

Form Approved
OMB No. 0704-0188

1. REPORT DATE	**2. REPORT TYPE**	**3. DATES COVERED**
1 October 2009	Annual	15 Sep 2008 – 14 Sep 2009

4. TITLE AND SUBTITLE

Neural Stem Cell Delivery of Therapeutic Antibodies to Treat Breast Cancer Brain Metastases

5a. CONTRACT NUMBER

5b. GRANT NUMBER
W81XWH-08-1-0468

5c. PROGRAM ELEMENT NUMBER

6. AUTHOR(S)

Brunhilde Felding-Habermann, Ph.D.

E-Mail: brunie@scripps.edu

5d. PROJECT NUMBER

5e. TASK NUMBER

5f. WORK UNIT NUMBER

7. PERFORMING ORGANIZATION NAME(S) AND ADDRESS(ES)

The Scripps Research Institute
La Jolla, CA 92037

8. PERFORMING ORGANIZATION REPORT NUMBER

9. SPONSORING / MONITORING AGENCY NAME(S) AND ADDRESS(ES)
U.S. Army Medical Research and Materiel Command
Fort Detrick, Maryland 21702-5012

10. SPONSOR/MONITOR'S ACRONYM(S)

11. SPONSOR/MONITOR'S REPORT NUMBER(S)

12. DISTRIBUTION / AVAILABILITY STATEMENT
Approved for Public Release; Distribution Unlimited

13. SUPPLEMENTARY NOTES
mechanisms and therapeutic targets for inhibition of breast cancer brain metastasis, establishment of cell and animal models that emulate all steps of clinical breast cancer brain metastasis, development of treatment approaches

14. ABSTRACT
Our goal is to develop a therapeutic approach for clinical inhibition of breast cancer brain metastasis. Our work has identified a new molecular target for treatment of metastatic brain disease in breast cancer patients and provided antibody tools that successfully interrupt breast cancer metastasis in a mouse model. Systemic application of the antibodies does not sufficiently reach brain lesions to interfere with their development and progression. Therefore, we are developing delivery strategies to bring therapeutic antibodies to brain metastatic lesions and inhibit their proliferation. We have established and validated unique new breast cancer brain metastasis cell models and adapted mouse models to emulate all steps of human breast cancer brain metastasis development and invasive progression. These models are essential new tools for the evaluation of successful new therapies against widespread metastatic brain disease as seen in breast cancer patients. By investigating initial as well as late stages of brain metastasis development in the animal model, we have identified host cell responses that can be potentially used as therapeutic targets and for delivery of therapeutic molecules to disseminated breast cancer brain lesions. With these advances, we have made tangible progress toward new treatment options for breast cancer patients with cerebral metastasis.

15. SUBJECT TERMS
Identification of activated breast cancer cell integrin v 3 as therapeutic target for inhibition of brain metastases; mechanism of action of activated v 3 in brain lesion growth; identification of microglia as a potential therapy delivering host cell type

16. SECURITY CLASSIFICATION OF:			**17. LIMITATION OF ABSTRACT**	**18. NUMBER OF PAGES**	**19a. NAME OF RESPONSIBLE PERSON**
					USAMRMC
a. REPORT	**b. ABSTRACT**	**c. THIS PAGE**			**19b. TELEPHONE NUMBER** *(include area code)*
U	U	U	UU	83	

Standard Form 298 (Rev. 8-98)
Prescribed by ANSI Std. Z39.18

Table of Contents

Grant: W81XWH-01-1-0468
Title: **Delivery of Therapeutic Antibodies to Treat Breast Cancer Brain Metastases**

Report: Sept 2008 – Sept 2009

Introduction

Brain metastases are among the most feared complications in breast cancer[1-3]. Today, nearly 30% of patients with advanced breast cancer are eventually diagnosed with brain lesions, making breast tumors the main source of metastatic brain disease in women[4-5]. However, treatment options are limited and in most cases prolong patient survival only for a few weeks or months, often associated with severe side effects. Current treatment options are surgery, if isolated brain lesions can be safely removed, gamma knife surgery and whole brain radiation. Unfortunately, cases with operable lesions are rare and brain metastatic disease is most often widespread and ultimately fails to respond to these therapies. Therefore, it is imperative to develop new, effective regimens that prevent and control this stage of the disease. Thus, the goal of our project is to develop mechanisms through which therapeutic antibodies can be successfully delivered to breast cancer brain lesions to effectively interfere with intracranial tumor cell growth and expansion. Today's clinical regimen of antibodies against metastatic breast cancer progression include Herceptin, a human antibody directed against the Her2 receptor expressed on an aggressive subgroup of breast cancer types that frequently metastasizes to all major target organs of breast cancer metastasis, including the brain. Herceptin treatment has been successfully used in the clinic and a high percentage of treated patients, at least initially, respond well to this therapy with regression of extracranial metastatic burden. However, the incidence of brain lesions in these patients is rising[6]. Failure of the therapeutic antibody to reach breast cancer cells has been held responsible for progression of brain metastasis in the central nervous system under the antibody treatment[7-10].

As antibodies could potentially serve as effective anti-cancer agents against brain metastases, a major hurdle to overcome in treatment of breast cancer brain metastases is to develop delivery systems that will allow antibody molecules, or their effective fragments, to pass the blood brain barrier and reach widespread lesions within the central nervous system.

Body

The aims of our study are:

1. To develop components for a functional and clinically relevant model of breast cancer brain metastasis and neural progenitor cell scFv therapy
2. To generate a pre-clinical model of neural progenitor-scFv therapy and test its efficacy in vivo

During the past funding period, we have made major progress toward these aims and reached several of our milestones defined in the statement of work. Guided by our results, we have also expanded the questions addressed, to optimize the outcome toward better understanding of breast cancer brain lesions development and finding of effective ways to treat lesions in the central nervous system.

Milestones reached:

Clinically relevant model of breast cancer brain metastasis

- We have developed mouse models that emulate all stages of breast cancer brain metastasis.
- We analyzed early as well as late stages leading to the development of breast cancer brain lesions and expansion of cerebral metastases.

- We analysis the initial brain colonization of circulating breast cancer cells from the blood stream and investigated the timing and mechanism involved in tumor cell penetration of the blood brain barrier
- We identified early as well as persisting host cell reactions to the arrival of breast cancer cells in the brain and began to investigate mechanisms through which astrocytes and microglial cells interact with brain metastatic breast cancer cells and influence the development of breast cancer brain lesions.

As brain metastases are difficult to treat and mostly develop late during progressive metastatic disease, breast cancer patients at risk would benefit from the development of prevention as well as improved treatments. This requires knowledge of the initial events that lead to brain metastasis. Our study revealed cellular events during the initiation of brain metastasis by breast cancer cells and documents the earliest host responses to incoming cancer cells after carotid artery injection in immune deficient and immune competent mouse models. Our findings capture and characterize heterogeneous astrocytic and microglial reactions to the arrest and extravasation of cancer cells in the brain, showing immediate and drastic changes in the brain microenvironment upon arrival of individual cancer cells. We identified reactive astrocytes as the most active host cell population that immediately localizes to individual invading tumor cells and continuously associates with growing metastatic lesions. Up-regulation of MMP-9 associated with astrocyte activation in the immediate vicinity of extravasating cancer cells might support their progression. Early involvement of different host cell types indicates environmental clues that might co-determine whether a single cancer cell progresses to macrometastasis or remains dormant. Thus, information on the initial interplay between brain homing tumor cells and reactive host cells may help develop strategies for prevention and treatment of symptomatic breast cancer brain metastases.

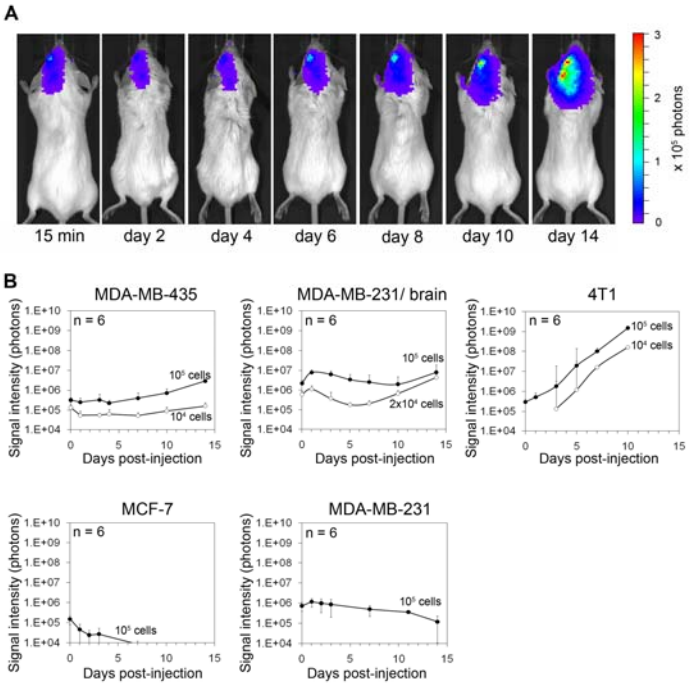

Figure 1. Brain colonization by breast cancer cell lines after carotid artery injection in mice monitored by bioluminescence imaging. (A) Increase of bioluminescence signal indicates growth of F-*luc* tagged MDA-MB-435 cells shown in a representative animal at various time points after injection of 10^5 cancer cells. **(B)** Survival and growth of F-*luc*-tagged MDA-MB-435, MDA-MB-231 parental, MDA-MB-231/brain, MCF7 (injected into immunosuppressed CB17/SCID mice) and 4T1 cells (injected into immunocompetent BALB/c mice) after injection into the left carotid artery followed over time. Only live cells produce signal. Number of injected cells as indicated.

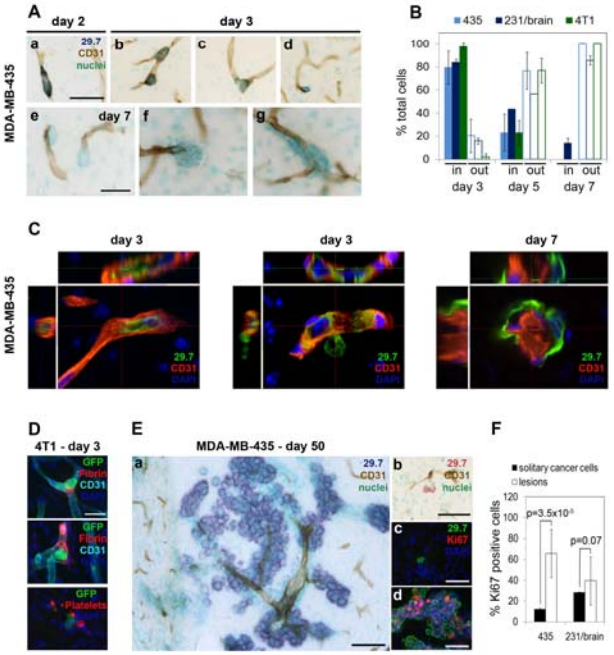

Figure 2. Cancer cell extravasation and growth in the brain. (A) MDA-MB-435 cells were visualized by anti-human CD44 (mab 29.7) and blood vessels by CD31 staining using immunohistochemistry (IHC). **a:** An elongated cancer cell within a capillary on day 2 post injection. **b:** Rounding of intra-vascular cancer cells on day 3. **c:** Cancer cell on day 3 breaking through the vessel wall during extravasation. **d:** Extravasated cancer cell on day 3. **e-g:** Extra-vascular cancer cells on day 7. Bars: 50 µm (a-d), 25 µm (e-g). **(B)** Percentage of cancer cells located inside versus outside blood vessels. The quantification was performed for 3 different cells lines: MDA-MB-435, MDA-MB-231/brain, and 4T1. **(C)** Analysis of early cell location by confocal microscopy. Cancer cells were stained for human CD44 (green) and blood vessels for CD31 (red). An intravascular cell (left), a cell in the process of extravasation (middle), and extravascular cells (right) are shown.

(D) Association of intravascular 4T1 cancer cells with fibrin and platelets ($GPIb_{\alpha}$ staining) on day 3. Bar: 25 µm. **(E)** Day 50: Long-term fate of MDA-MB-435 cells was monitored by IHC (a,b) and immunofluorescence (c,d). **a:** Intra-parenchymal macrometastases grew preferentially around co-opted blood vessels. **b,c:** solitary tumor cells outside blood vessels on day 50, detected by anti human CD44 (mab 29.7) are mostly negative for Ki67. **d:** In contrast, most cells within lesions as shown in (a) are Ki67 positive. Bars: 200 µm (a), 50 µm (b-d). **(F)** Quantification of Ki67-positive cells within the solitary cancer cell population and within the macrometastatic lesions for MDA-MB-435 and MDA-MB-231/brain cells 30 to 50 days post-injection.

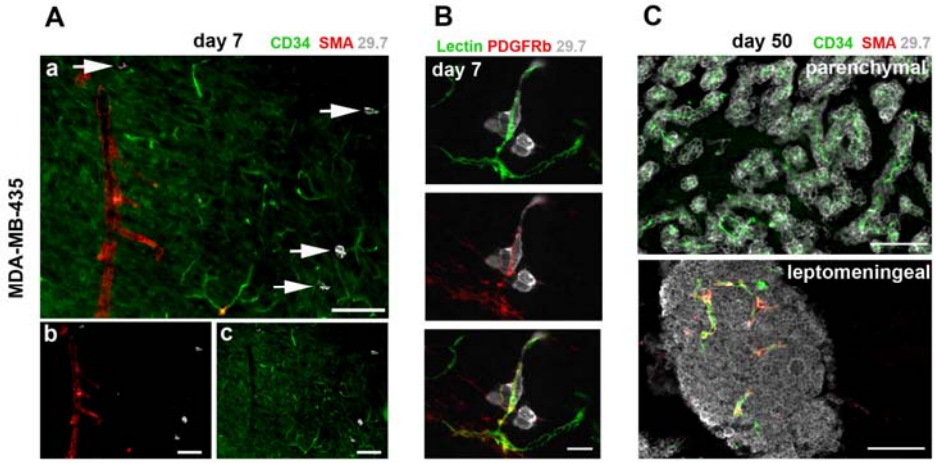

Figure 3. Blood vessel types involved in cancer cell extravazation and growth.
Blood vessel types were analyzed by immunofluorescence. Representative images for MDA-MB-435 cells are shown. **(A)** Day 7: In the brain parenchyma, cancer cells (white, see arrows) arrest and extravasate exclusively from capillaries or post capillary venules positive for CD34 and lacking smooth-muscle cells (no smooth muscle actin (SMA) signal). Bars: 100 µm. **(B)** Day 7: Blood vessels from which cancer cells (gray) extravasate are surrounded by PDGFRβ-positive pericytes. **Top:** BS-1 lectin; **middle:** anti-PDGFRβ; **bottom:** merge. Bar: 20 µm. **(C)** Day 50: intra-parenchymal metastases grow around co-opted capillaries lacking smooth-muscle cells. Leptomeningeal metastases contain capillaries as well as larger, smooth-muscle cell-positive vessels. Bars: 100 µm.

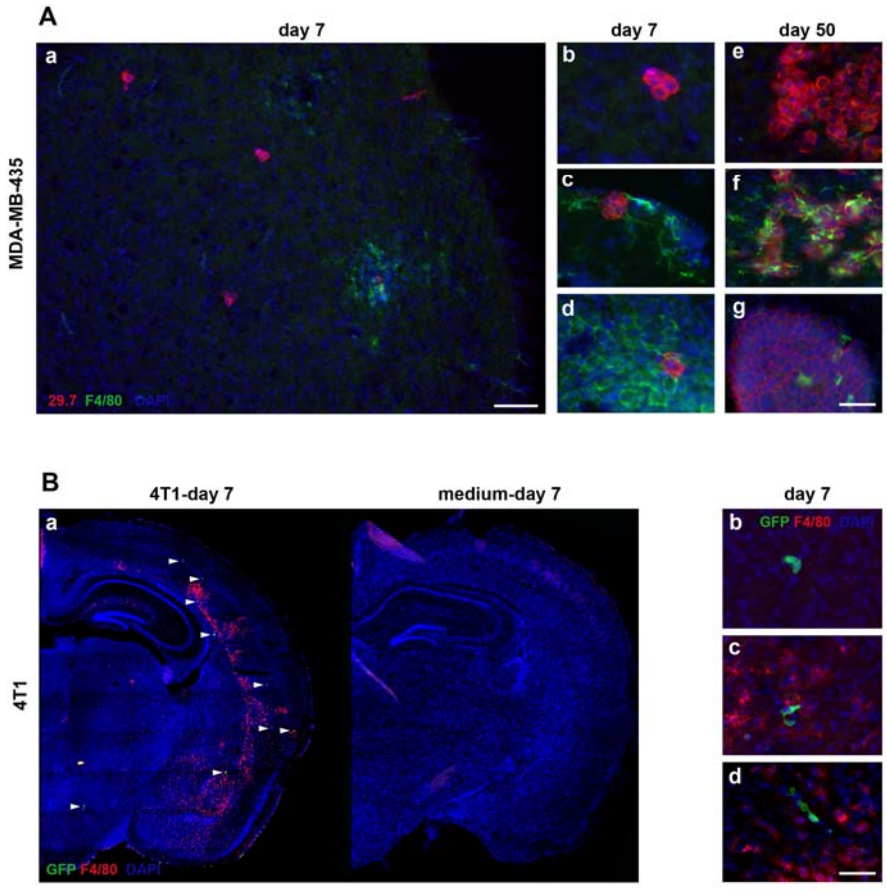

Figure 4. Microglial cell responses to invading cancer cells are heterogeneous. Microglial activation in response to cancer cell invasion varies at early as well as late stages, as detected by immunofluorescence analysis. **(A)** MDA-MB-435 cells in immunosuppressed mice; **a:** Diverse microglial responses (green) to incoming cancer cells (red) on day 7. Responses include **b:** absence of microglial cells, **c:** presence of hypertrophic stellate activated, or **d:** amoeboid reactive microglial cells. Similarly, on day 50, **e:** some macrometastases show no microglial involvement, or **f:** contain stellate or **g:** amoeboid microglia. Bars: 100 µm (a), 50 µm (b-g). **(B)** 4T1 cells in immunocompetent mice; **a:** Distribution of activated microglia (red) in the mouse brain 7 days after carotid artery injection of cancer cells (left) or medium alone (right). White arrowheads mark the GFP-labeled cancer cells (green). Diverse microglial responses to cancer cells include **b:** absence of microglial cells, **c:** presence of hypertrophic stellate, or **d:** reactive amoeboid microglial cells. Bar: 50 µm.

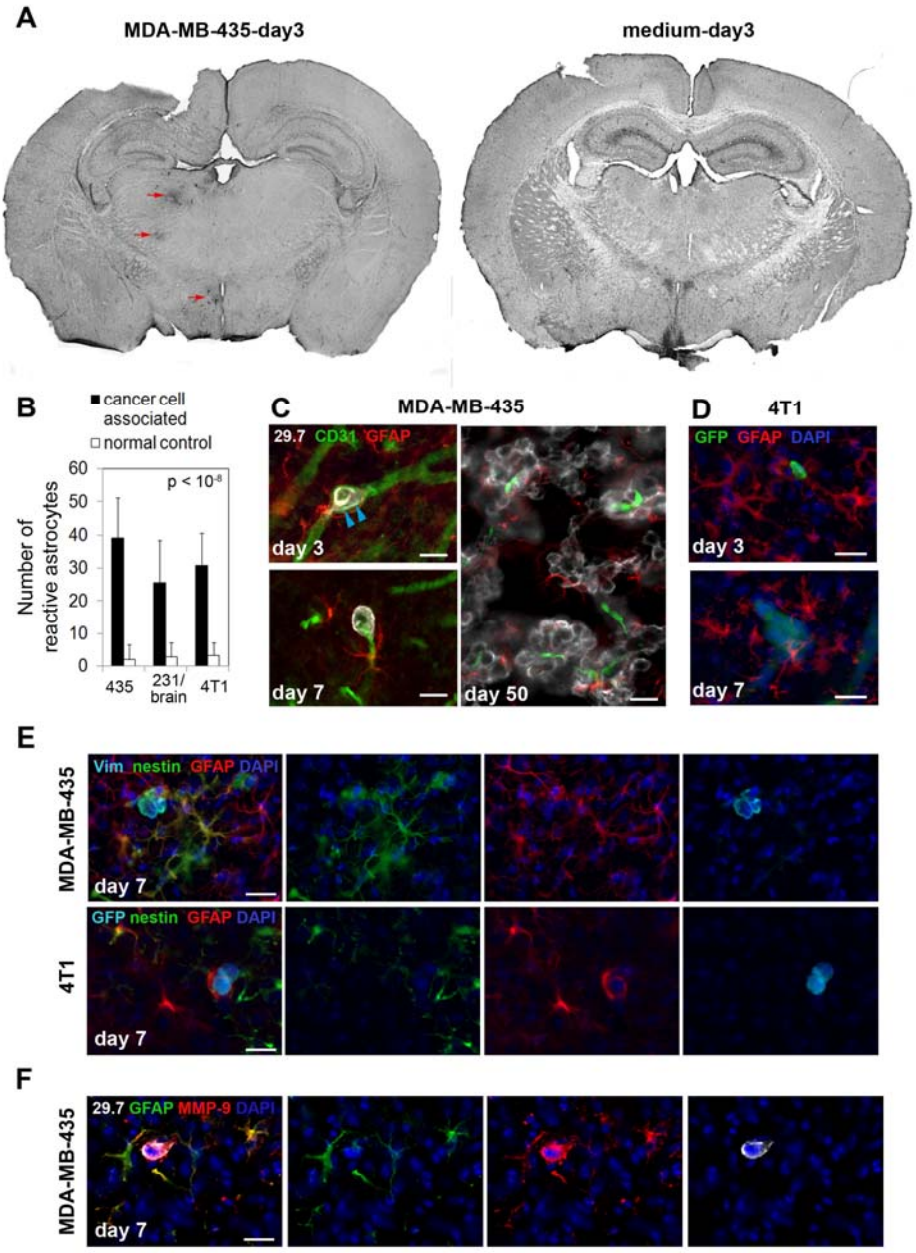

Figure 5. Cancer cell invasion induces strong astrocytic responses. Astrocytes were investigated by immunofluorescence staining. **(A) Left:** On day 3 after cancer cell injection into the left carotid artery, GFAP in astrocytes is already up-regulated strongly in the vicinity of intravascular arrested cancer cells (MDA-MB-435, red arrows). Astrocyte activation can be detected in the left hemisphere in brain overview sections, while the corresponding area of the contralateral hemisphere is devoid of GFAP reactivity. **Right:** Also, no GFAP activity was found in the brain of control animals injected with medium alone. **(B)** Number of reactive astrocytes 3 days after carotid artery injection of cancer cells, quantified within the 150 µm distance from cancer cells (cancer cell associated) and within the corresponding region of the contralateral hemisphere that lacks cancer cells (normal control). **(C)** Activated astrocytes with thick processes and up-regulated expression of GFAP are detected next to MDA-MB-435 cancer cells that are still intravascular. Note the cytoplasmic protrusions of cancer cells on day 3 post-inoculation that apparently cause stretching of the vessel wall (blue arrowheads) (day 3, upper left). GFAP positive astrocytes stay close to extravasated tumor cells (day 7, lower left). Reactive astrocytes persist close to cancer cells throughout their development into macrometastases (day 50, right). Bars: 20 µm. **(D)** Activated astrocytes are also present in the vicinity of 4T1 breast cancer cells injected into the carotid artery of syngeneic BALB/c mice. Bars: 20 µm. **(E)** In addition to GFAP up-regulation, some reactive astrocytes simultaneously express nestin. Merged images are shown on the left. Human vimentin or GFP (light blue), nestin (green), GFAP (red), Dapi (dark blue).Bar: 20 µm. **(F)** Strong up-regulation of MMP-9 is detected in reactive astrocytes located in the immediate vicinity of extravasated MDA-MB-435 tumor cell. Bar: 20 µm.

Identification of the activated form of breast cancer cell integrin αvβ3 as a therapeutic target for therapy of breast cancer brain metastasis

Lorger M, Krueger JS, O'Neal M, Staflin K, Felding-Habermann B (2009) Proc Natl Acad Sci USA 104 (21): 9024-9028

We had previous evidence that integrin αvβ3 can exist on breast cancer cells in distinct states of activation. We showed that a metastatic subset of breast cancer cells carry the adhesion receptor in a constitutively activated, high affinity form. The high affinity form of αvβ3 is characterized by its ability to bind ligands from solution, as for example in blood plasma when circulating tumor cells are on their way to metastasize to distant organs. However, the activated form of αvβ3 apparently also endows the breast cancer cells with specific properties that support their metastatic growth in a microenviroment specific manner.

In this study, we analyzed if and through which mechanism the expression of activated integrin αvβ3 supports brain metastatic growth. This information is of particular importance for this project because we had chosen to investigate if antibodies directed to the active form of integrin αvβ3 might interfere with breast cancer brain metastasis. We now demonstrated a crucial role for high affinity tumor cell integrin $\alpha_v\beta_3$ in brain metastatic growth and recruitment of blood vessels. While $\alpha_v\beta_3$ is frequently upregulated in primary brain tumors[13-16] and metastatic lesions of brain homing cancers, we showed that it is the $\alpha_v\beta_3$ activation state that is critical for brain lesion growth. Activated but not non-activated tumor cell $\alpha_v\beta_3$ supports efficient brain metastatic growth through continuous up-regulation of VEGF protein under normoxic conditions. In metastatic brain lesions carrying activated $\alpha_v\beta_3$, VEGF expression is controlled at the post-transcriptional level and involves phosphorylation and inhibition of translational respressor 4E-binding protein (4E-BP1). In contrast, tumor cells with non-activated $\alpha_v\beta_3$ depend on hypoxia for VEGF induction, resulting in reduced angiogenesis, tumor cell apoptosis and inefficient intracranial growth. Importantly, the microenvironment critically influences the effects that activated tumor cell $\alpha_v\beta_3$ exerts on tumor cell growth. While strongly promoting intracranial growth, the activation state of the receptor did not influence tumor growth in the mammary fat pad as a primary site. Thus, we identified a mechanism by which metastatic cells thrive in the brain microenvironment and utilize the high affinity form of an adhesion receptor to grow and secure host support for proliferation. Targeting this molecular mechanism could therefore prove valuable for the inhibition of brain metastasis[17-22].

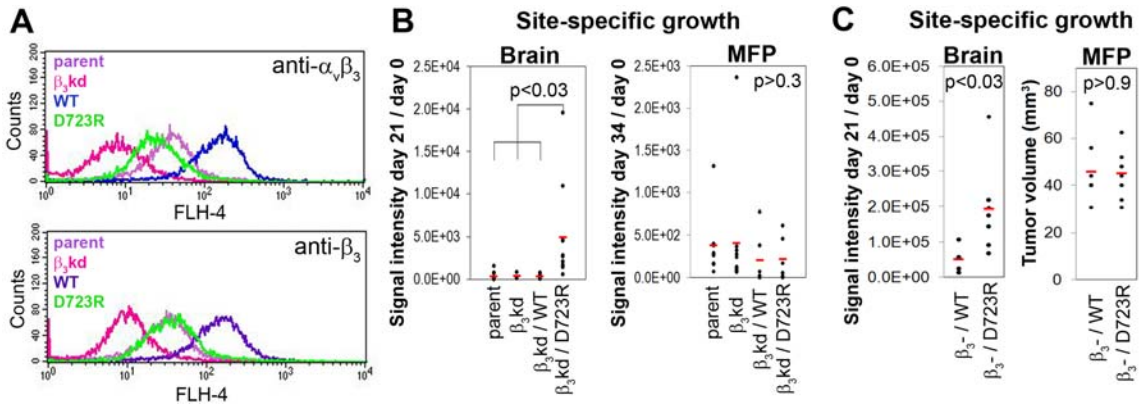

Fig.1 Impact of tumor cell integrin $\alpha_v\beta_3$ expression and activation on lesion growth in the brain and mammary fat pad (MFP)
(A) Analysis of integrin $\alpha_v\beta_3$ expression by flow cytometry. **Parent**: MDA-MB-435 transduced with control shRNA ScrB; **$\beta_3$kd**: MDA-MB-435 transduced with β_3 shRNA; **WT**: MDA-MB-435/$\beta_3$kd reconstituted with wild-type β_3 (non-activated $\alpha_v\beta_3$); **D723R**: MDA-MB-435/$\beta_3$kd reconstituted with β_3D723R (activated $\alpha_v\beta_3$). **(B)** Lesion growth in the brain (day 0 - 21) or MFP (day 0-34) based on bioluminescence signal of *F-luc* tagged tumor cells by non-invasive in vivo imaging. **(C)** Lesion growth in the brain (day 0-21) or MFP (day 0-36) of MDA-MB 435/β_3^- cells selected from parental cells with saporin-anti-β_3 antibody and reconstituted by transfection with β_3WT of β_3D723R based on in vivo imaging (brain) or caliper measurement (MFP). Each dot represents one animal and red lines the mean values per group (group sizes in **B**: brain: parent and $\beta_3$kd n=6, β_3WT and β_3D723R n=11; MFP: parent n=10, $\beta_3$kd n=8, β_3 and β_3D723R n=6; **C**: all groups n=7); p-values obtained by 2-tailed Student's T-test with unequal variance.

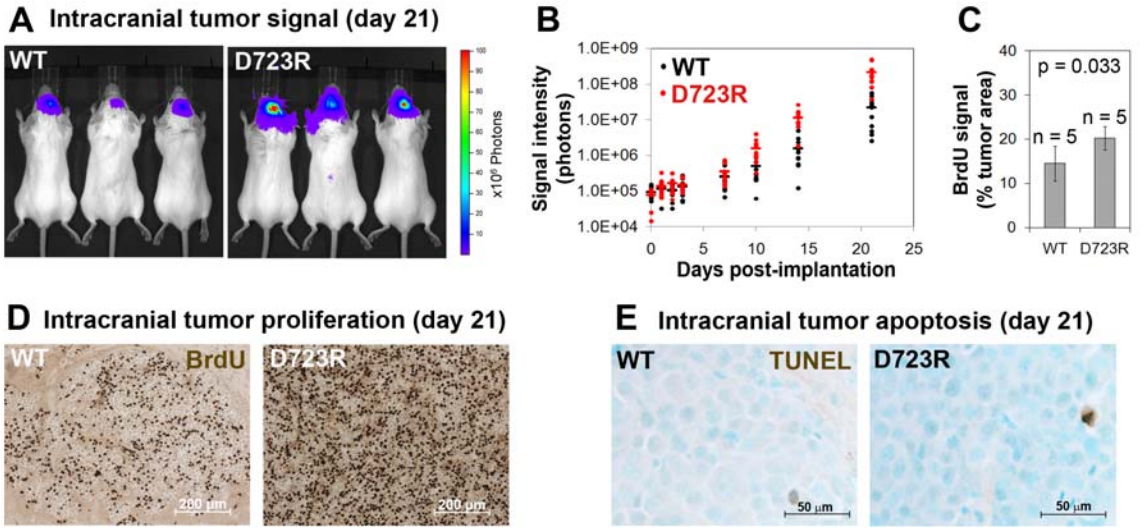

Fig.2 Tumor cell integrin $\alpha_v\beta_3$ activation enhances proliferation in the brain
(A) Non-invasive bioluminescence imaging 21 days after intracranial implantation of $1x10^4$ β_3WT *(left)* or β_3D723R *(right)* expressing MDA-MB-435 tumor cells. **(B)** Growth of β_3WT and β_3D723R expressing tumor cells in the brain. Each dot represents one animal and horizontal lines the mean values per group. **(C,D)** Intracranial proliferation of β_3WT and β_3D723R expressing cells in brain lesions by in vivo BrdU uptake; n=5 per group, p-values obtained by 2-tailed Student's T-test with unequal variance. **(E)** Apoptosis in β_3WT and β_3D723R brain lesions by TUNEL staining (brown).

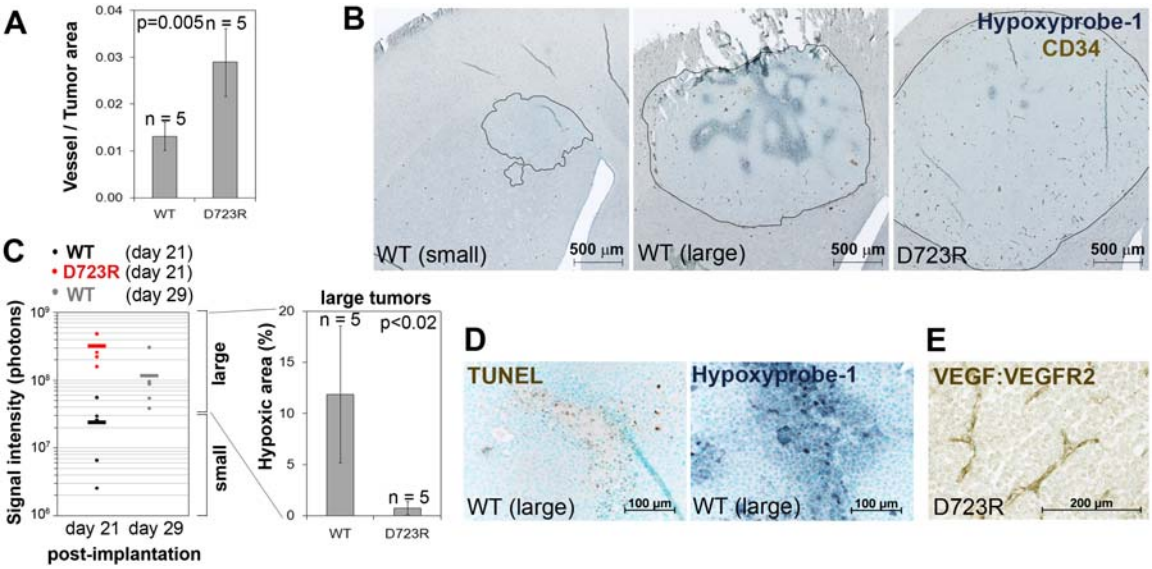

Fig.3 Tumor cell integrin $\alpha_v\beta_3$ activation increases angiogenesis and reduces hypoxia in brain lesions
(A) Quantification of the total vessel area in β_3WT and β_3D723R brain lesions 21 days after tumor cell implant. Vessels were visualized by CD34 staining. **(B)** Immunohistochemistry of tumor vessels (brown) and hypoxic regions (grey-blue) in brain lesions on day 21. Borders between tumor area and brain parenchyma are outlined showing representative small (≤ 1.5 mm) and large (≥ 1.5 mm) β_3WT lesions. All β_3D723R lesions were > 2 mm. **(C)** *Left:* In vivo signal of β_3WT (black) and β_3D723R (red) brain lesions on day 21, and on day 29 for β_3WT (gray) to obtain larger lesions for this group. Only lesions with a diameter ≥ 1.5 mm (approximately $5x10^7$ bioluminescence photons in vivo) were included in the quantification of hypoxic tumor regions (marked with a bracket as large tumors). *Right*: Percentage of hypoxic area in brain lesions > 1.5 mm in diameter; n=5 per group; p-values based on 2-tailed Student's T-test with unequal variance. **(D)** Large β_3WT lesions (> 1.5 mm) show increased apoptosis (left; TUNEL staining: brown; nuclei: green) within hypoxic regions (right; Hypoxyprobe-1 staining: grey-blue; nuclei: green) in adjacent sections. **(E)** Formation of the VEGF:VEGFR2 complex on tumor vessels in β_3D723R brain lesions (Gv39M staining: brown).

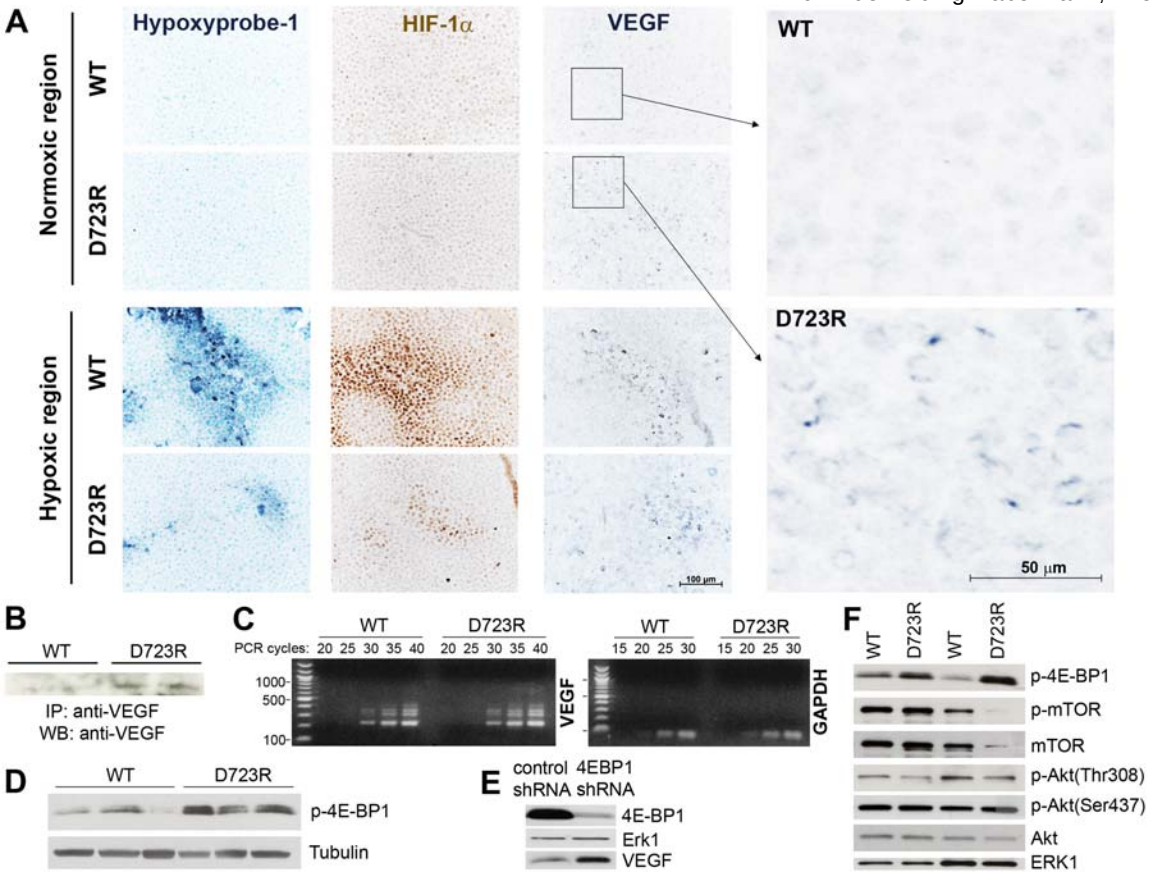

Fig.4 Tumor cell integrin $\alpha_v\beta_3$ activation increases VEGF expression in the brain post-transcriptionally by 4E-BP phosphorylation

(A) VEGF protein expression in normoxic (upper panels) versus hypoxic areas (lower panels) of β_3WT and β_3D723R brain lesions by immunohistochemistry. Hypoxic regions defined by positive staining for Hypoxyprobe-1 (left) and HIF-1α (middle). β_3WT and β_3D723R lesions express VEGF in hypoxic regions. In normoxic regions, only β_3D723R lesions express VEGF (right and enlarged on far right). **(B)** VEGF protein levels in micro-dissected β_3WT and β_3D723R brain lesions 21 days post tumor cell implant (Immunoprecipitation (IP): VEGF; Western blot (WB): VEGF). **(C)** VEGF mRNA levels in micro-dissected β_3WT and β_3D723R brain lesions on day 21 post implant (RT-PCR). Lesions from 3 different mice per group. **(D)** Phospho-4E-BP1 signal in micro-dissected β_3WT and β_3D723R brain lesions 21 days post tumor cell implant (Western blot with anti-phospho-4E-BP1 and anti-tubulin antibodies). **(E)** Down-regulation of 4E-BP1 in β_3WT cells by shRNA results in a strong increase of VEGF protein level under normoxia in vitro. VEGF was immunoprecipitated from cell culture supernatants prior to Western blot analysis. **(F)** Detection of mTOR and Akt activation levels with phospho-specific antibodies in micro-dissected β_3WT and β_3D723R brain lesions 21 days post tumor cell implant.

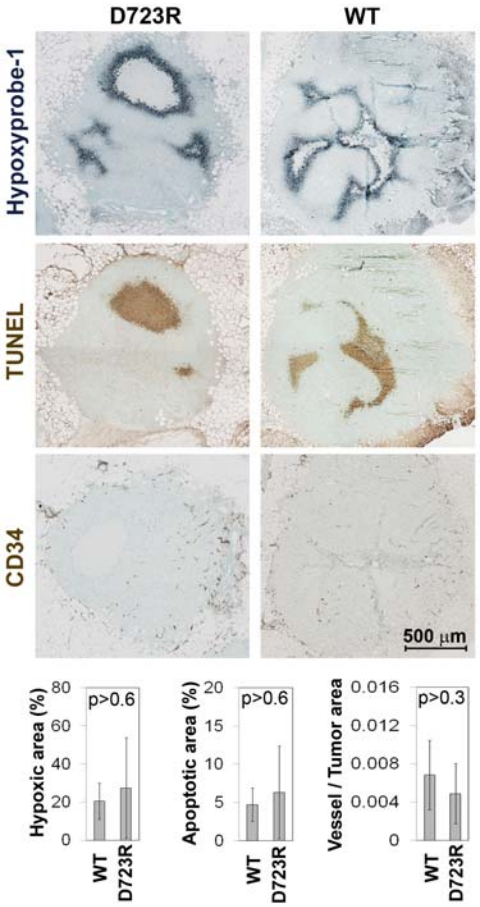

Fig.5 Tumor cell integrin $\alpha_v\beta_3$ activation does not prevent hypoxia in mammary fat pad tumors. Hypoxia (Hypoxyprobe-1 in gray-blue, upper), apoptosis/necrosis (TUNEL staining in brown, middle) and blood vessel denstity (CD34 in brown, lower) in MFP tumors 34 days after implanting $1x10^4$ β_3WT or β_3D723R expressing tumor cells. Quantifications are included (n=5 per group). p-values based on 2-tailed Student's T-test with unequal variance. Note: all 34-day old MFP tumors were smaller than 21-day old β_3D723R brain lesions.

Ongoing and future activities based on these findings:

It is important to note that the activated conformer of integrin $\alpha v\beta 3$ specifically supports an advantageous mechanism of new blood vessel recruitment in the brain micronenvironment and not in the mammary fat pad. It is plausible that the tumor cells expressing the constitutively activated integrin already pre-existed in the initial primary breast tumor, or that this trait was acquired during an evolutionary process during breast cancer progression. The results clearly show that high affinity $\alpha v\beta 3$ provides metastatic breast cancer cells with a unique ability to thrive in the brain microenvironment. Therefore, this molecule is a very promising functional target on breast cancer cells for therapeutic inhibition of breast cancer brain metastasis.

Our goal toward translation into clinical therapy, we are currently focusing on two directions: First, we are investigating an angle from which we can target the mechanism through which activated integrin $\alpha v\beta 3$ induces angiogenesis in brain metastatic breast cancer cells. Second, we are assessing treatment options to target the activated conformer of breast cancer cell integrin $\alpha v\beta 3$ in brain metastasis, using the scFv antibody fragments that we developed earlier from the immune repertoire of cancer patients[21].

The study below, currently under review for publication, highlights our efforts of using our previously isolated scFv antibodies directed against the high affinity $\alpha v\beta 3$ integrin for therapeutic inhibition of advanced metastatic disease in breast cancer, including brain metastasis.

Pre-clinical model of neural progenitor-scFv therapy

In preparation for the demanding task of developing a neural progenitor delivered scFv therapy against breast cancer brain metastases, we first sought to establish clinically relevant therapeutic activity of the scFv antibodies directed against the high affinity form of integrin αvβ3.

Targeting activated integrin αvβ3 with patient-derived antibodies impacts late-stage multiorgan Metastasis

Staflin K, Krueger JS, Hachmann J, Forsyth JS, Lorger M, Steiniger SC, Pop C, Salvesen G, Janda KD, Felding-Habermann B
Submitted

Advanced multi-organ metastasis is difficult to manage, and therapies will benefit from new functional targets that are critical for breast cancer progression. We identified the high affinity conformer of breast cancer cell integrin αvβ3 as a potential target for inhibition of metastatic growth, particularly in the brain microenvironment. Integrin αvβ3 is an important player in tumor angiogenesis, but it also promotes tumor cell adhesion, invasion migration and survival. The expression of αvβ3 in tumors and the tumor associated vasculature correlates with tumor grade and progression in several tumor types, most prominently in melanoma, glioma, and breast cancer. Integrin αvβ3 antagonists, including antibodies, can disrupt tumor-induced angiogenesis in animal models and interfere with metastasis promoting tumor cell functions. We documented that the activation state of αvβ3 is critical for supporting metastatic progression, and that the immune repertoire of cancer patients can contain anti-tumor antibodies, which specifically react with the high affinity form of αvβ3 expressed on a metastatic subset of tumor cells. This was shown by panning of a combinatorial single chain (scFv) antibody library from cancer patient leukocytes against highly metastatic human breast cancer cells.
With this approach, we isolated two antibodies that mimic ligands of αvβ3 and are specific for this receptor. We showed that these antibodies can inhibit early steps of hematogenous metastasis, including cancer cell arrest within the vasculature and tissue invasion. The ligand-mimetic properties of the antibodies are caused by an Arg-Gly-Asp (RGD) sequence within the antibodies' CDR-H3 region and account for the ability of the molecules to interfere with tumor cell adhesive functions.

Here, we characterized the binding properties of the scFv antibodies in detail and asked whether targeting the high affinity conformer of integrin αvβ3 can impact human breast cancer metastasis at late stages of the disease. This was examined in immune deficient mice after inducing advanced metastatic burden with human breast cancer cells, and following disease progression and response to treatment by noninvasive bioluminescence imaging. We found that widespread late-stage metastatic disease can respond to only a few doses of high affinity αvβ3-directed scFv antibodies and that the therapeutic antibody fragments localize to metastatic lesions in the treated animals. Comparing different routes of administration, we found that the phage displayed scFvs were able to reach most major target organs of breast cancer metastasis, but had a weak distribution to the brain. In agreement with this finding, the therapeutic responses of metastatic lesions to scFv treatment were primarily seen in extracranial metastases with little effect on breast cancer spread to the central nervous system.

Analyzing the mechanisms involved in the anti-cancer treatment responses, we found that the observed antimetastatic properties of the scFv antibodies are due to their ability to specifically bind and inhibit the activated conformer of integrin αvβ3 with specific binding dynamics that allows for antibody mediated interruption of integrin αvβ3 mediated tumor cell interaction with its natural ligands and downstream cellular functions that support tumor cell adhesion, migration and survival. Thus, activated αvβ3 appears as a suitable target for the inhibition of widespread metastatic disease in breast cancer. Our fully human antibodies and their derivatives, or compounds with similar specific properties, might provide a basis for powerful therapeutic intervention of advanced metastasis.

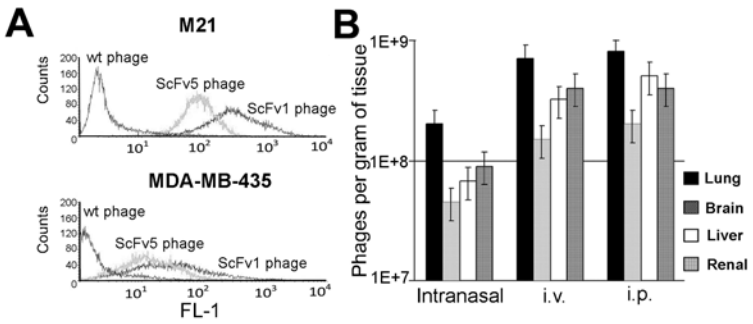

Figure 1
Antibody binding validation and routes of administration
(A) Before use in animals, the binding properties of each scFv phage batch were analyzed by flow cytometry on tumor cells expressing high affinity integrin $\alpha v\beta 3$. scFv phage was tested in the presence of calcium on M21 human melanoma cells that carry activated αvβ3 and on MDA-MB 435 cells which express mutant $\alpha v\beta 3_{D723R}$. **(B)** scFv phage organ distribution in the mouse model. Phage were injected i.v., i.p. or applied intranasally to non-tumor bearing mice to determine phage organ distribution 24 h later.

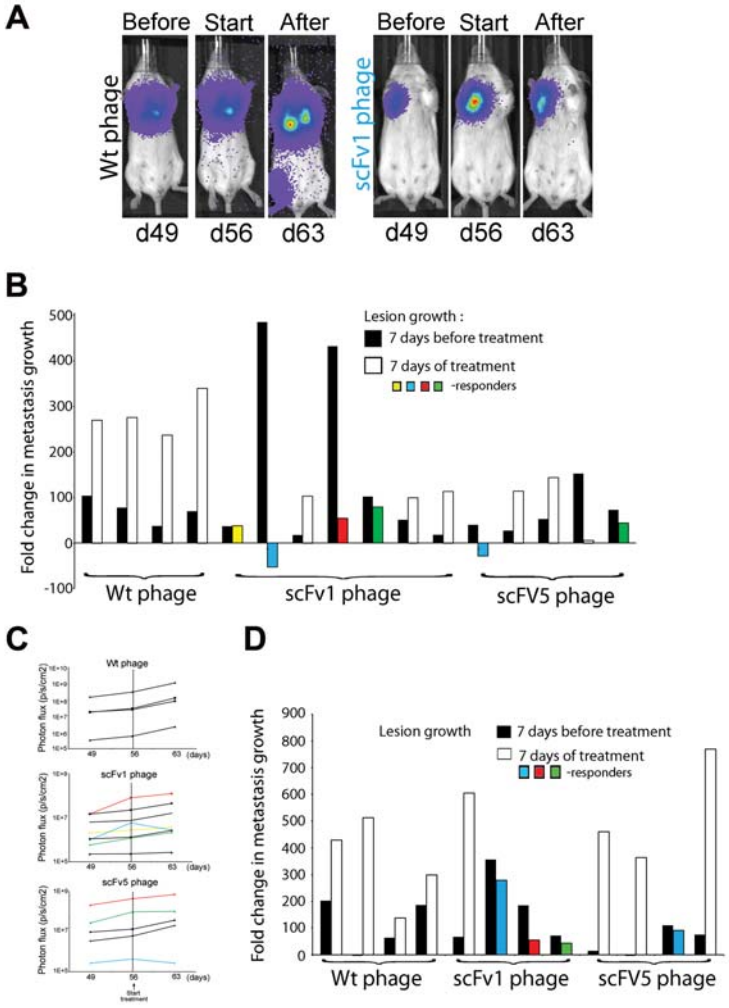

Figure 2
Lung metastases regress in response to treatment with scFv 1 or scFv 5.
F-luc tagged MDA-MB-435 cells were injected i.v. and lesion development monitored by non-invasive bioluminescence imaging (photons/second/cm^2) over time. Treatment with scFv phage ($5x10^{10}$ per dose) started on day 56 post tumor cell injection. **(A)** Non-invasive bioluminescence imaging of representative animals before treatment on day 49, at treatment onset on day 56, and after 4 doses of treatment on day 63. Reduced progression in lung lesions is seen after treatment with scFv1 but not with Wt-phage. **(B)** Response to treatment given every 48 h (4 doses). Fold-changes of lesion growth were calculated based on growth during 7 days before treatment compared to 7 days under treatment. ScFv1-phage treatment yielded a 57% animal response rate in lung burden and one animal with stabilization of lesion growth. ScFv5-phage treatment resulted in a 60% animal response rate for lung burden. Wt-phage gave no reduction in tumor growth. **(C)** *Non*-invasive bioluminescence imaging of lung burden (photons/second/cm^2) over time before and during treatment. Animals were treated every 48h for (4 doses). Lung lesion growth was monitored pre-treatment (day 49-56) and during treatment until day 63 (the end of treatment). Dashed vertical lines indicate the start of treatment on day 56. Animals responding to treatment are colored. **(D)** Response to treatment given every 24h (8 doses) to animals with very advanced metastatic burden. Treatment with Wt-phage gave no response, whereas regression and reduced tumor progression was seen in the scFv treated animals. ScFv1-phage treatment yielded a response in 75% of the animals, and scFv5-phage in 25%. Animals responding to treatment are colored.

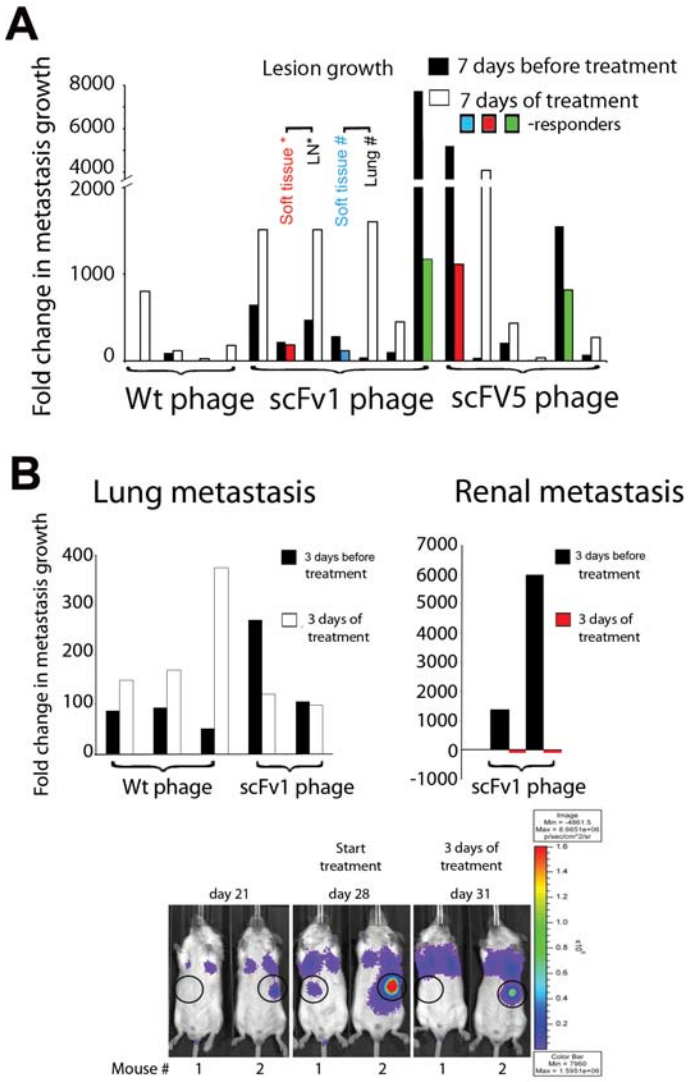

Figure 3
Advanced multi-organ metastases in the lung and soft tissues can regress or stabilize after treatment with scFv 1 or scFv5.
(A) *F-luc* tagged, *in vivo* selected and highly metastatic MDA-MB-435-met cells were injected i.v. to induce multiorgan metastasis. Metastatic progression was monitored by non-invasive bioluminescence imaging (photons/second/cm^2) over time. Animals with the largest tumor burden were selected for daily treatment with either scFv5-phage, or scFv1 phage for 7 days, beginning on day 41. Wt-phage was used as control. Metastases at individual sites showed reduced progression or a stabilization of lesion growth in response to scFv1 or scFv5 treatment. Fold-change in lesion growth was calculated for individual lesions during an equal number of days before treatment and under treatment. Animals responding to treatment are colored. The control group treated with Wt phage did not show tumor regression. Bars represent lung metastatic burden, except where specified otherwise. Tumor lesions originating in the same animal are denoted with an * or $^{\#}$. Lesions were frequently found in the liver, adrenal glands, lymph node, lung, brain, and within soft tissues below the spine. **(B)** Examples of animals with regression in both lung and renal metastases in response to 3 daily doses of scFv 1. Lung metastatic burden partially regressed or stabilized in the treated group and renal metastases regressed considerably. Wild type (wt)-phage treatment had no effect. Fold-change in metastatic burden shown for tumor growth before and during treatment. *In vivo* images confirm regression of renal lesion signal.

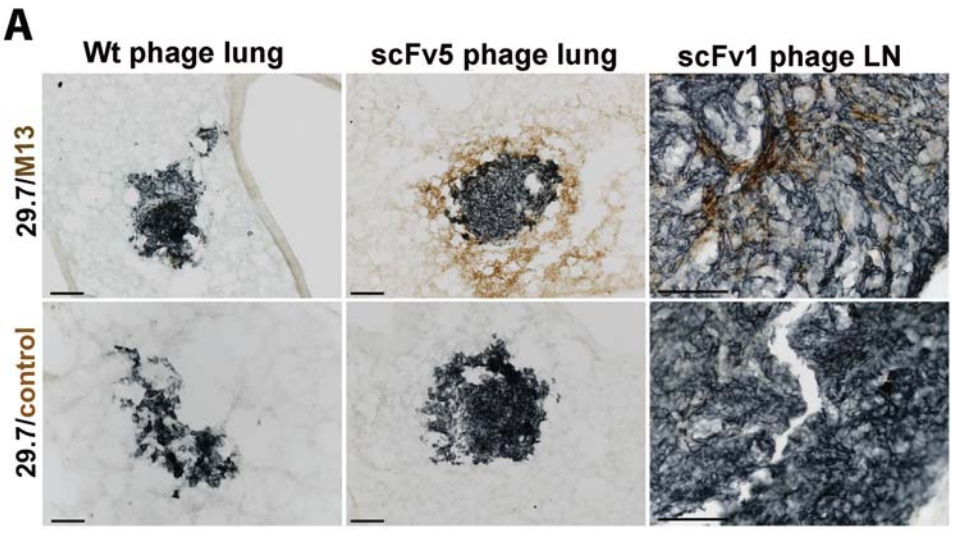

Figure 4
Localization of scFv1 or scFv 5 phage to areas in and around metastatic lesions in mice with multi-organ metastasis.
(A) Immunohistochemical detection of phage homing to metastases in the lungs and lymph node. ScFv phage, or wt control phage, were injected i.p. daily for 7 days into tumor bearing mice. 24h after the last scFv dose, the animals were terminally perfused and frozen tissue sections stained with mAb 29.7 (dark blue), specific for human CD44 indicating the tumor cells, and anti-M13 mAb to detect phage (DAB, brown). Animals treated with wt-phage did not show phage localization to tumor metastases (left panels), but lung metastasis from scFv5-phage treated animals showed phage localization in the tumor proximity as well as within the lung lesion (middle). A lymph node metastasis from an animal treated with scFv1-phage showed phage localizing to the tumor bulk as well as to the outer border of the lesion (right). Controls treated with secondary antibody and substrate did not show specific staining in or around any lesions. Scale bars indicate 100µm.

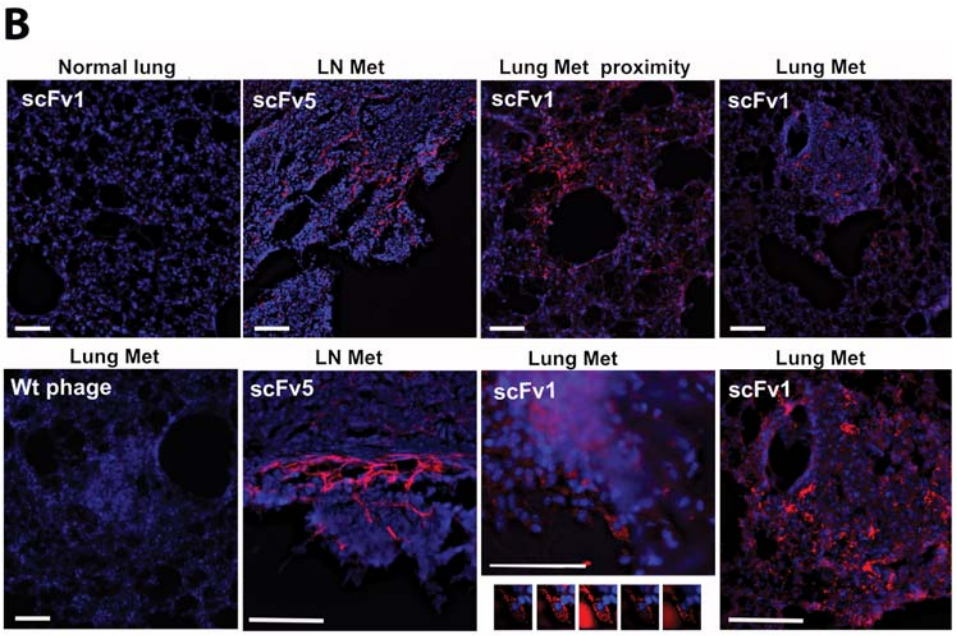

Figure 4 (B) (B) Fluorescence microscopy detecting phage (red). (Upper row) M13 phage was detected in and around lung metastases of scFv1-phage treated animals (right), as well as within the near proximity of the tumor lesions (second right), with minimal phage signal in the unaffected lung tissue away from a tumor lesion (left). Lymph node metastasis showed scFv1-phage localization in the tumor mass and within the tumor proximity (second left, top and bottom). Animals treated with wt-phage showed no specific staining in tumor lesions. Only a weak signal was sometimes seen in non-tumor bearing parts of the tissues, comparable to that seen for scFv phage in unaffected areas of lung tissue (lower left). Using optical sectioning and deconvolution of *z*-stack images, scFv phage was specifically detected associated with tumor cells (lower second right). Scale bars indicate 100 µm.

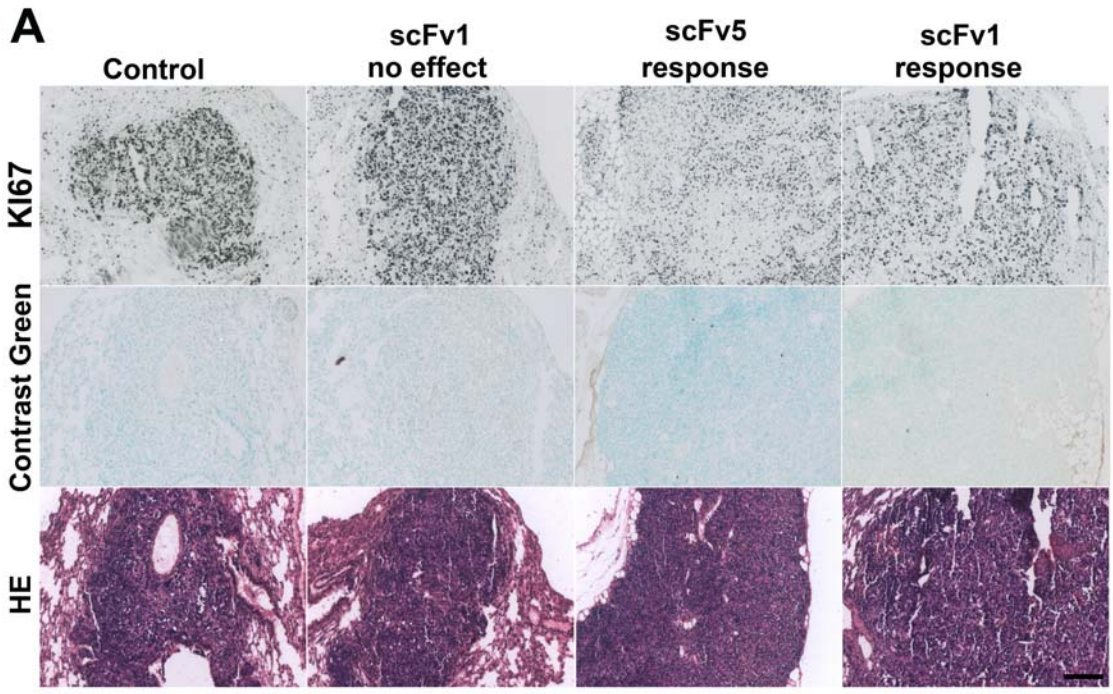

Figure 5
Effects of scFv treatment on tumor cells in vivo and host cell infiltration
(A) Ki67 staining on lung metastases treated with wt-phage or scFv1/5-phage (top panel). Lesions in animals responding to treatment showed fewer proliferating cells. Nuclear staining with contrast green (middle), H&E staining (lower panel). **(B)** F4/80 macrophage staining of lung metastases in mice treated with wt-phage or scFv1/5-phage. An increased infiltrate was seen in lesions responding to treatment. Scale bars indicate 100 µm in all sections. (Panel B is shown on the next page)

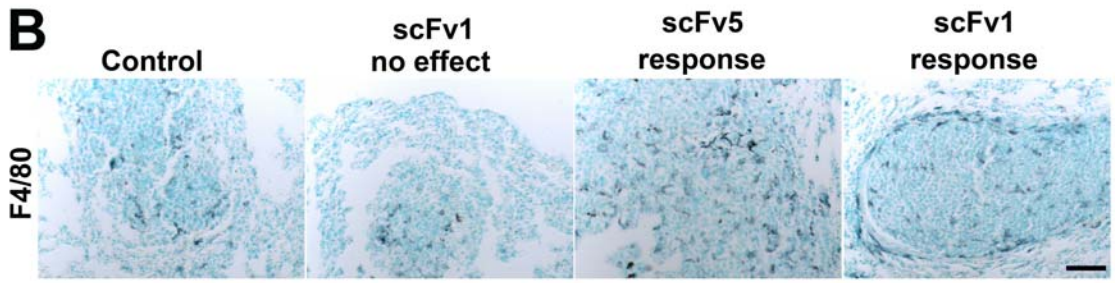

Fig. 5B

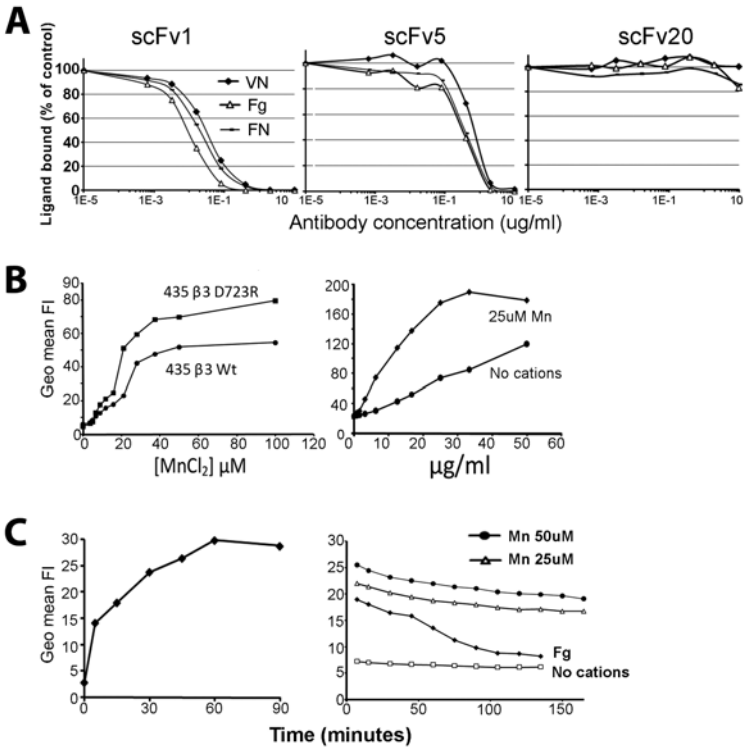

Figure 6
Inhibitory and binding properties of scFv 1 and scFv5.
(A) Biotinylated natural ligands of αvβ3: vitronectin (VN), fibronectin (FN) or fibrinogen (Fg) (10μg/ml) were incubated with purified immobilized αvβ3 receptor protein in TBS containing Ca^{2+}, Mg^{2+}, and Mn^{2+} (1mM each), in the presence of increasing concentrations of purified scFv protein. A non-function blocking scFv directed against the integrin αv subunit, scFv 20, was used as a control. **(B)** Flow cytometric binding analysis of fluorescinated scFv5 protein and MDA-MB 435 human tumor cells, expressing either activated high-affinity $\alpha v\beta 3_{D723R}$ or non-activated $\alpha v\beta 3_{WT}$. Binding was experimentally maximized in the presence of Mn^{2+}, known to induce a high affinity state in integrin heterodimers. Using a Mn^{2+} concentration (25 μM) that supports suboptimal scFv5 binding to tumor cells expressing activated $\alpha v\beta 3_{D723R}$, antibody was titrated to determine binding saturation. **(C)** Kinetics of scFv cell association and dissociation were analyzed by flow cytometry with FITC-labeled scFv protein at half maximal Mn^{2+} concentration and saturating scFv concentration, using MDA-MB-$435_{\beta 3D723R}$ cells. (Left) Association time was measured after removing unbound ligand in 10 min intervals. (Right) Dissociation was determined after allowing cells to bind scFv for 1 h to reach binding saturation, followed by removal of unbound ligand, washing and measuring scFv that remained bound in 10 min intervals. FITC-labeled fibrinogen (Fg) was used as a natural ligand for comparison. All incubations were done on ice using ice-cold buffers to prevent scFv or ligand internalization. No binding was detected in the absence of divalent cations.

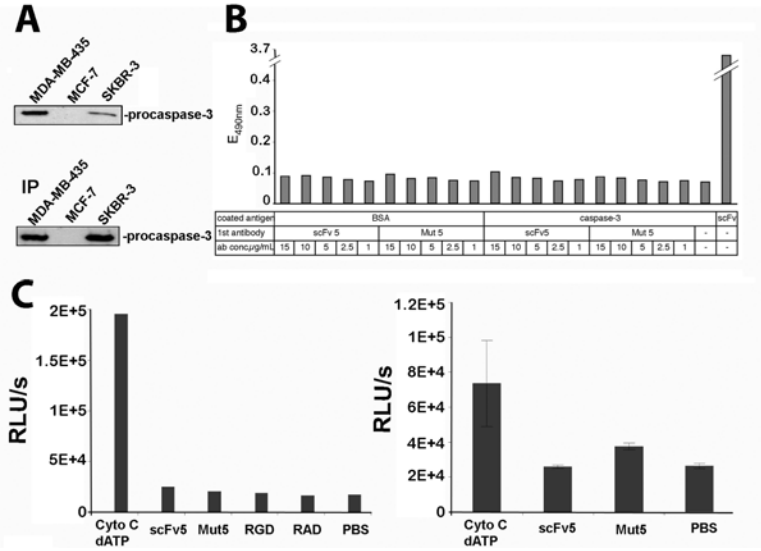

Figure 7
Caspase-3 expression in the target tumor cells and analysis of caspase-3 binding and activation by RGD-containing scFv1 and scFv5.
(A) (Top) Western blot analysis of caspase-3 expression in MDA-MB-435, MCF-7 (negative control) and SKBR-3 (positive control) cells. (Bottom) Verification for procaspase-3 by immunoprecipitation of caspase-3 from tumor cell lysates. **(B)** ELISA-based analysis of caspase-3 and scFv antibody interaction. Plates were coated with recombinant pro-caspase-3 or BSA (negative control) or scFv 5 (positive control). Addition of RGD-containing scFv 5 or RGE-containing scFv Mut 5 antibody, at concentrations as indicated showed no specific binding to caspase-3. **(C)** Analysis of caspase-3 activation by scFv antibodies. Hypotonic cell lysates, depleted of mitochondria, were combined with either scFv 5 or scFvMut 5 (4 μM), or RGD or RAD peptides (1 mM) (left panel). Cytochrome c/dATP were used as positive control and PBS as negative control in a bioluminescence assay.

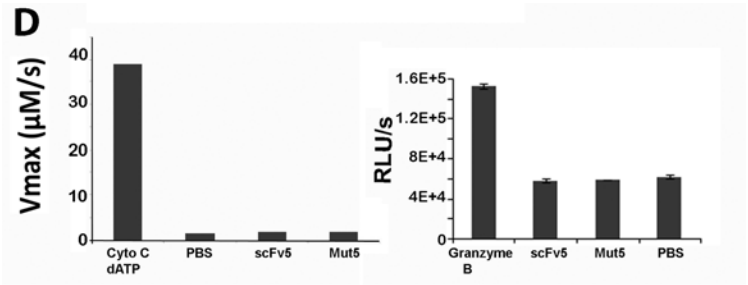

Cytochrome c and dATP were able to activate caspase-3 in the lysates, whereas all other samples showed only background signal. A higher scFv concentration was used to verify the lack of activation (10 µM) in the presence of Mg^{2+} (right panel). **(D)** Continuous measurement of caspase-3 activity in cell lysates based on chromogenic substrate reaction. Cleavage of colorimetric capsase 3 substrate N-acetyl-Asp-Glu-Val-Asp-*p*-nitroanilide (Ac-DEVD-*p*NA) was measured after combining hypotonic cell lysates with either scFv 5 or scFvMut 5 (2 µM). Absorption was measured continuously for 2 h at 37˚C (left panel). Activation measurement of recombinant caspase-3 by scFv 5 or scFvMut 5 in the presence of Mg^{2+} using Granzyme B as positive and PBS as negative control. After 30 min incubation at 37˚C, Glo reagent was added and bioluminescence measured after 30 min incubation at RT (right panel).

Ongoing and future activities based on these findings:

While treatment of mice bearing late stage breast cancer metastasis with antibodies against high affinity integrin $\alpha v\beta 3$ induced therapeutic responses in extracranial lesions, brain metastases were rarely affected. For our treatment regimens, we generated 'experimental patients' with advanced metastatic breast cancer by injecting human tumor cells into the venous circulation of immune deficient mice. Reminiscent of the situation in human breast cancer patients, metastases were widespread with extensive lung burden in almost every animal and additional lesions in the liver, bone, adrenal glands and occasionally in the brain. Due to the route of tumor cell implantation, pulmonary burden was likely somewhat overrepresented, compared to the situation seen in human breast cancer patients. Due to this distribution of metastatic disease, our evaluation of treatment responses focused on lung lesions, also assessing other sites of metastasis for therapeutic effects by whole body non-invasive imaging of disease burden. In accordance with the initially seen biodistribution of our therapeutic antibodies, responses of brain lesions were limited and not statistically significant.

In light of the central role of high affinity breast cancer cell integrin $\alpha v\beta 3$ in brain metastatic growth, our current efforts focus on expressing the scFv antibody fragments in neural progenitor cells to use these cells as vehicles for delivering the therapeutic molecules to sites of widespread breast cancer brain metastasis development.

Generation of two new, unique models of breast cancer brain metastasis

A major drawback in research directed at breast cancer brain metastasis has been that there are no true models of the disease currently available. Therefore, a priority in our study is to establish new cell and animal models that faithfully recapitulate breast cancer brain metastasis, as closely as possible as it occurs in breast cancer patients.

To accomplish this, we generated two novel and unique cell lines from surgical specimens of brain metastatic lesions removed from breast cancer patients. We refer to these cells as RJBr1 and RJBr2. When implanted into the frontal lobe of female SCID mice by stereotactic injection, both cell lines develop rapidly growing intracranial lesions (Fig.1). Importantly, these cell models also mimic the clinical situation of breast cancer brain metastasis, as they are able to colonize the brain from the blood stream. After injection into the left internal carotid artery, the tumor cells invade the brain parenchyma and develop multifocal and widespread breast cancer brain lesions. We detected brain metastases even after mammary fat pad injection of the tumor cells. This demonstrates that our new breast cancer brain metastasis cell models are capable of fully recapitulating the human disease in the SCID mouse model. *These cells are unique in the field, as no directly*

breast cancer brain metastasis derived cell models have been developed to date that emulate all steps of the human disease. Thus, our new cell models will be of critical importance for the planned project and provide direct clinical relevance for our studies on targeting breast cancer brain metastasis with antibodies delivered by brain homing progenitor cells.

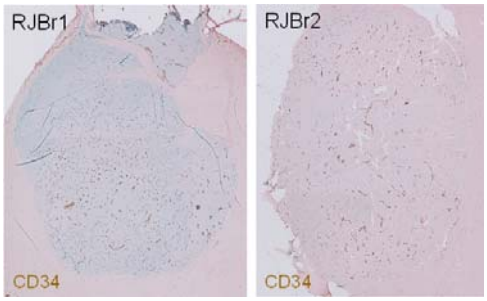

Fig.1 Intracranial lesions in the SCID mouse brain from RJBr1 and RJBr2 human brain metastatic breast cancer cells.
RJBr1 or RJBr2 cells (10^4) were implanted into the left frontal lobe. Lesions are shown by histology on day 56 post implant. Brown signal (CD34) represents the microvasculature of the lesions.

To follow brain lesion development and progression of metastatic brain disease, we genetically tagged the tumor cells stably with firefly luciferase and can detect lesion location and growth by non-invasive bioluminescence imaging. Figure 2 shows this for RJBr1cells after intracranial implantation on day 56 in a group of mice (left), and after carotid artery injection in one individual mouse at different time points. With this new and unique development, we have new models with which we can generate widespread brain metastatic disease of breast cancer. Therefore, these models provide a clinically most relevant foundation for evaluating a progenitor-based therapy for delivering function blocking antibodies to metastatic brain disease in breast cancer.

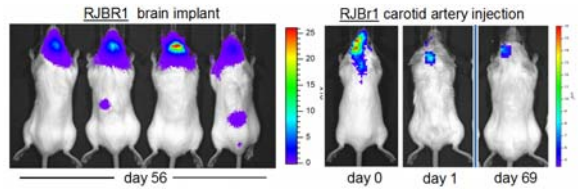

Fig.2 Development of intracranial lesions after frontal lobe implantation or carotid artery injection of RJBr1 cells. Four different mice after brain implant (10^4 cells) (left). The same mouse imaged over time after carotid artery injection (10^4 cells) (right).

Key Research Accomplishments

- We developed new human breast cancer brain metastasis and animal models that emulate all stages of brain metastasis in breast cancer
- We defined the timing and initial mechanisms through which circulating breast cancer cells invade the blood brain barrier and brain tissue
- We identified initial and persisting host cell responses to invading breast cancer cells within the brain tissue
- Among the earliest and persisting host cell responses are microglial localization and activation in the immediate vicinity of incoming and expanding breast cancer brain metastatic cells
- With these findings, we identified microglial cells and potentially their precursor cells as possible alternative host cells for delivery of therapeutic molecules to early as well as widespread breast cancer brain metastases.

- We identified the activated conformer of tumor cell integrin αvβ3 as a therapeutic target for inhibition of breast cancer brain metastasis

- We unraveled the mechanism through which activated integrin αvβ3 endows brain metastatic breast cancer cells with critical advantages for intracranial growth

- With this information, we identified a new pathway as therapeutic target for inhibition of breast cancer brain metastasis.

- We analyzed the therapeutic efficacy of human scFv antibody fragments directed against the activated form of tumor cell integrin αvβ3 for inhibition of breast cancer metastasis in a mouse model.

- We documented that the therapeutic antibodies, given systemically, specifically localize to extracranial lesions

- We found that targeting activated αvβ3 with the human scFv antibodies can interfere with advanced and widespread metastatic disease in breast cancer

- We found that treatment with the αvβ3 directed scFv antibodies causes growth retardation in extracranial breast cancer metastases and leads to increased immune cell infiltration into the lesions.

- We also found that phage delivery of the αvβ3 directed scFv antibodies does not reach the brain with sufficient efficacy to interfere with brain metastatic growth.

- We investigated the mechanism of interaction between activated tumor cell integrin αvβ3 and the therapeutic scFv antibodies and ruled out an alternative mechanism through binding of internalized scFv antibody to intracellular caspase-3 and direct induction of tumor cell apoptosis.

Reportable Outcomes

List of publications with DOD grant W81XWH-01-1-0468

Lorger M, Krueger JS, O'Neal M, Staflin K, Felding-Habermann B (2009) Activation of tumor cell integrin αvβ3 controls angiogenesis and metastatic growth in the brain. Proc Natl Acad Sci USA 106(26): 10666-71.

Katz J, Krueger JS, Felding-Habermann B, Snyder EY (2009) Maintaining and engineering neural stem cells for delivery of genetically encoded therapy to brain tumors. Methods Mol Biol 568:249-59.

Lorger M, Felding-Habermann B Capturing changes in the brain microenvironment during initial steps of brain metastasis. Am J Pathol *In revision*

Staflin K, Krueger JS, Hachmann J, Forsyth JS, Lorger M, Steininger SC, Pop C, Salvesen G, Janda KD, Felding-Habermann B Targeting activated integrin αvβ3 with patient-derived antibodies impacts late-state multiorgan metastasis. Clinical and Experimental Metastasis *In review*

Symposium Abstracts and Lectures associated with DOD grant W81XWH-01-1-0468

Felding-Habermann B, Chen EI, Krueger JS, Lorger M, Staflin K, Yates JR, Steeg PS, Palmier D, Kroener J 2008
Metabolic Changes in breast cancer brain metastasis

Annual Meeting of the American Association for Cancer Research Seminar presentation

Felding-Habermann B., Chen E.I., Krueger J.S., Lorger M., Staflin K., Yates J.R., Steeg P.S., Palmieri D., Kroener J. 2008
Mechanisms of breast cancer brain metastasis. *AACR 99th Annual Meeting, San Diego, CA* Poster

Staflin K, Krueger JS, Lorger M and Felding-Habermann B 2008
Tumor cell integrin activation in breast cancer brain metastasis
Annual Meeting of the American Association for Cancer Research Poster

Lorger M, Felding-Habermann B 2008
An RNA library screening approach to understanding breast cancer cell invasion of the brain
Annual Meeting of the American Association for Cancer Research Poster

Lorger M., Lee H., Felding-Habermann B. 2008
Mechanisms that control cancer cell penetration of the blood-brain barrier. *AACR 99th Annual Meeting, San Diego, CA* Poster

Felding-Habermann B, Krueger KS, O'Sullivan DM, Lorger M, Staflin K, Fernandez-Santidrian A, Jandial R, Kroener JF 2008
Intracranial growth in breast cancer brain metastasis
AACR Meeting of the Metastasis Research Society Invited lecture

Hassenpflug W.A., Lorger M., Forsyth J., Torbett B.E., Felding-Habermann B. 2008
Osteopontin promotes osteosarcoma metastasis to the lung through interaction with integrin $\alpha_V\beta_3$. *AACR 99th Annual Meeting, San Diego, CA* Poster

Felding-Habermann B, Lorger M, Fernandez-Santidrian A, Weber M, Krueger JS 2008
Mechanisms of tumor cell interaction with vascular cells
Barcelona BioMed Conference on Metastasis Genes and Functions Invited Lecture

Santidrian AF, Seo BB, Matsuno-Yagi A, Yagi T, and Felding-Habermann B 2009
Mitochondrial complex I modulation of cellular redox potential regulates tumorigenicity in breast cancer
AACR Special Conference on Metabolism in Cancer Poster

Staflin K, Fogal V, Fernandez-Santidrian A, Rouslahti E, and Felding-Habermann B 2009
A role of p32 in brain metastasis
AACR Special Conference on Metabolism in Cancer Poster

Lorger M. and Felding-Habermann B. 2009
Capturing the changes in brain microenvironment during the initial cancer cell invasion. *Society of Fellows Research Symposium, The Scripps Research Institute*, *La Jolla, CA* Poster

Lorger M., Krueger J.S., O'Neal M., Staflin K., Felding-Habermann B. 2009
Activation of tumor cell $\alpha_V\beta_3$ integrin controls metastatic growth in the brain. *AACR 100th Annual Meeting, Denver, CO* Poster

Wurdak H., Romero A., Lorger M., Zhu S., Watson J., Santidrian A.F., Chiang C.-Y.,Welch G., Tu B., Orth T., Steindler D., Harsh G., Felding-Habermann B., Miraglia L., Skirboll S., Rines D.R., Schultz P.G. 2009
Identification of signals regulating the fate of glioblastoma-initiating cells. *AACR 100th Annual Meeting, Denver, CO* Poster

Lorger M and Felding-Habermann B 2009
Capturing changes in the brain microenvironment during initial steps of breast cancer brain metastasis. *Annual CTRC-AACR San Antonio Breast Cancer Symposium* Poster

Invited oral presentations given by B. Felding-Habermann associated with DOD grant W81XWH-01-1-0468

1. Integrin activation in tumor metastasis
   Barcelona BioMed Conference on "Metastasis Genes and Functions" May 19-21, 2008
   Barcelona, Spain, 05/20/08 (invited speaker)

2. Mechanisms of breast cancer brain metastasis
   AACR Special Conference in Cancer Research, Joint Metastasis Research Society-AACR conference on "Metastasis", Vancouver, Canada, August 3-7, 2008
   Vancouver, Canada 08/04/08 (invited speaker)

3. Advanced progression in breast cancer: invasion and colonization of the brain
   Drexel University College of Medicine, Philadelphia, PA, 12/14/08 (invited lecture)

4. Development and progression of brain metastasis.
   MD Anderson Cancer Center, Department of Cancer Biology and Cancer Metastasis Research, Houston, TX, 06/30/09 (invited lecture)

5. Models and mechanisms of brain metastasis
   Sloan Kettering Memorial Cancer Center, Brain Tumor Center Seminar, New York, 11/16/09 (invited lecture)

Disclosures associated with DOD grant W81XWH-01-1-0468

Felding-Habermann B, O'Sullivan D, Smider V, Steele J 2009 "TES, a Human Breast Cancer Model to study the Biology, Clinical Progression and Therapy of Inflammatory, Triple Negative and Metaplastic Breast Cancers" (Disclosure)

Felding-Habermann B, Lorger M 2009 "Lentiviral cDNA expression of BMC1 human breast cancer cell and Adapter-flanked cDNA from human breast cancer cell lines TES-1, TES-2b, and TES-PE (Disclosure)

List of community presentations with DOD grant W81XWH-01-1-0468

2008 "Parlor Party" discussion round on progress in breast cancer research for participants of the Scripps initiative for breast cancer survivors and activists (Del Mar, CA)

2009 "Our research on breast cancer progression" Presentation at the Annual Fundraiser Ladies Golf tournament of the Lomas Santa Fe Country Club (Solana Beach, CA)

2009 "Brain metastasis in breast cancer" Lab Notes Lecture of The Scripps Research Institute, a public education event sponsored by the Philantropy Office. (La Jolla, CA)

2009 "Targeting invasive breast cancer" Presentation at the Initiation Event of the Elizabeth Smider Foundation for Metaplastic Breast Cancer. Lomas Santa Fe Country Club (Solana Beach, CA)

Conclusion

The goal of this study is to develop a new therapeutic approach for clinical inhibition of breast cancer brain metastasis. Our work to date has identified a new molecular target for treatment of metastatic brain disease in breast cancer patients and provided antibody tools that successfully interrupt breast cancer metastasis in a mouse model. Systemic application of the antibodies does not sufficiently reach brain lesions to interfere with their development and progression. Delivery strategies are being developed to bring therapeutic antibodies or their fragments to brain metastatic lesions and inhibit their proliferation. We have established and validated unique new breast cancer brain metastasis cell models and adapted mouse models to emulate all steps of human breast cancer brain metastasis development and invasive progression. These models are essential new tools for the evaluation of successful new therapies against widespread metastatic brain disease as seen in breast cancer patients. By investigating initial as well as late stages of brain metastasis development in the animal model, we have identified host cell responses that can be potentially used as therapeutic targets and for delivery of therapeutic molecules to disseminated breast cancer brain lesions. With these advances, we have made tangible progress toward new treatment options for breast cancer patients with cerebral metastasis.

References

(1) Kirsch DG, Loeffler JS. Brain metastases in patients with breast cancer: new horizons. Clin Breast Cancer 2005;6:115-24.

(2) Weil RJ, Palmieri DC, Bronder JL, Stark AM, Steeg PS. Breast cancer metastasis to the central nervous system. Am J Pathol 2005;167:913-20.

(3) Palmieri D, Chambers AF, Felding-Habermann B, Huang S, Steeg PS. The biology of metastasis to a sanctuary site. Clin Cancer Res 2007;13:1656-62.

(4) Clayton AJ, Danson S, Jolly S, Ryder WD, Burt PA, Stewart AL, et al. Incidence of cerebral metastases in patients treated with trastuzumab for metastatic breast cancer. Br J Cancer 2004;91:639-43.

(5) Kirsch DG, Ledezma CJ, Mathews CS, Bhan AK, Ancukiewicz M, Hochberg FH, et al. Survival after brain metastases from breast cancer in the trastuzumab era. J Clin Oncol 2005;%20;23:2114-6.

(6) Piccart-Gebhart MJ, Procter M, Leyland-Jones B, Goldhirsch A, Untch M, Smith I, et al. Trastuzumab after adjuvant chemotherapy in HER2-positive breast cancer. N Engl J Med 2005;353:1659-72.

(7) Peacock KH, Lesser GJ. Current therapeutic approaches in patients with brain metastases. Curr Treat Options Oncol 2006;7:479-89.

(8) Nieder C, Grosu AL, Astner S, Thamm R, Molls M. Integration of chemotherapy into current treatment strategies for brain metastases from solid tumors. Radiat Oncol 2006;1:19.:19.

(9) Lin NU, Bellon JR, Winer EP. CNS metastases in breast cancer. J Clin Oncol 2004;22:3608-17.

(10) Klos KJ, O'Neill BP. Brain metastases. Neurologist 2004;10:31-46.

(11) Chambers AF. MDA-MB-435 and M14 Cell Lines: Identical but not M14 Melanoma? Cancer Res 2009;96:5292-3.

(12) Hollestelle A, Schutte M. Comment Re: MDA-MB-435 and M14 cell lines: identical but not M14 Melanoma? Cancer Res 2009;69:7893.

(13) Lim M, Guccione S, Haddix T, Sims L, Cheshier S, Chu P, et al. alpha(v)beta(3) Integrin in central nervous system tumors. Hum Pathol 2005;36:665-9.

(14) Albelda SM, Mette SA, Elder DE, Stewart R, Damjanovich L, Herlyn M, et al. Integrin distribution in malignant melanoma: association of the beta 3 subunit with tumor progression. Cancer Res 1990;50:6757-64.

(15) Gingras MC, Roussel E, Bruner JM, Branch CD, Moser RP. Comparison of cell adhesion molecule expression between glioblastoma multiforme and autologous normal brain tissue. J Neuroimmunol 1995;57:143-53.

(16) Gladson CL, Hancock S, Arnold MM, Faye-Petersen OM, Castleberry RP, Kelly DR. Stage-specific expression of integrin alphaVbeta3 in neuroblastic tumors. Am J Pathol 1996;148:1423-34.

(17) Ding Q, Stewart J, Jr., Olman MA, Klobe MR, Gladson CL. The pattern of enhancement of Src kinase activity on platelet-derived growth factor stimulation of glioblastoma cells is affected by the integrin engaged. J Biol Chem 2003;278:39882-91.

(18) Brooks PC, Clark RA, Cheresh DA. Requirement of vascular integrin alpha v beta 3 for angiogenesis. Science 1994;264:569-71.

(19) Fujita Y, Abe R, Shimizu H. Clinical approaches toward tumor angiogenesis: past, present and future. Curr Pharm Des 2008;14:3820-34.

(20) Cai W, Chen X. Anti-angiogenic cancer therapy based on integrin alphavbeta3 antagonism. Anticancer Agents Med Chem 2006;6:407-28.

(21) Felding-Habermann B, Lerner RA, Lillo A, Zhuang S, Weber MR, Arrues S, et al. Combinatorial antibody libraries from cancer patients yield ligand-mimetic Arg-Gly-Asp-containing immunoglobulins that inhibit breast cancer metastasis. Proc Natl Acad Sci U S A 2004;101:17210-5.

(22) Felding-Habermann B, Fransvea E, O'Toole TE, Manzuk L, Faha B, Hensler M. Involvement of tumor cell integrin alpha v beta 3 in hematogenous metastasis of human melanoma cells. Clin Exp Metastasis 2002;19:427-36.

Appendices

Publications

Lorger M, Krueger JS, O'Neal M, Staflin K, Felding-Habermann B (2009) Activation of tumor cell integrin $\alpha v\beta 3$ controls angiogenesis and metastatic growth in the brain. Proc Natl Acad Sci USA 106(26): 10666-71.

Katz J, Krueger JS, Felding-Habermann B, Snyder EY (2009) Maintaining and engineering neural stem cells for delivery of genetically encoded therapy to brain tumors. Methods Mol Biol 568:249-59.

Lorger M, Felding-Habermann B Capturing changes in the brain microenvironment during initial steps of brain metastasis. Am J Pathol *In revision*

Staflin K, Krueger JS, Hachmann J, Forsyth JS, Lorger M, Steininger SC, Pop C, Salvesen G, Janda KD, Felding-Habermann B Targeting activated integrin $\alpha v\beta 3$ with patient-derived antibodies impacts late-state multiorgan metastasis. *In review*

Activation of tumor cell integrin $\alpha_v\beta_3$ controls angiogenesis and metastatic growth in the brain

Mihaela Lorger, Joseph S. Krueger, Melissa O'Neal, Karin Staflin, and Brunhilde Felding-Habermann[1]

Department of Molecular and Experimental Medicine, The Scripps Research Institute, 10550 North Torrey Pines Road, MEM-150, La Jolla, CA 92037

Edited by Richard O. Hynes, Massachusetts Institute of Technology, Cambridge, MA, and approved May 5, 2009 (received for review March 18, 2009)

The incidence of brain metastasis is rising and poses a severe clinical problem, as we lack effective therapies and knowledge of mechanisms that control metastatic growth in the brain. Here we demonstrate a crucial role for high-affinity tumor cell integrin $\alpha_v\beta_3$ in brain metastatic growth and recruitment of blood vessels. Although $\alpha_v\beta_3$ is frequently up-regulated in primary brain tumors and metastatic lesions of brain homing cancers, we show that it is the $\alpha_v\beta_3$ activation state that is critical for brain lesion growth. Activated, but not non-activated, tumor cell $\alpha_v\beta_3$ supports efficient brain metastatic growth through continuous up-regulation of vascular endothelial growth factor (VEGF) protein under normoxic conditions. In metastatic brain lesions carrying activated $\alpha_v\beta_3$, VEGF expression is controlled at the post-transcriptional level and involves phosphorylation and inhibition of translational respressor 4E-binding protein (4E-BP1). In contrast, tumor cells with non-activated $\alpha_v\beta_3$ depend on hypoxia for VEGF induction, resulting in reduced angiogenesis, tumor cell apoptosis, and inefficient intracranial growth. Importantly, the microenvironment critically influences the effects that activated tumor cell $\alpha_v\beta_3$ exerts on tumor cell growth. Although it strongly promoted intracranial growth, the activation state of the receptor did not influence tumor growth in the mammary fat pad as a primary site. Thus, we identified a mechanism by which metastatic cells thrive in the brain microenvironment and use the high-affinity form of an adhesion receptor to grow and secure host support for proliferation. Targeting this molecular mechanism could prove valuable for the inhibition of brain metastasis.

angiogenesis | brain metastasis | integrin activation | 4E-BP1

Brain metastases are diagnosed in 10% to 40% of patients with progressing cancer, and the incidence is rising as patients live longer and extracranial metastases respond to improved treatments. However, brain metastases still cannot be treated effectively, and mechanisms controlling brain metastatic growth are largely unknown (1–3).

Here, we demonstrate that the high-affinity state of tumor cell adhesion receptor integrin $\alpha_v\beta_3$ critically promotes metastatic growth and recruitment of supporting blood vessels within the brain microenvironment. Integrins are cell surface receptors composed of non–covalently linked α and β subunits that mediate cell–matrix and cell–cell interactions and transduce signals that have impacts on cell survival, proliferation, adhesion, migration, and invasion. Integrin signals can also originate inside cells, affect receptor affinity, and thereby control ligand binding, cross talk with other receptors, and alter cell adhesion and proliferation (4–6). Integrin $\alpha_v\beta_3$ also plays a role on sprouting endothelial cells and contributes to angiogenesis (7). In several tumor types, including glioma, breast cancer, and melanoma, expression of $\alpha_v\beta_3$ supports invasion and metastasis (8–11). Notably, these tumors either originate in the brain or frequently spread to the brain. Because of this correlation and our previous findings that expression of $\alpha_v\beta_3$ by tumor cells, particularly in its high-affinity form, promotes metastatic dissemination (12), we asked whether $\alpha_v\beta_3$ and the activation state of the receptor also play a role in metastatic growth within the brain microenvironment. To address this question directly, we generated and validated a human tumor cell model in which variants share a genetic background and express integrin $\alpha_v\beta_3$ either in a constitutively activated or non-activated functional form. Our results show that tumor cell $\alpha_v\beta_3$ activation promotes tumor cell growth in the brain but not in the mammary fat pad (MFP) as a primary site, pointing to a critical influence of the tissue environment on the ability of high-affinity $\alpha_v\beta_3$ to enhance tumor growth. Our study suggests that the mechanism through which activated $\alpha_v\beta_3$ supports brain metastatic growth is based on elevated expression of vascular endothelial growth factor (VEGF) because of inhibition of translational repressor 4E-BP1, resulting in efficient tumor angiogenesis under normoxic conditions. This function prevents development of hypoxia, associated tumor cell apoptosis, and retardation of lesion growth. Thus, as an initiator of this process, activated integrin $\alpha_v\beta_3$ could potentially serve as a target against brain metastasis.

Results

Tumor Cell Integrin $\alpha_v\beta_3$ Activation Enhances Metastatic Growth in the Brain. We chose MDA-MB-435 human cancer cells for our analysis because they are highly metastatic, can spread to the brain, and express $\alpha_v\beta_3$, and because the activation state of the receptor strongly affects metastasis to extracranial sites (12). To generate cell variants that express $\alpha_v\beta_3$ in defined states of activation, endogenous $\alpha_v\beta_3$ was knocked-down, targeting the 3′UTR of the β_3 subunit gene and then reconstituted either with non-activated β_3WT or constitutively activated mutant β_3D723R (12, 13). In MDA-MB-435 cells, $\alpha_v\beta_3$ is the only β_3 integrin. Thus, targeting β_3 by stable transduction with lentiviral shRNA resulted in 80% reduction of total β_3 protein (Western blot, not shown) and 70% reduction in $\alpha_v\beta_3$ surface expression (Fig. 1*A*), without affecting other integrins. This was confirmed by fluorescence activated cell sorter (FACS) analysis of a panel of integrins, including $\alpha_v\beta_5$ and $\alpha_v\beta_6$ (not shown). Importantly, β_3 down-regulation remained stable in tumor xenografts [supporting information (SI) Fig. S1]. The cDNA constructs used for reconstitution with β_3WT or β_3D723R lack 3′-UTRs and are therefore not affected by the β_3 shRNA. $\alpha_v\beta_3$ surface expression in β_3D723R cells resembled that of the parental cells, whereas β_3WT cells expressed twice as much $\alpha_v\beta_3$ (Fig. 1*A*). Notably, $\alpha_v\beta_3$ activation by mutant β_3D723R was stable after tumor cell implantation into the brain or MFP.

When implanted into the forebrain (striatum), tumor cells expressing activated β_3D723R exhibited a significant growth advantage over $\beta_3$kd cells, cells expressing non-activated β_3WT, and parental cells transduced with scrambled shRNA used as a

Author contributions: M.L., J.S.K., and B.F.-H. designed research; M.L., J.S.K., M.O., and K.S. performed research; M.L., J.S.K., and B.F.-H. analyzed data; and M.L. and B.F.-H. wrote the paper.

The authors declare no conflict of interest.

This article is a PNAS Direct Submission.

Freely available online through the PNAS open access option.

[1]To whom correspondence should be addressed. E-mail: brunie@scripps.edu.

This article contains supporting information online at www.pnas.org/cgi/content/full/0903035106/DCSupplemental.

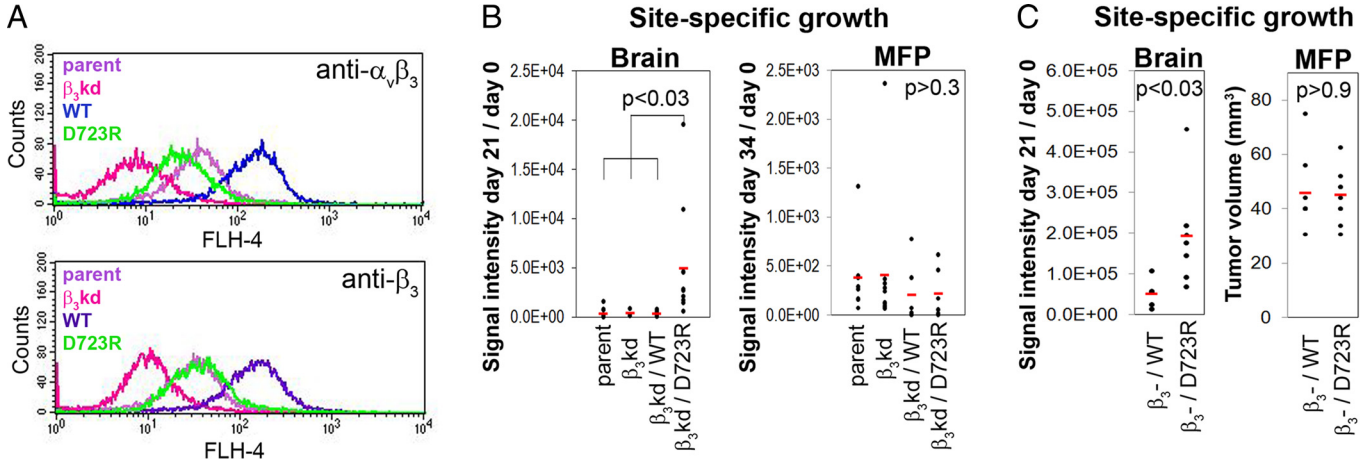

Fig. 1. Impact of tumor cell integrin $\alpha_v\beta_3$ expression and activation on lesion growth in the brain and mammary fat pad (MFP). (*A*) Analysis of integrin $\alpha_v\beta_3$ expression by flow cytometry. Parent, MDA-MB-435 transduced with control shRNA ScrB; $\beta_3$kd, MDA-MB-435 transduced with β_3 shRNA; WT, MDA-MB-435/$\beta_3$kd reconstituted with wild-type β_3 (non-activated $\alpha_v\beta_3$); D723R, MDA-MB-435/$\beta_3$kd reconstituted with β_3D723R (activated $\alpha_v\beta_3$). (*B*) Lesion growth in the brain (days 0–21) or MFP (days 0–34) based on bioluminescence signal of *F-luc*–tagged tumor cells by non-invasive in vivo imaging. (*C*) Lesion growth in the brain (days 0–21) or MFP (days 0–36) of MDA-MB 435/β_3- cells selected from parental cells with saporin-anti-β_3 antibody and reconstituted by transfection with β_3WT of β_3D723R based on in vivo imaging (brain) or caliper measurement (MFP). Each dot represents one animal and red lines the mean values per group; group sizes in (*B*): brain: parent and $\beta_3$kd, $n = 6$; β_3WT and β_3D723R, $n = 11$; *MFP*: parent, $n = 10$; $\beta_3$kd, $n = 8$; β_3 and β_3D723R, $n = 6$; (*C*), all groups, $n = 7$. *P* values obtained by a two-tailed Student's *t* test with unequal variance.

control (Figs. 1*B*, 2*A*). In contrast, in the MFP, mimicking a primary tumor site, expression of activated β_3D723R did not accelerate tumor growth, which was generally slower than in the brain (Fig. 1*B*). Notably, β_3WT and β_3D723R cells displayed identical growth rates in vitro (Fig. S2*A*).

The site-specific growth phenotype seen in β_3WT and β_3D723R cells was also observed with MDA-MB-435 β_3-/WT and β_3-/D723R cells (Fig. 1*C*). The previously described β_3- cells (12) were obtained through selection with a saporin-conjugated anti-β_3 antibody and used to generate β_3WT and β_3D723R re-expressing variants by plasmid transfection, and antibiotic selection (12). The organ-dependent growth behavior observed in both independently generated cell models confirmed that the phenotype is indeed due to the $\alpha_v\beta_3$ activation state. Thus, activation of integrin $\alpha_v\beta_3$ critically enhances tumor cell growth in the brain but is not required for growth in the MFP, implying that $\alpha_v\beta_3$ activation promotes metastatic growth in a microenvironment-dependent manner.

To investigate the mechanism involved, we followed tumor cell growth in the brain over time and realized initially no difference between cells expressing activated versus non-activated $\alpha_v\beta_3$. However, 10 days after implantation of 10^4 tumor cells, a significant growth difference became evident and then increased continuously (Fig. 2*B*). This difference was caused by an enhancement in tumor cell proliferation. On day 21, in vivo BrdU incorporation was 25% higher in β_3D723R than in β_3WT implants (Figs. 2*C*, 2*D*). Both lesion types showed low and comparable levels of apoptosis (<1%) by terminal deoxynucleotidyl transferase dUTP nick end labeling (TUNEL) staining (Fig. 2*E*). Thus, once lesions in the brain reach an initial critical

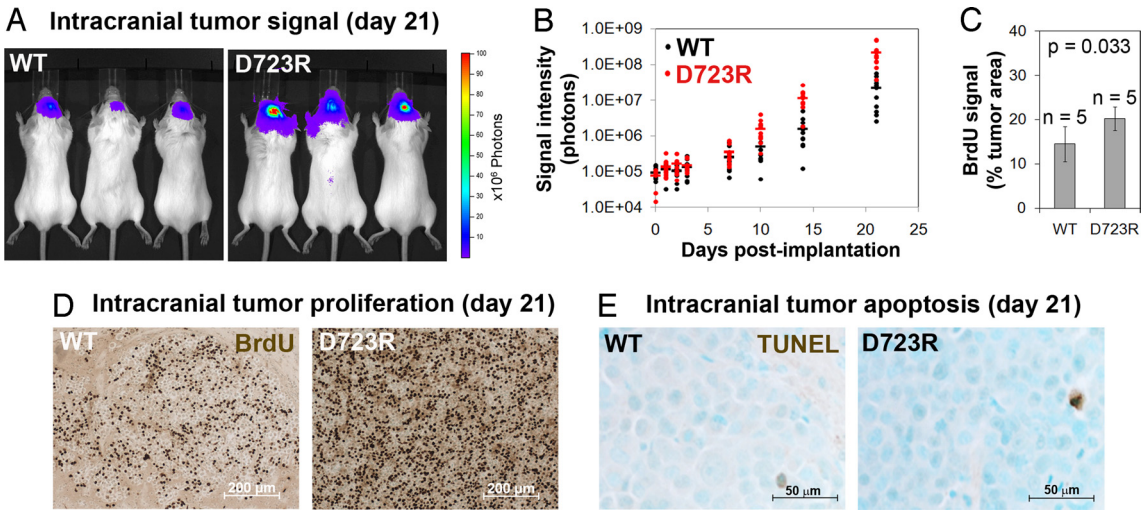

Fig. 2. Tumor cell integrin $\alpha_v\beta_3$ activation enhances proliferation in the brain. (*A*) Non-invasive bioluminescence imaging 21 days after intracranial implantation of 1×10^4 β_3WT- (*Left*) or β_3D723R- (*Right*) expressing MDA-MB-435 tumor cells. (*B*) Growth of β_3WT and β_3D723R-expressing tumor cells in the brain. Each dot represents one animal; horizontal lines represent mean values per group. (*C and D*) Intracranial proliferation of β_3WT- and β_3D723R-expressing cells in brain lesions by in vivo BrdU uptake; $n = 5$ per group, *P* values obtained by a two-tailed Student's *t* test with unequal variance. (*E*) Apoptosis in β_3WT and β_3D723R brain lesions by TUNEL staining (brown).

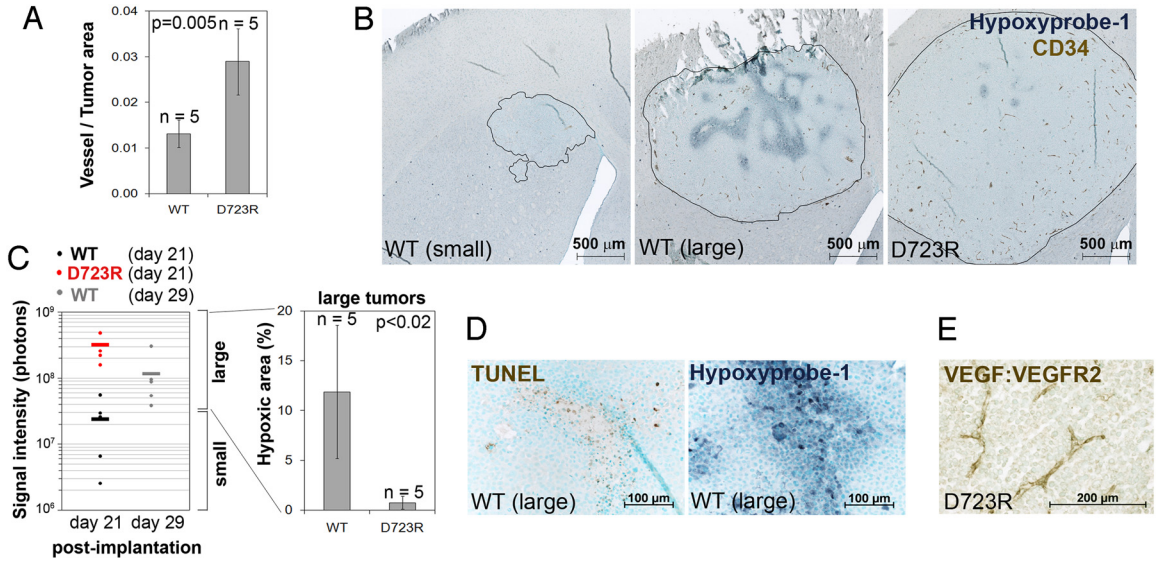

Fig. 3. Tumor cell integrin $\alpha_v\beta_3$ activation increases angiogenesis and reduces hypoxia in brain lesions. (*A*) Quantification of the total vessel area in β_3WT and β_3D723R brain lesions 21 days after tumor cell implantion. Vessels were visualized by CD34 staining. (*B*) Immunohistochemistry of tumor vessels (brown) and hypoxic regions (gray-blue) in brain lesions on day 21. Borders between tumor area and brain parenchyma are outlined showing representative small (≤1.5 mm) and large (≥ 1.5 mm) β_3WT lesions. All β_3D723R lesions were >2 mm. (*C*) (*Left*) In vivo signal of β_3WT (black) and β_3D723R (red) brain lesions on day 21, and on day 29 for β_3WT (gray) to obtain larger lesions for this group. Only lesions with a diameter ≥1.5 mm (≈5×10^7 bioluminescence photons in vivo) were included in the quantification of hypoxic tumor regions (marked with a bracket as large tumors). (*Right*) Percentage of hypoxic area in brain lesions >1.5 mm in diameter; $n = 5$ per group; *P* values based on two-tailed Student's *t* test with unequal variance. (*D*) Large β_3WT lesions (> 1.5 mm) show increased apoptosis (*Left;* TUNEL staining, brown; nuclei, green) within hypoxic regions (*Right;* Hypoxyprobe-1 staining, gray-blue; nuclei, green) in adjacent sections. (*E*) Formation of the VEGF:VEGFR2 complex on tumor vessels in β_3D723R brain lesions (Gv39M staining, brown).

size, tumor cell integrin $\alpha_v\beta_3$ activation strongly enhances proliferation, without affecting cell survival.

Tumor Cell Integrin $\alpha_v\beta_3$ Activation Promotes Angiogenesis and Prevents Development of Hypoxia in Brain Lesions. Having observed that the growth advantage of brain implants expressing activated β_3D723R became apparent once the lesions reached an initial critical size, we asked whether a host response contributes to the accelerated tumor growth. In vivo labeling and detailed immunohistochemistry revealed two major points. First, the tumor area covered by blood vessels (CD34 stain) was significantly larger in lesions expressing activated β_3D723R than in those expressing non-activated β_3WT (Fig. 3*A*). This included all tumors, regardless of size. Notably, on day 21 post-implantation, five of five lesions in the β_3D723R group were large and measured 2 to 3 mm in diameter, whereas only one in five in the β_3WT group reached a threshold size of 1.5 mm. Second, whereas microvessels were distributed evenly throughout the large tumor areas in the β_3D723R group with no or minimal hypoxic regions (<1%), vessels in the β_3WT group were located mainly along the lesion margins. The only lager tumor in this group had developed extensive hypoxic regions in the poorly vascularized central area (Fig. 3*B*).

To investigate whether the development of hypoxic regions in the β_3WT group is a function of lesion size, we allowed implants of β_3WT-expressing cells to grow longer and become larger, making it possible to compare them to β_3D723R-expressing lesions. An association between hypoxia development and tumor size in lesions expressing non-activated β_3WT would further point to angiogenesis as a growth limiting factor. On day 29 post-implantation, four of five β_3WT lesions were larger than 1.5 mm, and they were used for comparison with β_3D723R lesions of the same or larger size (Fig. 3*C*). Although β_3D723R lesions developed no or only minimal hypoxia, β_3WT lesions harbored large hypoxic regions (Fig. 3*C*) with increased tumor cell apoptosis (Fig. 3*D*). Thus, expression of activated $\alpha_v\beta_3$ by the tumor cells is associated with their enhanced ability to attract new blood vessels, thereby avoiding hypoxia and protecting the growing tumor cells from apoptosis. *De novo* angiogenesis, rather than tumor cell growth around exiting vessels (vessel co-opting), was confirmed by expression of VEGF:VEGFR2 complex on the tumor vessels (Fig. 3*E*), identifying the angiogenic state of the endothelial cells (14).

Tumor Cell Integrin $\alpha_v\beta_3$ Activation Promotes VEGF Expression at the Post-Transcriptional Level in Normoxic Brain Lesions. To identify a mechanism by which activated tumor cell integrin $\alpha_v\beta_3$ promotes angiogenesis in the brain, we focused on VEGF, a major promoter of endothelial proliferation (15). As hypoxia potently induces VEGF via transcription factor HIF-1α (16) or via induction of cap-independent internal ribosome entry site IRES-mediated translation (17), we analyzed VEGF expression in hypoxic versus normoxic tumor regions, identifying hypoxia by staining for Hypoxyprobe-1 and probing for HIF-1α. In hypoxic regions, VEGF protein expression was strong and associated with increased HIF-1α signal regardless of the $\alpha_v\beta_3$ activation state of the tumor lesions (Fig. 4*A*), indicating VEGF up-regulation at the transcriptional level. In contrast, in normoxic tumor regions devoid of Hypoxyprobe-1 and HIF-1α signal, VEGF was detected only in β_3D723R but not in β_3WT lesions (Fig. 4*A*).

To determine whether $\alpha_v\beta_3$ activation in normoxic regions regulates VEGF expression at the transcriptional or post-transcriptional level (18, 19), proteins and total RNA were extracted from microdissected β_3WT- and β_3D723R-expressing lesions of mouse brains 21 days after tumor cell implantation. All analyzed β_3WT lesions were smaller than 1.5 mm and still without hypoxic areas. β_3D723R lesions, although larger, also showed no or minimal hypoxia (<1%) (Fig. 3). Western blot analysis of VEGF immunoprecipitated from brain tumor lysates confirmed increased VEGF protein levels in β_3D723R-expressing lesions (Fig. 4*B*). Reverse transcription–polymerase

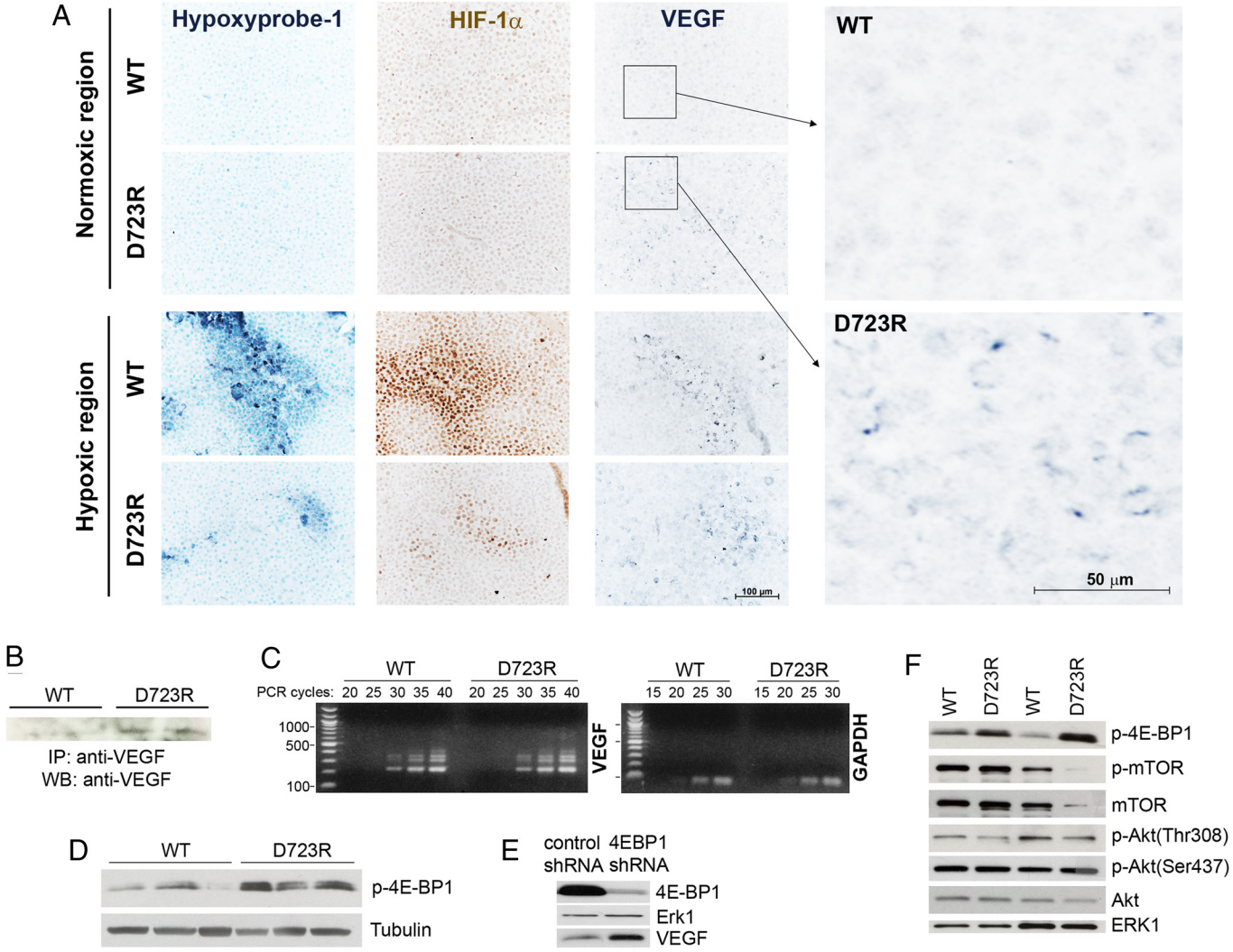

Fig. 4. Tumor cell integrin $\alpha_v\beta_3$ activation increases VEGF expression in the brain post-transcriptionally by 4E-BP phosphorylation. (*A*) VEGF protein expression in normoxic (*upper panels*) versus hypoxic areas (*lower panels*) of β_3WT and β_3D723R brain lesions by immunohistochemistry. Hypoxic regions defined by positive staining for Hypoxyprobe-1 (*Left*) and HIF-1α (*Middle*). β_3WT and β_3D723R lesions express VEGF in hypoxic regions. In normoxic regions, only β_3D723R lesions express VEGF (*Right*; enlarged on *far right*). (*B*) VEGF protein levels in microdissected β_3WT and β_3D723R brain lesions 21 days after tumor cell implantation (immunoprecipitation [IP], VEGF; Western blot [WB], VEGF). (*C*) VEGF mRNA levels in microdissected β_3WT and β_3D723R brain lesions on day 21 post-implantation (RT-PCR). Lesions from three different mice per group. (*D*) Phospho-4E-BP1 signal in microdissected β_3WT and β_3D723R brain lesions 21 days after tumor cell implantation (Western blot with anti-phospho-4E-BP1 and anti-tubulin antibodies). (*E*) Down-regulation of 4E-BP1 in β_3WT cells by shRNA results in a strong increase of VEGF protein level under normoxia in vitro. VEGF was immunoprecipitated from cell culture supernatants before Western blot analysis. (*F*) Detection of mTOR and Akt activation levels with phospho-specific antibodies in microdissected β_3WT and β_3D723R brain lesions 21 days after tumor cell implantation.

chain reaction (RT- PCR) with VEGF-specific primers yielded four distinct PCR products (230, 310, 365, and 430 bp) (Fig. 4*C*), corresponding to splice variants $VEGF_{121}$, $VEGF_{145}$, $VEGF_{165}$, and $VEGF_{189}$ (20), with no differences in mRNA levels or isoform patterns between β_3WT- and β_3D723R-expressing lesions (Fig. 4*C*). Thus, under normoxic conditions, tumor cell integrin $\alpha_v\beta_3$ activation regulates VEGF expression at the post-transcriptional level.

To investigate the mechanism involved, we focused on VEGF mRNA regulation. VEGF mRNA is "weakly" transcribed because of its highly structured 5′UTR, and its translation under normoxia strongly depends on the availability of eukaryotic initiation factor eIF4E (19, 21). eIF4E is bound and inhibited by eIF4E binding protein 1 (4E-BP1), which, when phosphorylated, no longer binds eIF4E and makes it available for translation of weak RNAs (22). 4E-BP1 was significantly stronger phosphorylated in β_3D723R- than β_3WT-expressing brain lesions (Fig. 4*D*), suggesting that increased VEGF expression is due to phosphorylation and inactivation of 4E-BP1. A causal relationship between 4E-BP1 inhibition and VEGF production under normoxia was confirmed by the finding that shRNA knock-down of 4E-BP1 in β_3WT cells strongly increased VEGF protein levels in vitro (Fig. 4*E*). Similar to β_3WT and β_3D723R cells, 4E-BP1 knock-down and control cells also showed identical growth rates in culture (Fig. S2*B*).

We further investigated mTOR and Akt as major constituents of pathways controlling the 4E-BP1 protein (22). The mTOR protein is large and prone to degradation during tissue processing. We therefore compared the ratio between phosphorylated mTOR(Ser-2481) and total mTOR and found no difference between β_3WT- and β_3D723R-expressing lesions (Fig. 4*F*). Similarly, Akt activation measured by phosphorylation on Ser-308 and Thr-437 was also not altered because of $\alpha_V\beta_3$ activation (Fig. 4*F*). Thus, enhanced phosphorylation of 4E-BP1 associated

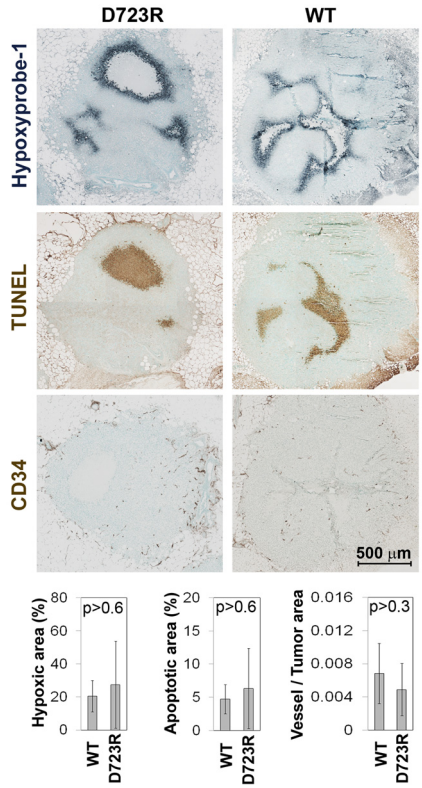

Fig. 5. Tumor cell integrin $\alpha_v\beta_3$ activation does not prevent hypoxia in mammary fat pad tumors. Hypoxia (Hypoxyprobe-1 in gray-blue, *Upper*), apoptosis/necrosis (TUNEL staining in brown, *Middle*) and blood vessel density (CD34 in brown, *Lower*) in MFP tumors 34 days after implanting 1×10^4 β_3WT- or β_3D723R-expressing tumor cells. Quantifications are included ($n = 5$ per group). *P* values are based on two-tailed Student's *t* test with unequal variance. Note: All 34-day old MFP tumors were smaller than 21-day-old β_3D723R brain lesions.

with $\alpha_V\beta_3$ activation of the tumor cells is apparently not controlled by mTOR or Akt activation.

Tumor Cell Integrin $\alpha_v\beta_3$ Activation Does Not Prevent Hypoxia in Mammary Fat Pad Tumors. Although tumor cell integrin $\alpha_v\beta_3$ activation significantly increased growth of MDA-MB-435 cell implants in the brain, it had no impact on tumor growth in the MFP (Fig. 1*B*, 1*C*). There, $\beta_3$kd as well as β_3WT- and β_3D723R-expressing cells grew more slowly than in the brain, and $\alpha_v\beta_3$ activation made no difference. In fact, MFP lesions expressing β_3WT or β_3D723R showed much lower blood vessel densities than brain lesions and developed extensive hypoxic regions with strong apoptosis and necrosis (Fig. 5). Hypoxic areas and some of the surrounding tissue strongly expressed VEGF in β_3WT as well as β_3D723R derived MFP lesions (Fig. S3). Because of the extensive expansion of hypoxic regions in MFP tumors, seen even in early lesions still smaller than 1 mm (not shown), it was not possible to define clearly normoxic areas and to analyze VEGF expression there. Thus, in the MFP, tumor cell $\alpha_v\beta_3$ activation is not sufficient to enhance recruitment of tumor blood vessels, prevent hypoxia, and accelerate tumor cell growth. Therefore, tumor cell integrin $\alpha_v\beta_3$ activation selectively enhances cancer growth in a microenvironment-dependent manner, strongly supporting lesion growth in the brain, a particularly feared metastatic site.

Discussion

We analyzed a role of integrin $\alpha_v\beta_3$ activation in tumor cell growth in the brain and mammary fat pad to represent clinically highly relevant metastatic and primary sites. We focused explicitly on $\alpha_v\beta_3$ in tumor cells, as it is largely unknown how the activation state of this receptor affects cancer progression whereas the endothelial receptor has been widely studied in angiogenesis. We show that tumor cell integrin $\alpha_v\beta_3$ activation strongly promotes metastatic growth in the brain by enabling tumor cells to attract blood vessels independently of hypoxia and thereby avoiding hypoxia-related growth stagnation and apoptosis. In contrast, in the mammary fat pad, tumor cell $\alpha_v\beta_3$ had no effect on lesions growth, which was generally slower than in the brain, poorly vascularized, extensively hypoxic, and associated with apoptosis and necrosis. Expression of activated tumor cell integrin $\alpha_v\beta_3$ could not overcome this limitation as it did in the brain. Therefore, the specific ability of activated tumor cell integrin $\alpha_v\beta_3$ to enhance angiogenesis clearly depends on the tissue microenvironment. Organ-dependent differences in growth factors, chemokines, cytokines, and matrix proteins, as well as stromal and immune components, may distinctly affect tumor cell growth and endothelial behavior in the mammary fat pad versus the brain (23) and may synergize with (brain) or antagonize (MFP) growth-promoting functions of activated tumor cell $\alpha_v\beta_3$.

Intracranial MDA-MB-435 lesions expressed four different VEGF isoforms, including freely diffusible $VEGF_{121}$ and partially diffusible $VEGF_{165}$, the most frequent isoform in VEGF-secreting cells (15, 19). Because of the strong hypoxia in the MFP environment, we were unable to reliably define normoxic MFP tumor areas and determine VEGF expression there. However, as previously shown, over-expression of $VEGF_{121}$ in glioma cells increased angiogenesis in the brain, but not in the subcutaneous environment (24). This suggests that even though MDA-MB-435 β_3D723R tumors might express VEGF in normoxic regions in the MFP, this might not be sufficient to promote angiogenesis. Similarly, HIF-1α knockout in transformed astrocytes reduced their growth in the subcutis but promoted it in the brain (25). Thus, the inability of the mammary fat pad to support continuous, hypoxia-independent angiogenesis may be related to the nature and responsiveness of vascular development in the mammary fat pad compared with the brain.

It was previously shown that VEGF can promote breast cancer cell survival in an autocrine manner (26). However, in our model, tumor cell survival was not limiting, and we found increased proliferation but no evidence for enhanced survival of tumor cells upon $\alpha_v\beta_3$ activation in normoxic brain lesions. Integrins can signal through different growth promoting pathways, including Src and MAPK (27–30). However, we detected no significant differences in pSrc and pERK levels between β_3WT- and β_3D723R-expressing brain lesions (not shown). In fact, all of our data point to increased vascularization as the main mechanism through which activated tumor cell integrin $\alpha_v\beta_3$D723R accelerates lesion growth in the brain: increased vascular density, strongly reduced hypoxia, and formation of VEGF:VEGFR2 complex indicating an angiogenic switch. Furthermore, divergence in growth rates between β_3WT- and β_3D723R-expressing brain lesions became obvious only after the tumors reached a size at which blood supply became limiting in β_3WT tumors.

Although lesions expressing activated or non-activated $\alpha_v\beta_3$ up-regulated VEGF protein in hypoxic regions, only lesions with the activated receptor expressed elevated VEGF under normoxia. This was caused by $\alpha_v\beta_3$ activation–dependent control of VEGF at the post-transcriptional level. Our data indicate that activated $\alpha_v\beta_3$ promotes VEGF protein expression through inhibition of 4E-BP1, a repressor of mRNA translation. $\alpha_v\beta_3$ Activation in brain lesions induced phosphorylation and thereby inactivation of 4E-BP1, which is known to result in the release of eIF4E and increased translation of VEGF mRNA (21). A causal relationship between VEGF increase and 4E-BP1 inhibition in our model was provided by knock-down of 4E-BP1 in

β_3WT cells, as this resulted in increased VEGF production under normoxic conditions. Notably, under hypoxia, 4E-BP1 might exert an opposite effect on VEGF, as its over-expression has been shown to increase IRES-dependent VEGF translation (17). In the current study, however, we focused on normoxia, because increased VEGF expression resulting from $\alpha_v\beta_3$ activation occurred in normoxic brain lesions. Thus, our findings establish a link between the activation state of integrin $\alpha_v\beta_3$, regulation of translation, and angiogenesis in vivo.

Several integrins, including $\alpha_6\beta_4$, $\alpha_{IIb}\beta_3$, and $\alpha_2\beta_1$, can promote translation of weak mRNAs through the PI3K-Akt-mTOR pathway (31, 32). In contrast, activation of integrin $\alpha_v\beta_3$ did not result in enhanced activation of mTOR or Akt in brain lesions, suggesting that a different mechanism is involved. Notably, mTOR-independent phosphorylation of 4E-BP1 in breast cancer cells has been previously documented (33).

The incidence of brain metastases in tumor patients is rising. However, although therapies for primary tumors and extracranial metastases are improving, effective treatments for brain metastases are still missing (1–3). Our data define the activated, high-affinity conformer of tumor cell integrin $\alpha_v\beta_3$ as a potential new therapeutic target in brain metastasis. Moreover, our study points to the importance of the tumor microenvironment when considering different treatment options for cancer. Beyond drug accessibility, brain metastases apparently require specific targeting. Thus, information on mechanisms that promote metastatic growth in the brain as presented here can be a basis for the development of novel, effective therapies.

Materials and Methods

Tumor Cell Model. MDA-MB-435 adenocarcinoma cells were from J.E. Price (M. D. Anderson), cultured as previously described (12), and stably tagged with Firefly luciferase (*F-luc*) using a lentiviral transduction system (34). For generation of MDA-MB-435 $\beta_3$kd, β_3WT, β_3D723R, β_3-/WT, β_3-/D723R, and 4E-BP1 knock-down cells, see *SI Methods*.

Animal Experiments. Female 6- to 8-week-old CB17/SCID mice were injected with 1×10^4 *F-luc*–tagged cancer cells either stereotactically into the striatum (2.5 mm right from the midline, 2.5 mm anterior from bregma, and 3 mm deep) or into the axillary mammary fat pad and imaged once (mfp) or twice (brain) weekly using an IVIS200 bioluminescence imaging system (Xenogen). BrdU (Sigma) (1 ml of 1 mg/ml) was injected intraperitoneally at 24 hours, and Hypoxyprobe-1 (NPI) (150 μl of 10 mg/ml) intraperitoneally 60 minutes before tissue harvest. All animal work complied with National Institutes of Health and institutional guidelines (TSRI is AAALAC accredited).

For detailed protocols of immunohistochemistry, RNA, and protein expression, see *SI Methods*.

ACKNOWLEDGMENTS. This study was supported by National Institutes of Health grants CA095458 and CA112287 (to B.F.H.), CBCRP grants 12NB0176 and 13NB0180 (to B.F.H.), a UCSD NNC project grant (to B.F.H.), and fellowships from SG Komen (to M.L. and J.S.K.), and the Swedish Government to K.S.. We thank Bruce Torbet for F-*luc* expressing lentiviral constructs. Dr. Ernest Beutler, a NAS member, a leader in biomedical research and our Department Chair, contributed to this work based on numerous scientific discussions.

1. Ranasinghe MG, Sheehan JM (2007) Surgical management of brain metastases. *Neurosurg Focus* 22:E2.
2. Lin NU, Bellon JR, Winer EP (2004) CNS metastases in breast cancer. *J Clin Oncol* 22:3608–3617.
3. Weil RJ, Palmieri DC, Bronder JL, Stark AM, Steeg PS (2005) Breast cancer metastasis to the central nervous system. *Am J Pathol* 167:913–920.
4. Arias-Salgado EG, Lizano S, Shattil SJ, Ginsberg MH (2005) Specification of the direction of adhesive signaling by the integrin beta cytoplasmic domain. *J Biol Chem* 280:29699–29707.
5. Ginsberg MH, Partridge A, Shattil SJ (2005) Integrin regulation. *Curr Opin Cell Biol* 17:509–516.
6. Stupack DG (2007) The biology of integrins. *Oncology (Williston Park)* 21(9 Suppl 3):6–12.
7. Brooks PC, Clark RA, Cheresh DA (1994) Requirement of vascular integrin alpha v beta 3 for angiogenesis. *Science* 264:569–571.
8. Albelda SM, et al. (1990) Integrin distribution in malignant melanoma: association of the beta 3 subunit with tumor progression. *Cancer Res* 50:6757–6764.
9. Gingras MC, Roussel E, Bruner JM, Branch CD, Moser RP (1995) Comparison of cell adhesion molecule expression between glioblastoma multiforme and autologous normal brain tissue. *J Neuroimmunol* 57:143–153.
10. Natali PG, et al. (1997) Clinical significance of alpha(*v*)beta3 integrin and intercellular adhesion molecule-1 expression in cutaneous malignant melanoma lesions. *Cancer Res* 57:1554–1560.
11. Pignatelli M, Cardillo MR, Hanby A, Stamp GW (1992) Integrins and their accessory adhesion molecules in mammary carcinomas: loss of polarization in poorly differentiated tumors. *Hum Pathol* 23:1159–1166.
12. Felding-Habermann B, et al. (2001) Integrin activation controls metastasis in human breast cancer. *Proc Natl Acad Sci USA* 98:1853–1858.
13. Hughes PE, et al. (1996) Breaking the integrin hinge. A defined structural constraint regulates integrin signaling. *J Biol Chem* 271:6571–6574.
14. Bergers G, et al. (2000) Matrix metalloproteinase-9 triggers the angiogenic switch during carcinogenesis. *Nat Cell Biol* 2:737–744.
15. Karamysheva AF (2008) Mechanisms of angiogenesis. *Biochemistry (Mosc)* 73:751–762.
16. Kunz M, Ibrahim SM (2003) Molecular responses to hypoxia in tumor cells. *Mol Cancer* 2:23.
17. Braunstein S, et al. (2007) A hypoxia-controlled cap-dependent to cap-independent translation switch in breast cancer. *Mol Cell* 28:501–512.
18. Gray MJ, et al. (2005) HIF-1alpha, STAT3, CBP/p300 and Ref-1/APE are components of a transcriptional complex that regulates Src-dependent hypoxia-induced expression of VEGF in pancreatic and prostate carcinomas. *Oncogene* 24:3110–3120.
19. Kevil CG, et al. (1996) Translational regulation of vascular permeability factor by eukaryotic initiation factor 4E: Implications for tumor angiogenesis. *Int J Cancer* 65:785–790.
20. Zygalaki E, et al. (2005) Real-time reverse transcription-PCR quantification of vascular endothelial growth factor splice variants. *Clin Chem* 51:1518–1520.
21. De Benedetti A, Harris AL (1999) eIF4E expression in tumors: its possible role in progression of malignancies. *Int J Biochem Cell Biol* 31:59–72.
22. Sonenberg N, Gingras AC (1998) The mRNA 5′ cap-binding protein eIF4E and control of cell growth. *Curr Opin Cell Biol* 10:268–275.
23. Witz IP (2008) Tumor-microenvironment interactions: Dangerous liaisons. *Adv* Cancer Res 100:203–229.
24. Guo P, et al. (2001) Vascular endothelial growth factor isoforms display distinct activities in promoting tumor angiogenesis at different anatomic sites. *Cancer Res* 61:8569–8577.
25. Blouw B, et al. (2003) The hypoxic response of tumors is dependent on their microenvironment. *Cancer Cell* 4:133–146.
26. Bachelder RE, et al. (2001) Vascular endothelial growth factor is an autocrine survival factor for neuropilin-expressing breast carcinoma cells. *Cancer Res* 61:5736–5740.
27. Huveneers S, et al. (2007) Integrin alpha v beta 3 controls activity and oncogenic potential of primed c-Src. *Cancer Res* 67:2693–2700.
28. Meier F, et al. (2005) The RAS/RAF/MEK/ERK and PI3K/AKT signaling pathways present molecular targets for the effective treatment of advanced melanoma. *Front Biosci* 10:2986–3001.
29. Vellon L, Menendez JA, Lupu R (2006) A bidirectional ''alpha (v) beta(3) integrin-ERK1/ERK2 MAPK'' connection regulates the proliferation of breast cancer cells. *Mol Carcinog* 45:795–804.
30. Illario M, et al. (2005) Fibronectin-induced proliferation in thyroid cells is mediated by alphavbeta3 integrin through Ras/Raf-1/MEK/ERK and calcium/CaMKII signals. *J Clin Endocrinol Metab* 90:2865–2873.
31. Chung J, Bachelder RE, Lipscomb EA, Shaw LM, Mercurio AM (2002) Integrin (alpha 6 beta 4) regulation of eIF-4E activity and VEGF translation: a survival mechanism for carcinoma cells. *J Cell Biol* 158:165–174.
32. Pabla R, et al. (1999) Integrin-dependent control of translation: engagement of integrin alphaIIbbeta3 regulates synthesis of proteins in activated human platelets. *J Cell Biol* 144:175–184.
33. Avdulov S, et al. (2004) Activation of translation complex eIF4F is essential for the genesis and maintenance of the malignant phenotype in human mammary epithelial cells. *Cancer Cell* 5:553–563.
34. Chen EI, et al. (2007) Adaptation of energy metabolism in breast cancer brain metastases. *Cancer Res* 67:1472–1486.
35. Felding-Habermann B, Habermann R, Saldivar E, Ruggeri ZM (1996) Role of beta3 integrins in melanoma cell adhesion to activated platelets under flow. *J Biol Chem* 271:5892–5900.

Chapter 16

Maintaining and Engineering Neural Stem Cells for Delivery of Genetically Encoded Therapy to Brain Tumors

Jennifer Katz, Joseph Krueger, Brunhilde Felding-Habermann, and Evan Y. Snyder

Summary

Despite advances for the treatment of cancer, the prognosis for patients suffering from malignant brain tumors remains dismal. High-grade neoplasms, such as gliomas, are highly invasive and spawn widely disseminated microsatellites that have limited the efficacy of surgical and adjunctive therapies. The cancer stem cell hypothesis suggests that conventional chemotherapeutic treatments kill differentiated and differentiating cells which often form the bulk of the tumor. One major concern is that the cells which give rise to the tumor, the cancer stem cells, remain untouched and may be responsible for a relapse of the disease. Therefore, an adjunctive therapy to current cancer treatment is critical for the survivability of patients suffering from brain tumors. We have successfully engineered tumor-tropic neural stem cells to deliver antineoplastic gene products directly to the tumor-producing cells. This potential therapeutic strategy may safely eradicate tumor-producing cells in the brain while minimizing damage to normal, healthy cells.

Key words: Neural stem cells, Gene therapy, Brain tumors, Viral constructs, Transfection, Lentiviral transduction

1. Introduction

The neural stem cell began receiving attention once scientists recognized that it was a primordial self-renewing cell that can give rise to neurons, astrocytes, and oligodendroglia of the mature nervous system. Since neural stem cells can be isolated, expanded in culture and then reimplanted, the potential that neural stem cells hold as therapeutic agents for a variety of neuropathological conditions is promising *(1)*. Furthermore, it has previously

John S. Yu (ed.), *Cancer Stem Cells,* Methods in Molecular Biology, vol. 568
DOI 10.1007/978-1-59745-280-9_16,

been reported that neural stem cells administered intracranially, migrate to and infiltrate experimental orthotopic primary brain tumors and deliver therapeutic agents that successfully inhibit tumor growth *(2, 3)*.

The protocol outlined in this chapter describes techniques that modify the cellular genome of murine neural stem cells for gene delivery approaches in brain tumor therapy. It is important to note, however, that stem cells isolated from origins other than mouse or the neuroectoderm have also been genetically modified to produce molecules of therapeutic value *(4–6)*. The transduction techniques summarized later are not specific for neural stem cells and may be performed on a variety of mammalian cell lines. However, due to the capacity of neural stem cells to differentiate in vivo following transplantation, as well as their ability to home toward brain tumors and track migrating tumor cells, the neural stem cell ;may be the optimal vehicle for delivery of genetically encoded therapy in the CNS *(3)*. Neural stem cells have been successfully engineered to deliver a variety of therapeutically relevant molecules, such as prodrug-converting enzymes *(3, 6, 7)* (e.g., cytosine deaminase, carboxylesterase, HSV-TK) or bioactive genes, including interleukin-12 *(8, 9)* and TRAIL *(10)*. Still, it is up to the user to determine the optimal stem cell source and therapeutic gene for their study.

The final step in generating a therapeutically useful neural stem cell line is to create neural stem cells that express the therapeutic protein. Modern retroviral and lentiviral transduction has dramatically improved the efficiency and stability of vector-based expression over traditional expression vectors and transfection techniques. In this regard, lentivirus is far more efficient at transducing mammalian cells than retrovirus due to its ability to infect both proliferative and nonproliferative cells, as well as its ability to infect each cell multiple times (multiplicity of infection [MOI]). The HIV-1-derived self-inactivating lentiviral constructs have proven to be useful for high-efficiency transfection of a variety of cell types *(11)*. Nonconcentrated viral preparations often give a rate of transduction approaching 100%, with high MOI, allowing sufficient expression of a therapeutic protein of interest (POI) *(12)*. The expression of this protein can be controlled under constitutive (cytomegalovirus [CMV]), ligand-activated (tetracycline-on/off), strong or weak and lineage-specific promoters; giving the user the desired control overexpression of the POI. The use of lentivirus ensures homogeneity in the transduced cells, without the need for clonal selection techniques that may introduce artifacts into the system. Beyond this, good lentiviral transduction eliminates the need for an antibiotic selection step, considerably decreasing the amount of time and effort required to generate a useful neural stem cell line.

2. Materials

2.1. Maintenance of Neural Stem Cells

1. Neural stem cell medium: Dulbecco's Modified Eagle's Medium + GlutaMax (DMEM) containing 10% fetal bovine serum (FBS), 5% inactivated horse serum, and 1% penicillin–streptomycin; store at 4°C.
2. 1× Dulbecco's Phosphate-Buffered Saline without calcium & magnesium.
3. 0.05% trypsin–ethylenediamine tetraacetic acid (EDTA); store at –20°C.
4. Sterile DMSO.
5. Falcon tissue-culture-treated dishes.
6. Cryogenic vials.

2.2. Producing Lentivirus in HEK 293T Cells

1. 0.1× TE buffer: 1 mM tris of pH 8.0, 100 μM EDTA of pH 8.0. Make stock buffer as 1× TE (10 mM tris of pH 8.0, 1 mM EDTA of pH 8.0). Sterile filter through a 0.22-μM filter; store at room temperature.
2. 2.5 M $CaCl_2$ in H_2O. Sterile filter through a 0.22-μM filter; store at –20°C.
3. 2× HBS: 281 mM NaCl, 100 mM Hepes, 1.5 mM Na_2HPO_4, pH 7.12. Sterile filter through a 0.22-μM filter; store at –20°C.
4. 293T medium: DMEM containing 5% FBS, 4 mM L-Glutamine, 1 mM MEM Sodium Pyruvate, 0.1 mM MEM Nonessential Amino Acids, and 1% penicillin–streptomycin.

2.3. Titering Your Lentiviral Stock

1. 293T medium: DMEM containing 5% FBS, 4 mM L-Glutamine, 1 mM MEM Sodium Pyruvate, 0.1 mM MEM Nonessential Amino Acids, and 1% penicillin–streptomycin.
2. Your lentiviral supernatant.
3. 6 mg/mL Polybrene® in H_2O.

2.4. Transduction of Cells

1. Your lentiviral supernatant (store at –80°C until use).
2. Mammalian cell line of choice (e.g., neural stem cells).
3. Complete culture medium for your cell line.
4. 6 mg/mL Polybrene in H_2O.
5. Appropriately sized tissue culture plates for your application.
6. Selection agent (if selecting for stably transduced cells).

3. Methods

Maintenance of Neural Stem Cells. Neural stem cell cultures should be maintained in a standard humidified incubator (37°C, 5% CO_2). Once the lines are established they can be carried in 10-cm tissue-culture-treated dishes. It is important to split cell lines only once a week at no more than a 1:10 dilution. Neural stem cells are contact inhibited and therefore cultures can become confluent during normal growth periods. However, there are some general guidelines to consider before proceeding with transplantation or injection of neural stem cells. When working with cells that have been previously frozen, do not use those that have been passaged for more than 6 weeks after the initial thaw. Cultures should be no more than 90% confluent, or they will begin to produce an extracellular matrix causing clumping of cells and yielding poor results. If cells do not appear as a single-cell suspension then they should not be used for in vivo experiments. The proper confluence can be maintained by splitting cultures at a dilution of 1:10 72–96 h before transplantation or injection. It is important to plate cells during the last split for immunocytochemical analysis to confirm undifferentiated state at the time of use.

Considerations for Choice of Viral Constructs. The general backbone for HIV-1-derived lentiviral constructs contains flanking HIV-1 long terminal repeats, (delta U3) regions for self-inactivation, and a (R region) polyadenylation signal ***(13)***. Commercially available and privately generated HIV-1-based lentiviral vectors are similar in this manner; however, the addition of several elements to the viral backbone can improve stability and expression in transduced cells. These include the addition of the IFN-beta scaffold attachment region to increase expression, the central polypurine tract to facilitate nuclear import, and the woodchuck hepatitis virus posttranslational regulatory element to stabilize the mRNA ***(14)***. These additional elements may be integrated into the lentiviral vector you plan to use, and improve the expression of the POI and thus therapeutic potential when arming stem cells.

The choice of promoter should also be considered when choosing a lentiviral construct. Typically, the CMV promoter is used for its strong induction of transcription and usefulness in a wide variety of neural cell types ***(15)***. However, this strong promoting activity can possibly lead to toxicity through an overabundance of expressed protein. The use of a weaker promoter, such as the myeloproliferative sarcoma virus long terminal repeat negative control region deleted (MND promoter), allows sufficient expression in some cell types at a level lower than the CMV promoter ***(15)***. Alternatively, the use of the Ubiquitin promoter

has been proven to be effective for use in both human and murine cells *(16)*. Other lineage-specific neural promoters may be used if appropriate for the experiment planned.

For in vitro and in vivo studies, the ability to efficiently track the stem cells during the studied processes is critical. Thus, the lentiviral vector must contain a genetic tag for following the cells in live animals or fixed tissues *(17)*. For this, an arsenal of proteins that are detected in live or fixed cells through direct, substrate-based, or immunohistochemical means are available. For in vivo and in vitro tracking of live cells, choose fluorescent proteins such as GFP, YFP, CFP, etc. and bioluminescent proteins such as Firefly and Renilla luciferase. In fixed tissues, enzymatic reporters such as B-galactosidase and Alkaline Phosphatase are sensitive means to detect cells. Epitope tags such as the myc tag (myc), hemagglutin (HA), or histidine (HIS) tag fused to the POI are a good alternative for fixed tissues and cells. Any of these proteins or tags listed can be detected through typical antibody approaches. The genetic tag can either be present on the same expression vector as your POI, or otherwise independently expressed. In the latter case, using a different virus stock to label the cells from the stock used to force expression of your POI is suitable. However, modified lentiviral vectors that incorporate the internal ribosome excision sequence (IRES) allow simultaneous expression of both POI and reporter. Here, the IRES is sandwiched between the POI gene and reporter gene; thus, transcription of both proteins is driven by the same promoter. In this way, the delivery of the therapeutic protein and detection of the stem cells can occur with only one transduction.

3.1. Producing Lentivirus in 293T Cells

This procedure is to generate viral supernatant. Generally, this is sufficient for transfection of most cells. This protocol uses $CaCl_2$ precipitation for transfection of two 10-cm plates. Transformed Human Embryonic Kidney (HEK293T; 293T) cells are used for viral packaging. The actual construction of your packaging and expression constructs varies, so specific amounts mentioned in this protocol may vary. However, this protocol is fairly robust and should work for most types of lentiviral systems.

3.1.1. Day 1: Plating

1. Treat 10-cm plates with poly-L-lysine for 15 min at room temperature (50 μg/mL final)
2. Plate out 2×10^6 cells in 10 mL complete DMEM.
3. Grow overnight in 5% CO_2.

3.1.2. Day 2: Transfection

Generation of the lentivirus must be performed in a biosafety level 3 (BSL-3) facility. Make sure to follow your institutional guidelines.

1. In a laminar flow hood, using sterile tubes (FACS tubes are ideal), place packaging plasmids (13 μg GAG/POL, 7 μg VSV-G, 5 μg REV) and 10 μg lentiviral expression vector in 900 μL 0.1× TE. Make sure to dilute plasmids in sterile H_2O to appropriate volume and add 1× TE to make 0.1× TE.
2. Add 100 μL $CaCl_2$ solution, and vortex.
3. Add 1 mL of 2× HBS dropwise to tube, mixing slightly during this process.
4. Immediately add this solution dropwise onto the plate, spreading it out over the plate, gently swirling the plate as you add the solution.
5. Place cells into 5% CO_2 overnight (16 h).

3.1.3. Days 3–4: Viral Production

1. The next morning, change the media (use 10 mL). Note that the VSV G glycoprotein can cause 293T cells to fuse. They can appear as large, multinucleated cells (syncytia). This does not affect production of the lentivirus.
2. Grow 30–36 h, and then collect the media. Sterile filter (0.22 μM) and aliquot the supernatant into 1-mL aliquots. This supernatant is ready to use. Store virus aliquots at –80°C.

(Alternatively)

Harvest the viral supernatants up to 48 h posttransfection (Day 4).

(Alternatively)

After first supernatant harvest at 30–36 h, add 10 mL fresh media and collect new viral supernatant at 72 h. The viral yield for this collection will be substantially lower.

Caution: Remember that you are working with a nonreplicating, yet infectious, virus when you handle the supernatant. Use the appropriate precautions (BSL-2 precautions are recommended – follow your institutional guidelines).

3.2. Titering Your Lentiviral Stock

To easily perform a viral titer, a marker is needed to identify cells which have virus. In general, serial dilutions of the virus are made and the cells transduced. The marker is analyzed and the percentage of cells which express the marker is used to determine the titer. For this purpose, green fluorescent protein (GFP) is highly recommended due to the ability to quantitatively determine transduction efficiency using FACS analysis.

This protocol serves two purposes: To find the viral titer, and find the right concentration of virus to use if you wish to obtain an MOI of 1.0. Too much virus will give greater MOIs, which is good for protein expression but may cause toxicity.

1. Prepare tenfold serial dilutions ranging from 1×10^2 to 1×10^6 in 1 mL of culture media. You may prepare a wider range of serial dilutions (up to 1×10^{10}) if desired. Mix each dilution gently by inversion.

2. Follow the normal transduction protocol described later, using the entire 1-mL dilution.
3. Assay the cells for transduction efficiency. The lowest dilution that efficiently transduces all the cells (less than 5% nontransduced) is used to calculate the titer; any higher titration will result in an MOI greater than 1.
4. The exact MOI of 1.0 can be found between the tenfold dilution that leaves significant (more than 5%) nontransduced cells and the tenfold dilution that transduces all the cells. If desired, you may narrow this range down further by performing twofold dilutions in this range to find the exact MOI of 1.0. Keep in mind that there is a range of efficiencies in each transfection, and a calculated MOI of about 1.2 should be used to a practical MOI of 1.0.

3.2.1. Troubleshooting

If no or poor transduction efficiency is observed, perform the following diagnostics in this order:

1. Verify that your expression construct is correct (i.e., the gene is present, in frame, and not truncated or mutated).
2. Verify that your packaging plasmids are correct.
3. Verify your viral titer using an established reporter virus. Problems with virus production is usually a result of problems transfecting the packaging cells. The $CaCl_2$ transfection method is robust, but can be faulty if the HBSS is added improperly. If desired, switch to a lipid-based transfection technique.
4. If all the above are correct, consider the design of your expression construct. The use of the CMV promoter is not always appropriate. For example, the CMV promoter does not result in significant transcription in many stem cell types and murine cells. Consider a different promoter such as the Ubiquitin promoter.
5. Concentrate your virus if everything else seems fine (see the following section).

3.3. Concentration of Virus

Concentrating of virus is usually not necessary for in vitro transduction. One simple way to increase the concentration of virus for in vitro transduction is to simply use one-half of the media (5 mL instead of 10 mL) during viral production. However, if you plan to use the virus for in vivo transduction, you most often need a very concentrated virus. To accomplish this, simply centrifuge your viral supernatant at 50,000×*g* for 90 min. Carefully decant the supernatant and resuspend the viral pellet in 100 μL-1 mL of plain media (without FBS, etc.) or PBS.

3.4. Thawing Neural Stem Cell Lines

1. Thaw a frozen vial by placing the vial in a water bath maintained at a temperature of 37°C for 1–2 min. Do not agitate cells.
2. Remove the vial from the water bath as soon as the cells have thawed and decontaminate by wiping the vial down with 70% ethanol (*see* **Note 1**).
3. Pipet the contents of the vial (approximately 1–2 × 10^6 cells/vial) equally into one 10-cm dish containing 8 mL of prewarmed feeding medium.
4. Rinse the vial two times with 1 mL feeding medium and transfer to the dish.
5. Gently swirl each dish to evenly distribute cells.
6. Place dishes into the incubator.
7. Change the medium once the cells have attached to the plate (approximately 8 h).
8. Once cells have become confluent they can be trypsinized and gradually expanded as described in the next step.

3.5. Maintaining Neural Stem Cell Lines

1. Remove and discard culture medium by aspiration (*see* **Note 2**).
2. Rinse cell layer twice with 1× PBS (5 mL/10 cm dish) to remove all traces of serum.
3. Add 2 mL of 0.05% Trypsin–EDTA solution to the dish and incubate at 37°C for 2–5 min, then observe cells under an inverted microscope until cell layer is dispersed. (The serum in the medium deactivates the Trypsin–EDTA, so this is a crucial step that should not be left out). The dish can be gently tapped to help the cells detach. Cells that are difficult to detach can be placed back in the incubator for an additional 1–2 min.
4. Add 3 mL of feeding medium and aspirate cells by gently pipetting. Be careful not to introduce air bubbles while triturating.
5. Transfer 1 mL of the total 5 mL in the 10-cm dish equally (0.5 mL/dish) to two new 10-cm dishes containing 10 mL of prewarmed feeding medium. This should be done in a dropwise manner to ensure that each dish receives 10% of the original population. Fresh media can be added to the original dish so that the cells will reattach and proliferate as a backup should the split be unsuccessful.

3.6. Transduction of Neural Stem Cells

1. Day 1: The day before transduction, detach and count the cells, plating them in a six-well plate so they will be 40–60% confluent at the time of transduction. This is typically 2 × 10^5 cells per well. Make sure there is 1.5 mL of media in each well. Incubate cells per their normal growth conditions overnight.

2. Day 2: On the day of transduction, add 1 μL of 6 mg/mL (final concentration of 6 μ;g/mL) Polybrene to your cells. Swirl gently to mix. For high transduction efficiency and high MOI, simply add 500 μL of your thawed lentiviral supernatant to the media. Swirl gently to mix. Incubate cells per their normal growth conditions overnight (*see* **Note 3**). If you wish to more precisely transduce cells with low MOI, you will have to perform a viral titer (see prior section).
3. Day 3: The following day remove the media containing virus and replace it with 2 mL of complete culture medium. Aspirate this media and replace it two more times to remove any excess virus. Incubate cells per their normal growth conditions overnight, then passage and expand or harvest cells for expression analysis (*see* **Note 4**).

3.7. Preparing Neural Stem Cells for Transplantation or Injection

1. Remove and discard culture medium from dish.
2. Rinse cell layer twice with 1× PBS (5 mL/10-cm dish) to remove all traces of serum.
3. Add 2 mL of 0.05% Trypsin–EDTA solution to the dish and incubate at 37°C for 2–5 min, then observe cells under an inverted microscope until cell layer is dispersed.
4. Add 3 mL of feeding medium and aspirate cells by gently pipetting. Be careful not to introduce air bubbles while triturating.
5. Pipet cells into a 15-mL tube and centrifuge for 1 min at 1,000×*g*.
6. Remove supernatant by aspiration being careful to not disturb the cellular pellet.
7. Wash the cells by resuspending them in 10 mL of 1× PBS and gently triturate to form a single-cell suspension.
8. Centrifuge for 1 min at 1,000×*g*.
9. Repeat **steps 7** and **8**.
10. After the last spin, remove the supernatant by aspiration and resuspend the pellet in 10 mL of 1× PBS and gently triturate cells. Take 10 μL of cell solution and count the number of cells.
11. Centrifuge the cell solution at 1,000×*g* and resuspend the pellet in the appropriate volume of 1× PBS at a concentration of 4×10^4 cells/μL.
12. Place cells on ice until ready to use (*see* **Note 5**).

3.8. Freezing Neural Stem Cells

1. Make freezing medium (e.g., 67% feeding medium + 20% FBS and filter; add 13% sterile DMSO).
2. Remove and discard culture medium from dish.

3. Rinse cell layer twice with 1× PBS (5 mL/10-cm dish) to remove all traces of serum.
4. Add 2 mL of 0.05% Trypsin–EDTA solution to the dish and incubate at 37°C for 2–5 min, then observe cells under an inverted microscope until cell layer is dispersed. Cells that are difficult to detach can be placed back in the incubator for an additional 1–2 min.
5. Add 3 mL of freezing medium and aspirate cells by gently pipetting. Be careful not to introduce air bubbles while triturating.
6. Pipet an equal volume of cells into cryogenic vials (approximately $1–2 \times 10^6$ cells per 1 mL).
7. Slow freeze cells by first placing vials of cells at –80°C for 24 h. Transfer the vials to –140°C for long-term storage.

4. Notes

1. All protocols involving neural stem cells should be carried out under aseptic conditions in the hood.
2. Volumes used in this protocol for neural stem cell culture are intended to be used with 10-cm dishes. Be sure to reduce or increase proportionally the amount of solutions for culture dishes of other sizes.
3. Transduction rates approaching 100% are typical of this protocol. However, depending on your cells, the POI expressed, and the viral titer some variability may occur. If you have a low yield of transduction, follow the troubleshooting steps outlined in the "titering your lentiviral stock" section.
4. If you are transducing cells with untitered viral supernatant and are concerned about possible toxicity, it is possible to incubate cells for as little as 6 h prior to changing the medium. However, typically little or no toxicity is observed.
5. Prior to transplantation or injection, cells can be maintained on ice for 2–3 h.

Acknowledgments

This work was supported by a Susan G. Komen Breast Cancer Foundation grant PDF0403205 and a CBCRP grant12IB-0122 to B. Felding-Habermann in consortium with EY Snyder.

References

1. Snyder, EY., Deichter, DL., Walsh, C., Arnold-Aldea, S., Hartweig, EA., and Cepko, CL. Multipotent neural cell lines can engraft and participate in development of mouse cerebellum. Cell, 68: 33–51, 1992.
2. Yip, S., Aboody, KS., Burns, M., Imitola, J., Boockvar, JA., Allport, J., Park, KI., Teng, YD., Lachyankar, M., McIntosh, T., O'Rourke, DM., Khoury, S., Weissleder, R., Black, PM., Weiss, W., and Snyder, EY. Neural stem cell biology may be well suited for improving brain tumor therapies. Cancer J., 9: 189–204, 2003.
3. Aboody, KS., Brown, A., Rainov, NG., Bower, KA., Liu, S., Yang, W., Small, JE., Herrlinger, U., Ourednik, V., Black, PM., Breakefield, XO., and Snyder, EY. Neural stem cells display extensive tropism for pathology in adult brain: evidence from intracranial gliomas. Proc. Natl. Acad. Sci. USA., 97: 12846–12851, 2000.
4. Elzaouk, L., Moelling, K., and Pavlovic, J. Anti-tumor activity of mesenchymal stem cells producing IL-12 in a mouse melanoma model. Exp. Dermatology, 15: 865–874, 2006.
5. Song, K., Benhaga N., Anderson, RL., and Khosravi-Far, R. Transduction of tumor-necrosis factor-related apoptosis-inducing ligand into hematopoietic cells leads to inhibition of syngeneic tumor growth in vivo. Cancer Res., 66(12): 6304–6311, 2006.
6. Kim, SK., Kim, SU., Park, IH., Bang, JH., Aboody, KS., Wang, KC., Cho, BK., Kim, M., Menon, LG., Black, PM., and Carroll, RS. Human neural stem cells target experimental intracranial medulloblastoma and deliver a therapeutic gene leading to tumor regression. Clin Cancer Res., 12(18): 5550–5556, 2006.
7. Aboody, KS., Najbauer, J., Schmidt, NO., Yang, W., Wu, JK., Zhuge, Y., Przylecki, W., Carroll, R., Black, PM., and Perides, G. Targeting of melanoma brain metastases using engineered neural stem/progenitor cells. Neuro-Oncol., 8(2): 119–126, 2005.
8. Ehtesham, M., Kabos, P., Kabosova, A., Neuman, T., Black, KL., and Yu, JS. The use of interleukin 12-secreting neural stem cells for the treatment of intracranial glioma. Cancer Res., 62(20): 5657–5663, 2002.
9. Yang, YS., Hiu, L. and Zhang, JN. Gene therapy of rat malignant gliomas using neural stem cells expressing IL-12. DNA Cell Biol., 23(6): 381–389, 2004.
10. Ehtesham, M., Kabos, P., Guitierrez, MA., Chung, NH., Griffith, TS., Black, KL., and Yu, JS. Induction of glioblastoma apoptosis using neural stem cell-mediated delivery of tumor necrosis factor-related apoptosis-inducing ligand. Cancer Res., 62(24): 7170–7174, 2002.
11. Logan, AC., Haas, DL., Kafri, T., and Kohn, DB. Integrated self-inactivating lentiviral vectors produce full-length genomic transcripts competent for encapsidation and integration. J. Virol., 78: 8421–8436, 2004.
12. Logan, AC., Nightingale, SJ., Haas, DL., Cho, GJ., Pepper, KA., and Kohn, DB. Factors influencing the titer and infectivity of lentiviral vectors. Hum. Gene Ther., 15: 976–988, 2004.
13. Miyoshi, H., Smith, KA., Mosier, DE., Verma, IM., and Torbett, BE. Transduction of human CD34+ cells that mediate long-term engraftment of NOD/SCID mice by HIV vectors. Science, 283: 682–686, 1999.
14. Logan, AC., Lutzko, C., and Kohn, DB. Advances in lentiviral vector design for gene-modification of hematopoietic stem cells. Curr. Opin. Biotechnol., 13: 429–436, 2002.
15. Van Damme, A., Thorrez, L., Ma, L., Vandenburgh, H., Eyckmans, J., Dell'Accio, F., De Bari, C., Luyten, F., Lillicrap, D., Collen, D., VandenDriessche, T., and Chuah, MK. Efficient lentiviral transduction and improved engraftment of human bone marrow mesenchymal cells. Stem Cells, 24: 896–907, 2006.
16. Schorpp, M., Jager, R., Schellander, K., Schenkel, J., Wagner, EF., Weiher, H., and Angel, P. The human ubiquitin C promoter directs high ubiquitous expression of transgenes in mice. Nucleic Acids Res., 24: 1787–1788, 1996.
17. Torbett, BE. Reporter genes: too much of a good thing? J. Gene Med., 4: 478–479, 2002.

Capturing changes in the brain microenvironment during initial steps of breast cancer brain metastasis

Mihaela Lorger and Brunhilde Felding-Habermann

Department of Molecular and Experimental Medicine, The Scripps Research Institute,

10550 North Torrey Pines Road, MEM-150, La Jolla, CA 92037

Running head: Early host responses to brain metastasis
Suggested Categories: Tumorigenesis and neoplastic progression
Sources of support: Postdoctoral fellowship from the Susan G. Komen Breast Cancer Foundation PDF0707935 (to M.L.), National Institutes of Health grants CA095458 and CA112287 (to B.F.H.), CBCRP grants 12NB0176 and 13NB0180 (to B.F.H.) and DOD grant W81XWH-08-1-0468 (to B.F.H.)
Corresponding authors: Brunhilde Felding-Habermann and Mihaela Lorger, Department of Molecular and Experimental Medicine, The Scripps Research Institute, 10550 North Torrey Pines Road, MEM-150, La Jolla, CA 92037; phone: 858 784 2021, 858 784 2670; e-mail: brunie@scripps.edu, mlorger@scripps.edu

Abstract

Brain metastases are difficult to treat and mostly develop late during progressive metastatic disease. Patients at risk would benefit from the development of prevention and improved treatments. This requires knowledge of the initial events that lead to brain metastasis. The present study reveals cellular events during the initiation of brain metastasis by breast cancer cells and documents the earliest host responses to incoming cancer cells after carotid artery injection in immune deficient and immune competent mouse models. Our findings capture and characterize heterogeneous astrocytic and microglial reactions to the arrest and extravasation of cancer cells in the brain, showing immediate and drastic changes in the brain microenvironment upon arrival of individual cancer cells. We identified reactive astrocytes as the most active host cell population that immediately localizes to individual invading tumor cells and continuously associates with growing metastatic lesions. Up-regulation of MMP-9 associated with astrocyte activation in the immediate vicinity of extravasating cancer cells might support their progression. Early involvement of different host cell types indicates environmental clues that might co-determine whether a single cancer cell progresses to macrometastasis or remains dormant. Thus, information on the initial interplay between brain homing tumor cells and reactive host cells may help develop strategies for prevention and treatment of symptomatic breast cancer brain metastases.

Introduction

Brain metastases are diagnosed in 10 to 40% of all cancer patients, and the incidence is rising as patients live longer due to improved treatments for extracranial metastases[1, 2]. Brain lesions are most frequently associated with lung cancer, breast cancer, and melanoma[1, 2]. Unfortunately, brain metastases are still very difficult to treat and the mechanisms underlying their establishment and progression are poorly understood. Thus, information in this direction and models for analysis are a prerequisite for the development of new, efficient therapies.

The essential role of the tumor microenvironment in cancer progression has been well documented for extracranial malignancies, and recent findings indicate that the tumor microenvironment might be a suitable target in anti-cancer therapies, as well as a valuable biomarker for prognostic purposes[3-5]. The brain provides a unique environment with paracrine growth factors that differ from most other organs[6, 7]. The involvement of brain-resident cells including brain endothelial cells, microglia and astrocytes in the pathology of primary and metastatic brain tumors is only partially understood. Brain endothelial cells are the first host cell type that circulating cancer cells encounter when they arrest within the brain microvasculature. In addition to posing the initial barrier for brain invasion, endothelial cells and their basement membrane seem to play important roles in supporting the growth of brain metastases as well as brain tumor stem cells[8-10]. So far, only few studies documented cancer cell arrest and extravasation in the brain *in vivo*[11-13]. Once incoming cancer cells begin to infiltrate the brain tissue, they encounter a number of host cell types that may respond to their arrival. Microglia constitute the tissue macrophages of the central nervous system and are the main responders to primary brain tumors. Activated microglia can be frequently found in the vicinity of brain lesions[14-18] and the inhibition of microglial activation has been shown to significantly reduce glioma proliferation[14]. Microglia secrete multiple cytokines, growth factors and enzymes that can directly or indirectly lead to immunosuppression, angiogenesis, tumor proliferation and invasion[15, 17, 19, 20]. In contrast to these cancer promoting effects however, microglia has also been reported to elicit cytotoxicity towards lung cancer brain metastases[21]. Thus, microglial cells seem to play diverse roles in cancer progression, which might be related to their heterogeneity and distinct stages of activation. In addition to microglia, reactive astrocytes have been frequently observed in the vicinity of primary and metastatic brain tumors in animal models, as well as in human patients[6, 15, 22]. Astrocytes were shown to support brain tumor growth by secretion of cytokines, heparanase and neurotrophic factors such as TGF-α, CXCL12, S1P and GDNF[17, 23-25]. Furthermore, an immortalized astrocyte cell line has been recently shown to promote cell division and survival in lung adenocarcinoma cells *in vitro*[26].

While the microenvironment of established brain tumors has been intensively studied, the induction of changes in the brain during the initial steps of cancer cell invasion from the blood stream has not been previously described. This is probably due to challenges in the establishment of specialized animal models and techniques that allow efficient and detailed analysis of these early time-points. However, an understanding of early events in particular is essential for the development of preventive therapies, which are urgently needed. Breast cancer brain metastases are thought to develop at a late stage of progressive metastatic disease and ultimately fail to respond to treatment. Therefore, effective therapies for prevention could be life saving for patients who are at risk for developing brain lesions.

In the present study, we analyzed the brain microenvironment during the initiation of hematogenous breast cancer brain metastasis, using animal models that allowed us to capture the involvement of different brain-resident cells in this process. We found that cancer cells extravasated exclusively from capillaries. In some cell lines this step preceded their proliferation and establishment of metastatic foci, while other cell lines began to proliferate within the brain microvasculature. However, the timing between tumor cell arrest and extravasation was always the same and required several days. Thus, survival of arrested cancer cells within brain capillaries might be a rate-limiting step in metastatic progression. This might be true specifically for the brain, since cancer cell penetration of the vessel wall in the brain is much slower than in other organs[13, 27]. Strikingly, arrest of individual tumor cells in brain capillaries induced diverse astrocytic and microglial responses, even before the tumor cells extravasated. These responses resulted in heterogeneous local changes of the initial tumor microenvironment. We speculate that these changes might influence the fate of individual cancer cells, promoting or restricting their progression into macrometastases. In the future, our models should enable detailed *in vivo* analyses of these early interactions and contribute to the development of preventive therapeutic approaches that target early host responses within the brain microenvironment. Such strategies may hold particular promise since cancer cells may constantly change their phenotype due to genetic instability, in contrast to the more stable host microenvironment. Thus, microenvironment-based therapies might find broader application for different cancer types and affect different stages of progression.

Materials and Methods

In-vivo mouse models, bioluminescence imaging, and tissue preparation

MDA-MB-435, MDA-MB-231, MDA-MB-231/brain[28], 4T1, and MCF-7 cells were grown in EMEM supplemented with non-essential amino acids, vitamin mix, L-glutamin, pyruvate and 10% serum. 4T1 cells were stably transduced with lentiviral GFP-expressing vector to enable their detection by immunofluorescence. For *in vivo* imaging, all tumor cell lines were stably transduced with Firefly luciferase (F-luc) in a lentiviral construct[29]. F-luc tagged cancer cells (10^4, $2x10^4$ and/or 10^5) were injected into the left internal carotid artery of female BALB/c mice (4T1 cells) or CB17/SCID mice (all other cell lines) in EMEM without supplements in a total volume of 50 µl. For surgery, mice were anesthesized with isofluorane. To detect hypoxia, Hypoxyprobe (NPI) (150 µL of 10 mg/mL i.p.) was injected into the animals 45 minutes prior to tissue harvest. The surgery protocol and all animal work were approved by the institutional animal care and use committee (AAALAC accredited).

Tumor cell arrest and growth within the brain tissue were monitored by repeated non-invasive bioluminescence imaging using an IVIS 200 system (Xenogen, Alameda, CA) after luciferin injection (i.p.). On day 1, 2, 3, 5, 7, 10 and 50 - 70 post tumor cell injection, brain tissue was harvested after perfusing deeply anesthesized animals with 20 ml 0.9% NaCl, followed by 20 ml 4% paraformaldehyde (PFA) in PBS. Isolated brain tissue was post-fixed in 4% PFA for 4 to 8 hours at 4ºC, then incubated in 25% sucrose / 0.1M sodium phosphate buffer at 4ºC over night, and snap-frozen on dry ice. Brains were cut entirely into 30 µm cryosections, collected in Walter's antifreeze (30% (v/v) ethylenglycol, 30% (v/v) glycerol, 0.5 M phosphate buffer) and stored at -20ºC.

Immunohistochemistry and immunofluorescence

Before staining, floating sections were washed 3x in PBS, treated with 3% H_2O_2 / 10% methanol in PBS for 15 min, blocked in 10% goat serum / 0.3% triton-X-100 in PBS for 1 hour, and incubated with primary antibody over night, followed by incubation with secondary horse radish peroxidase (HRP)-, alkaline phosphatase (AP)- or biotin-conjugated antibodies (Jackson's ImmunoResearch, Vector Laboratories) for 2 hours. For double and triple staining, sections were incubated sequentially with one antibody at a time. Different HRP substrates (DAB, BD Pharmingen or Vector-SG, Vector Laboratories) and AP substrate (Vector-Red, Vector Laboratories) were used to visualize the antigens. Signal from biotinylated antibodies was amplified using an ABC kit (Vector Laboratories). After transferring the sections onto glass slides, nuclei were stained with Contrast Green (KPL) and the slides washed with isopropanol and briefly incubated in SafeClear II (Fischer Scientific) before mounting in Permount (Fischer Scientific).

For immunofluorescence, secondary antibodies conjugated with Alexa-488, Alexa-549, APC (Invitrogen), TRITC or FITC (Jackson's ImmunoResearch) were used, nuclei visualized with DAPI, and the slides mounted in Gel Mount (Biomeda).

Primary antibodies used were anti-CD34 (Abcam), anti-mouse-CD31 (BD Pharmingen), anti human CD44 (Mab 29.7)[30], anti-GFAP (Promega), anti-mouse Nestin Mab 353 (Chemicon), anti-MMP-9 (Ab-7,Oncogene), anti-SDF-1 (Santa Cruz Biotechnology), anti-Ki67 (BD Pharmingen), anti-smooth muscle actin (Sigma), anti-F4/80 (Cederlane), anti-PDGFRβ (eBioscience), anti-human vimentin (Dako), anti-GFP (Chemicon), anti-mouse $GPIb_\alpha$ (Emfret Analytics), anti-Hypoxyprobe (NPI), and anti-fibrin (murine Hybridoma HB8545, ATCC). BS-1 lectin was from Sigma. The TACS TdT kit (R&D Systems) was used for TUNEL staining.

Images were acquired with a Zeiss Axio Imager M1m microscope equipped with a digital camera, using 10x or 20x air objectives. Digital images were analyzed using AxioVision 4.6 software (Zeiss). Confocal images were acquired with an Olympus IX81 microscope equipped with UltraVIEW VoX Confocal Imaging System (Perkin Elmer), using a 40x water immersion objective. Images were acquired and analyzed using the Velocity software.

Quantification of tumor cell extravasation

To detect the tumor cells, tissues were stained with anti-GFP antibody (4T1), anti human CD44 (Mab 29.7) or human vimentin (human cell lines), and co-stained with anti-CD31 to visualize the vascular endothelium. The position of the tumor cells inside or outside blood vessels was determined for each detected tumor cell. For MDA-MB-435 cells, every 4th section throughout the entire brain was analyzed. At each time point (day 3, 5 and 7), n=4 brains were examined. On day 3, we found 253, 130, 90 or 301 tumor cells per brain respectively, and 15, 16, 48, or 196 tumor cells on day 5. For MDA-MB-231/brain and 4T1 cells, 60 randomly chosen events in each of 2 to 3 different animals were examined per time point. The percentage of intravascular versus extravascular tumor cells was calculated.

The gross quantification was performed using images acquired with Zeiss Axio Imager M1m microscope, which allowed for quantification of a large number of events. For a subset of events, the localization of cancer cells inside or outside the vasculature was confirmed by confocal microscopy.

Quantification of Ki67 positive cells

Tissue was co-stained for Ki67 and human CD44 (MDA-MB-435) or human vimentin (MDA-MB-231/brain). Every 4th section of the entire brain was analyzed in 2 to 3 different animals 30 to 50 days post-injection. The number of Ki67 positive and negative cells was counted for solitary cancer cells and for metastatic lesions containing more than 30 cells. For each of these lesion types, the percentages of Ki67-positive cells were calculated. Standard deviations and statistical significance were determined by two-tailed Student's T-test.

Quantification of astrocyte association with cancer cells

Three days after injection of cancer cells into the carotid artery, the brain tissue was stained for GFAP to detect astrocytes and co-stained for human CD44 (435), human vimentin (231/brain), or GFP (4T1) to detect the cancer cells. The number of reactive astrocytes located within a distance of 150 µm from the cancer cells (cancer cell associated) and the number of reactive astrocytes in the corresponding area of the non-afflicted contralateral hemisphere (normal control) was counted for 20 randomly chosen events per brain in 2-3 animals for each cancer cell line. Standard deviations and statistical significance were determined by two-tailed Student's T-test.

Results

Models and kinetics of initial cancer cell colonization of the brain

To define models suitable for studying the earliest steps of cancer cell brain colonization, we injected five different Firefly luciferase (F-luc) tagged breast cancer cell lines into the left internal carotid artery of female immunodeficient or immunocompetent mice, and followed cancer cell distribution and growth by non-invasive bioluminescence imaging (**Fig. 1**). CB17/SCID mice were used to analyze human tumor cells and BALB/c mice for syngeneic murine 4T1 breast cancer cells. Comparing MDA-MB-435, MDA-MB-231, MDA-MB-231/brain[28], MCF-7, and 4T1 cells, we found that all five cell lines were detectable within the brain area 15 minutes post-injection. Even though each of these cell lines initially localized to the brain area, only MDA-MB-435, MDA-MB231/brain, and 4T1 cells produced persistent and increasing signal over time, while MDA-MB-231 parental and MCF7 signal declined and eventually disappeared (**Fig. 1A,B**). Immediately after carotid artery injection of 10^4 or 10^5 MDA-MB-435 cells, strong bioluminescence signal was detected in the left hemisphere of the brain and the signal persisted without major change in intensity through days 5 to 7, before it increased continuously (**Fig. 1A and B**). Only live cells produce signal, indicating that the majority of the initially arrested cancer cells remained and survived this step. Just after carotid artery injection of MDA-MB-435 cells, a weak tumor cell signal was occasionally seen in the lungs, but this signal disappeared within a few days and never reappeared (not shown). The signal for MDA-MB-231/brain cells initially decreased slightly, indicating that some of the cancer cells were eliminated. Between day 5 and 10, the remaining signal then began to increase continuously. 4T1 murine breast cancer cells colonized the brain much more aggressively than the two human cell lines. The 4T1 signal started to increase immediately after tumor cell injection and continued to increase at a much faster rate than that of MDA-MB-435 and 231/brain cells.

To investigate the behavior of the bioluminescence producing tumor cells in more detail, we followed individual cells by histology on days 3, 5, and 7. We analyzed the entire brain of each animal by immunohistochemistry at each of these time points (n=2-4 mice per time and cell type). Human tumor cells were detected using two independent markers (human CD44 and human vimentin). Murine 4T1 cells were identified by their GFP label via anti-GFP staining. We found that MDA-MB-231 parental cells were rapidly cleared from the circulation of the brain parenchyma, and were undetectable inside or outside the vasculature of the brain tissue on day 3, 5, and 7 post injection. Residual bioluminescence signal of MDA-MB-231 parental cells in the brain

area seen through day 5 (**Fig. 1**) was likely due to tumor cells in the leptomeninges, which remained attached to the skull when the brains were removed for histology at these early time points. In contrast, MDA-MB-435, MDA-MB231/brain, and 4T1 cells were readily detected throughout the brain parenchyma very early (e.g. day 1, 2, 3, and 7) as well as at later time points. After 10 to 50 days, numerous macrometases were found in 100% of the animals (n=3-6/group) after injecting 10^4 to 10^5 of these tumor cells. 4T1 cells exhibited the most rapid growth in their immunocompetent hosts and produced extensive metastatic burden already after 10 days. MDA-MB-435 and brain homing MDA-MB-231/brain cells were previously reported to produce metastatic lesions in the brain when administered into the blood stream[28, 31], but the early colonization steps have not been previously investigated. MDA-MB-435 cells are aggressively metastatic breast cancer cells that share some characteristics with melanoma [32, 33], another tumor type that frequently causes brain metastasis in patients[1]. The MDA-MB-231/brain cell line was derived from MDA-MB-231 parental breast cancer cells after cardiac injection into immunodeficient mice and six cycles of isolating brain metastases and re-injection into the heart [28]. Here, we demonstrated that MDA-MB-231/brain cells, as well as MDA-MB-435 and 4T1 cancer cells are suitable models for studying cancer cell interaction with the brain microvasculature even at the earliest time points, for following the ability of cancer cells to survive and grow within the brain tissue, and for analyzing involved host cell responses.

Cancer cell extravasation, growth in the brain, and types of blood vessels involved

To analyze the mode and timing of cancer cell extravasation, their initial proliferation in the brain parenchyma, and the types of blood vessels involved in extravasation and lesion growth, we followed the cancer cells on days 1, 2, 3, 5, and 7 after carotid artery injection by immunohistochemistry.
The localization of cancer cells and blood vessels was determined by staining the human cancer cells with anti-human CD44 (mab 29.7)[30] or anti-human Vimentin, mouse 4T1 cells with anti-GFP, and the vasculature with anti-CD31 (**Fig. 2A and S1**). During the first two days after inoculation, all cancer cells were found inside blood vessels and displayed an elongated shape to fit into the narrow capillaries (**Fig. 2A-a**). On day 3 post-inoculation, for all three cell lines examined, the majority of cancer cells were still localized within the microvasculature (**Fig. 2A-b, B and S1**). Only a small percentage was extravasating (**Fig. 2A-c, 2C and S1**) or already located in the extra-vascular space, staying close to the vessels from which the cells had emerged (**Fig. 2A-d and S1**). Before or during extravasation, the cancer cells rounded up inside the vascular lumen and formed cytoplasmic protrusions, which apparently expanded the vessel wall that surrounded them (**Fig. 2A-b;** see also **5C, day3, blue arrowheads**). Intravascular cancer cells penetrating the blood vessel wall with their cytoplasmic protrusions were also detected (**Fig. 2C**, middle, and **S1**). Extravasation of individual cancer cells seemed to at least occasionally involve larger interruptions of the vessel wall (**Fig. 2A-c,d,e,f**). However, we could not detect any apoptosis or hypoxia associated with the endothelium at sites of cancer cell extravasation by TUNEL staining or hypoxyprobe, respectively. This suggests that the extravasation events were not associated with significant destruction of the vessel wall (data not shown). However, fibrin formation and platelet aggregation were detected at sites of 4T1 cell extravasation in BALB/c mouse brain on day 3, 5, and 7 post tumor cell injection (**Fig. 2D** and not shown). On day 5 post-inoculation, 20 to 40 % of the cancer cells were still intra-vascular (**Fig. 2B**). On day 7, all MDA-MB-435 and 4T1 tumor cells were found in the extravascular space, while approximately 15 % of MDA-MB-231/brain cells were still intravascular, suggesting a slightly slower extravasation kinetics (**Fig. 2A-e,f,g, B and S1**). At this time, for all three cell lines small groups of cancer cells were detected close to capillaries or lined up along the vessel wall at the parenchymal side, indicating initial cancer cell growth (**Fig. 2A-f,g and S1**). Notably, for MDA-MB-435 cells, extravasation always preceded cancer cell proliferation, since groups of two or more cancer cells were seen only in the extravascular space and never inside blood vessels (**Fig. 2A-c - g**). In contrast, groups of cancer cells within the vasculature were found for 4T1 cells, suggesting that these cells might proliferate even before extravasating. This is in line with the immediate increase in bioluminescence signal for this cell line from day 1 on (**Fig. 1B**).
By day 30 to 70, all mice injected with MDA-MB-435 or MDA-MB-231/brain cells harbored large metastatic lesions within the brain parenchyma and leptomeninges. At this stage, leptomeningeal metastases remained attached to the brain surface when the brains were harvested, allowing us to analyze these lesions in detail and to compare them to lesions within the brain tissue. While metastases in the brain parenchyma grew preferentially around capillaries, forming elongated clusters around these small vessels (**Fig. 2E-a, 3C**), leptomeningeal lesions were compact nodules and contained capillaries as well as larger vessels (**Fig. 3C**).
Due to the rapid intracranial growth of 4T1 cells, these experiments were terminated after 10-14 days. All animals harbored numerous macrometastases, tightly lined up along blood vessels within the brain parenchyma. No obvious leptomeningeal lesions were observed for this cell model.

During the initial steps of brain colonization within the parenchyma, cancer cells exclusively arrested within and extravasated from capillaries and/or post capillary venules. These vessels were identified by immunohistochemistry based on their size and lack of smooth muscle cells (**Fig. 3A**). The vessels were postitive for CD31 as well as for CD34, and were surrounded by PDGFRβ-positive pericytes (**Fig. 3B**). This indicates that parenchymal lesions stayed associated with the vessel type from which they initially emerged.

In addition to successfully growing large metastatic lesions, we detected many single cancer cells scattered throughout the brain at late time points for MDA-MB-435 and 231/brain cell models (day 30 – 70 post-injection). These cells were localized within the brain parenchyma next to capillaries (**Fig. 2E-b**). The majority of the solitary MDA-MB-435 cancer cells were not proliferating, as only 12 % of these cells were positive for cell cycle marker Ki67 (**Fig. 2E-c, F**). Thus, these solitary cancer cells were arrested in G_0 of the cell cycle and remained dormant after extravasation, while the majority of cancer cells within larger lesions (63 %) were Ki67 positive and proliferated actively (**Fig. 2E-d, F**). In contrast, there was no significant difference in the percentage of Ki67 positive cells between the solitary cancer cell population and macroscopic lesions for MDA-MB-231/brain cells (**Fig. 2F**). Notably, no solitary cancer cell population was detected for the aggressive murine 4T1 breast cancer cell line in their syngeneic BALB/c host model. All observed 4T1 cells grew in tight clusters around blood vessels 10 days after carotid artery injection (not shown).

Cancer cell arrest and extravasation in the brain induce diverse microglial and astrocyte responses

It is well established that the host microenvironment affects tumor growth and metastatic progression and impacts the success of tumor cells to survive and grow within the brain[6, 29, 34-36]. Therefore, we investigated the earliest responses of brain residing cells to incoming cancer cells during the initial steps of hematogenous brain metastasis. A major cell type of the brain known to respond to invading cells from the immune system during inflammatory brain disease and development of primary brain tumors is microglia[14-18]. We therefore investigated an involvement of microglia in the earliest steps of cancer cell brain colonization. F4/80 was used as a marker for microglia and macrophages. Our analysis revealed a varying accumulation of F4/80-positive cells with strongly increased F4/80 expression, indicative of microglial activation, around extravasated cancer cells on day 7 in all three cancer cell models (MDA-MB-435: **Fig. 4A**; 4T1: **Fig. 4B**; MDA-MB-231/brain: data not shown). Similar microglial responses were observed in immunosuppressed SCID mice and immunocompetent BALB/c mice. Some cancer cells that had left the vasculature recruited large amounts of activated microglia, while only few or no activated microglial cells could be detected in the vicinity of other cancer cells (**Fig. 4A-a, B-a left**). However, the microglial responses observed were specifically induced by the cancer cells, and were not a consequence of the surgical manipulation since activated microglial cells were never detected in the same brain regions of animals injected with medium alone (**Fig. 4B-a right**). Microglia associated with the initial micrometastases presented either as activated microglia displaying characteristic stellate morphology with thick cellular processes (**Fig. 4A-c, B-c**), or as reactive microglia with typical amoeboid morphology[37] (**Fig. 4A-d, B-d**). The heterogeneity in microglial responses persisted throughout metastatic lesion development. Even macrometastases on day 50 post tumor cell injection were either completely free of microglial cells (**Fig. 4A-e**), or found associated with activated stellate (**Fig. 4A-f**) or reactive amoeboid microglia (**Fig. 4A-g**). Thus, microglial responses to brain invading cancer cells can generate a variety of local microenvironments that may affect lesion growth. These responses could be dynamically regulated, potentially explaining their sporadic detection.

In addition to the variable microglial responses, astrocytes and their activation were consistently found associated with invading cancer cells from the earliest intravascular arrest steps on (**Fig. 5**). In addition to pericytes, brain capillaries are accompanied by astrocytes, which contribute to the tightness and functions of the blood-brain barrier (BBB)[38-40]. After interacting with endothelial cells, pericytes and astrocytes are the first host cell types that extravasating cancer cells encounter. Strikingly, in all three cancer cell models, arrest and extravasation of cancer cells consistently resulted in a strong local activation of astrocytes, detected by the up-regulation of glial fibrillar acidic protein (GFAP) as well as by the hyperdilation of astrocyte processes (MDA-MB-435: **Fig. 5A, C**; 4T1: **Fig. 5D**; MDA-MB-231/brain: data not shown). Astrocyte activation was always and exclusively seen in close proximity of cancer cells. In many cases, the astrocyte response was so strong that it could be detected in overviews of whole brain sections, even on day 3 post cancer cell injection (**Fig. 5A**). At this stage, reactive astrocytes were present in close proximity of individual cancer cells, even before those extravasated (**Fig. 5C**, day 3). Reactive astrocytes persisted throughout the extravasation process (**Fig. 5C and D,** day 7) and establishment of large metastatic lesions (**Fig. 5C**, day 50). Early astrocyte activation on day 3 was a specific response to the presence of cancer cells, since the injection of medium alone in sham operated animals did not result in any detectable astrocyte activation (**Fig. 5A**). Furthermore, no increase in reactive astrocytes was observed for the corresponding brain area in the contralateral brain hemisphere (**Fig. 5A**). Notably, injection of breast cancer cells into the left internal carotid artery resulted in tumor cell colonization of only the left hemisphere of the brain, while the right hemisphere remained unaffected. We therefore used the right, tumor cell free hemisphere as a control to quantify the number of reactive astrocytes associated with cancer cells in the left hemisphere. The results demonstrate a significant and specific increase in reactive astrocytes in the proximity of cancer cells on day 3 post-injection for all three breast cancer cell models (**Fig. 5B**).
In addition to elevated expression of GFAP, some cancer cell associated astrocytes simultaneously up-regulated expression of nestin, another marker of reactive astrocytes[41] (**Fig. 5E**). We confirmed that nestin staining was truly associated with astrocytes by co-staining blood vessels and microglia with nestin (**Fig. S2**). This result reflects a diversity of atrocytic responses to tumor cells.
An important consequence of astrocyte activation is their ability to secrete factors such as matrix metalloproteinase-9 (MMP-9)[42, 43]. MMP-9 can directly impact cancer cell invasion and has known pro-angiogenic and growth-promoting functions in brain tumors through release of growth factors from the extracellular matrix[34]. We found a strong expression of MMP-9 by MDA-MB-435 cells, as well as a strong up-regulation of MMP-9 protein in the immediate vicinity of extravasating cancer cells, associated with activated astrocytes that surrounded the tumor cells (**Fig. 5F**). Another factor also known to be released by reactive astrocytes is Stromal cell derived factor 1 (SDF-1)[44-47], but we did not detect SDF-1 in the context of astrocyte responses to cancer cell invasion (not shown). Together, astrocytes might provide early and continuous pro-angiogenic and/or survival signals that support cancer cell growth. The mechanism might involve release of MMP-9 into the immediate proximity of the cancer cells. Because of their consistent and very early response to arriving cancer cells in the brain, and the persistence of their association with proliferating tumor cells, astrocytes might provide a supportive microenvironment for the development of brain metastatic lesions.

Discussion

The present study provides detailed *in vivo* analyzes of breast cancer cell arrest and extravasation into the brain parenchyma. Furthermore, it captures the diversity of early host responses within the brain microenvironment during the initial steps of cancer cell invasion. Information on the first interaction between brain-homing tumor cells and reactive host cell types will contribute to a better understanding of critical early events in brain metastasis. This insight may help develop strategies for prevention and treatment of symptomatic brain lesions.
Our results show that breast cancer cells arrest exclusively in brain capillaries and/or post capillary venules. Comparing five different breast cancer cell models, we identified three as suitable models for detailed studies of the earliest critical events of breast cancer cell extravasation and initial brain colonization. Importantly, only these tumor cells consistently developed metastatic lesions. Reports in the literature differ on the time-course of cancer cell extravasation, likely due to the use of different cancer cell types, routes of inoculation, and primarily because of distinct microvascular structures within the target organs examined. In general, it takes significantly longer for cancer cells to extravasate into the brain parenchyma than into other organ tissues. For example, extravasation of lung cancer cells in the brain was reported to take 48 hours, while the same tumor cells extravasated into the liver within only 6 hours[13]. In another study, prostate cancer cells derived from brain metastases apparently remained inside brain capillaries for up to 5 days[27]. In our approach, breast cancer cells were injected into the left internal carotid artery of immunosupressed SCID mice or immunocompetent BALB/c mice. Importantly, we found that regardless of the host immune state, the timing of tumor cell arrest within the vasculature and extravasation was the same for all tumor cell models examined. We found the tumor cells arrested within the brain microvasculature and in the process of extravasation from day 3 on. Extravasation was completed on day 7, except for MDA-MB-231/brain cells, where a small percentage of cells was still intravascular. Thus, arrested cancer cells apparently have to survive within the brain vasculature for a significantly longer period of time than in other organs. Cancer cell survival in the vasculature is likely a critical step that limits the success rate of brain metastasis. This step is probably influenced by the ability of cancer cells to specifically interact with components of the vessel wall upon arrest. In line with this concept, it was recently reported[27] that the majority of DU145/RasB1 prostate cancer cells, which arrested in the brain vasculature, were eliminated before they could extravasate, pointing at intra-vascular survival as a rate limiting step. These studies were performed in immunodeficient mice. The presence of a fully competent immune system, especially natural killer cells[48], is expected to pose additional survival pressure on cancer cells that remain arrested within the vasculature for extended periods of time. However, our results indicate that arrested breast cancer cells can survive for several days within the cerebral microvasculature in the presence of a fully functional immune system. We found that 4T1 cells injected into BALB/c mice initiated growth very rapidly without any signs of cancer cell death by TUNEL staining (data not shown). In this model, we observed platelet accumulation and fibrin formation associated with intravascular cancer cells, potentially protecting them from the immune system.

Compared to the brain, intra-vascular survival may be less critical in other organs because of significantly shorter extravasation times. Recently, Bos et al.[49] identified genes that promote breast cancer brain metastasis through a gene profiling analysis. Importantly, these genes comprise a group of mediators of cancer cell extravasation in an *in vitro* model of the blood-brain barrier. Notably, the duration of transendothelial migration by cancer cells *in vitro* is significantly shorter (6-18 hours) than that required for extravasation into brain tissue *in vivo* (3 to 5 days). Furthermore, conditions in the vasculature are much more complex than can be recapitulated *in vitro*. While one can envision extravasation as a rate-limiting step for cancer types that are able to survive after arresting within the cerebral microcirculation, our results indicate that survival factors – in addition to mediators of extravasation – likely play a decisive role in the establishment of brain metastases.

Different modes of cancer cell extravasation have been described. These include extravasation of individual tumor cells without observable disruption of the microvasculature, as well as intra-vascular cancer cell proliferation followed by eventual vessel rupture, as reported for lung metastasis[50-53]. In the MDA-MB-435 model, we observed individual cancer cells within brain capillaries that initially assumed an elongated shape to fit into the significantly smaller vessels. Three days later, the tumor cells regained a round shape thereby stretching the vessel wall. In some cases, the vessels appeared disrupted upon extravasation. However, the absence of any detectable apoptosis or hypoxia associated with the vascular endothelium at these sites suggests that no significant damage of blood vessels occurs during the extravasation process. Notably, we also observed cancer cell protrusions stretching through the vessel wall, indicating that crossing of the blood brain barrier is an active, specific process initiated by the tumor cells. For MDA-MB-435 cells, we did not observe any intravascular proliferation. Groups of two or more cells appeared only in the extravascular space from day 5 on. Consistent with the histology, bioluminescence signal intensity reflecting the number of F-luc tagged cancer cells started to increase between days 5 and 7 when all of the cells had extravasated. In contrast, we observed intravascular groups of cells for both MDA-MB-231/brain and 4T1 cells, indicating that these might proliferate before extravasation. This finding correlates with the strong, immediate increase in bioluminescence signal for both MDA-MB-

231/brain and 4T1 cells within the first day after injection. For MDA-MB-231/brain cells, the signal intensity decreased after day 1, before it began to increase continuously between days 5 and 10, indicating that cancer cells were eliminated from the brain vasculature between days 2 and 5. Exit of cancer cells from capillaries or post capillary venules may involve mechanical forces caused by rounding of the cancer cells, formation of cytoplasmic protrusions, and most likely secretion of disruptive enzymes such as MMP-9 and heparanase, or their combinations[6, 12, 36, 54]. To our knowledge, only one study previously captured cancer cells in the process of extravasation into the brain, using a rat hepatoma cell line as a model[12]. In that model, extravasation apparently involved breaching or destruction of the endothelium. The results from our study with breast cancer cells suggest that different modes of extravasation for cancer cells in the brain might exist.

As lesions progressed, we observed macrometastases within the brain parenchyma, as well as in the leptomeninges. These locations represent distinct microenvironments within the brain[7, 36], which we found reflected by strikingly different phenotypes of parenchymal versus leptomeningeal metastases in our models. Throughout their development, metastases in the parenchyma grew mostly around small blood vessels similar to a phenotype previously reported[9, 11, 27, 55]. We identified these vessels as capillaries or post capillary venules based on their size and lack of smooth muscle cells. In contrast, metastases in the leptomeninges grew into dense, solid lesions that always contained larger vessels surrounded by smooth-muscle cells. Because of the fragility of the leptomeninges and their tendency to stay associated with the skull when the brains were removed early after cancer cell injection, our analysis of the initial colonization events focused on the parenchymal microenvironment. It is possible that the first steps of cancer cell arrest and extravasation within leptomeninges differ from the events seen within the brain parenchyma.

The brain is a very specialized environment with a unique cellular composition. Recent evidence suggests that adhesion of cancer cells to components of the vascular basement membrane provides essential survival cues for cancer cells, early during brain colonization[9]. In addition to initial signals from tumor cell adhesive interactions with the vessel wall, host cells in the immediate microenvironment of the tumor cells are most likely to impact their fate and ability to progress. In our study, we focused on host cell responses to the invading tumor cells. For established brain metastases, it has been well documented that reactive astrocytes and microglia surround the lesions[15, 22]. Furthermore, it is known that glial cells are activated in a response to brain injuries. However, responses of glial cells and astrocytes to the initial stages of tumor cell invasion have not been previously reported. We found that cancer cell arrest, extravasation and invasion of the brain parenchyma always induced a strong local activation of astrocytes, and activation of microglia to varying degrees. Astrocytic responses were heterogeneous in their intensity and cellular composition, involving cells with up-regulated expression of GFAP, nestin, or both. Reactive astrocytes occasionally strongly up-regulated expression of MMP-9, which is known to promote growth of primary brain tumors based on its pro-angiogenic activity by releasing VEGF from the surrounding matrix[34]. In addition, VEGF can also directly stimulate the proliferation of cancer cells[56]. Furthermore, astrocytes were shown to support brain metastatic growth by secretion of heparanase[24] and neurotrophins[23]. Thus, reactive astrocytes may provide initial cues for extravasating tumor cells to survive and proliferate within the brain parenchyma.
Some reactive astrocytes in the vicinity of cancer cells expressed nestin. Nestin is a marker of neuroepithelial stem cells, radial glia cells and progenitor cells, and is down-regulated during terminal differentiation to mature astrocytes. Nestin up-regulation in reactive astrocytes was found associated with brain injury from different causes[41, 57-59]. It has been long debated whether reactive astrocytes originate from progenitor cells that migrated from the sub-ventricular zone (SVZ), or if they derive from regional mature astrocytes. Recently, several groups showed that nestin-positive SVZ progenitors migrate to damaged areas in the brain cortex[60, 61]. Other groups demonstrated that mature astrocytes locally resume proliferation and dedifferentiate in response to brain injury and other stimuli[57, 62]. Thus, both scenarios can occur. In our study, nestin-positive reactive astrocytes were observed very early during cancer cell invasion of the brain parenchyma. The origin of these astrocytes remains to be elucidated.
The reactions of microglia to cancer cells were also diverse. In the normal brain, resting or ramified microglia with thin processes are distributed throughout the brain tissue. Upon stimulation, ramified microglia can be progressively converted into active microglia via at least two different and functionally distinct morphological states. These are termed activated and reactive microglia [37]. While activated microglia express only MHC-I, reactive microglia express both MHC-I and MHC-II, and show phagocytic activity. The microglial population we found associated with cancer cells was heterogeneous and consisted of both activated microglia with typical hypertrophic stellate appearance and reactive microglia with amoeboid cell morphology. Notably, microglial responses to cancer cells were similar in immunosuppressed and in immunocompetent mice. Microglial cells can have protective as well as cytotoxic functions[21, 22]. Thus, in addition to astrocytes, microglia may influence tumor cell survival and development into macrometastases.

In addition to macrometastases, we detected many solitary tumor cells distributed throughout the brain parenchyma, 30 to 70 days after carotid artery injection of MDA-MB-435 and MDA-MB-231/brain cells. The vast majority of solitary MDA-MB-435 cells were negative for Ki67 antigen, indicating their dormant state. In contrast, solitary MDA-MB-231/brain cells and macroscopic lesions displayed similar Ki67 expression. These observations are in line with previous reports demonstrating that cancer cells have different fates after arresting within the brain vasculature, as they may proliferate and progress to macrometastases, survive without growing (dormancy) or die and become eliminated[63, 64]. In addition to the impact of clonal heterogeneity of cancer cells, local differences within the brain microenvironment including large molecular diversity between astrocytes in different regions of the brain[65, 66], may influence the tumor cell fate. These parameters are known to affect nerogenesis and impact melanoma brain metastasis [7, 35, 67]. Our results demonstrate that in addition to these location-specific diversities, the invasion of brain tissue by individual cancer cells induces a variety of glial responses that add to the uniqueness of each local microenvironment. Distinct glial responses may help explain why cancer cells that arrested in the microvasculature can have different fates, even if they are located within the same brain area[63, 64]. Functional contributions of different astrocytic and microglial cell populations to very early steps of metastatic invasion remain to be elucidated. Unraveling the underlying mechanisms *in vivo* might lead to targeted manipulation of the brain microenvironment for clinical inhibition of brain metastasis. Similar approaches have already been used to convert a non-neurogenic into a neurogenic environment to promote neuron formation in the adult brain[67, 68]. Thus, in the future one could envision application of these principles for treatment of brain metastasis.

Acknowledgements
We would like to thank Hwajin Lee for his help with cutting brain cryosections, Karin Staflin for the introduction to the floating sections staining technique, Heiko Wurdak for help with confocal microscopy, and James Quigley for kindly providing Mab 29.7.

Figure 1. Brain colonization by breast cancer cell lines after carotid artery injection in mice monitored by bioluminescence imaging. (A) Increase of bioluminescence signal indicates growth of F-*luc* tagged MDA-MB-435 cells shown in a representative animal at various time points after injection of 10^5 cancer cells. **(B)** Survival and growth of F-*luc*-tagged MDA-MB-435, MDA-MB-231 parental, MDA-MB-231/brain, MCF7 (injected into immunosuppressed CB17/SCID mice) and 4T1 cells (injected into immunocompetent BALB/c mice) after injection into the left carotid artery followed over time. Only live cells produce signal. Number of injected cells as indicated.

Figure 2. Cancer cell extravasation and growth in the brain.
(A) MDA-MB-435 cells were visualized by anti-human CD44 (mab 29.7) and blood vessels by CD31 staining using immunohistochemistry (IHC). **a:** An elongated cancer cell within a capillary on day 2 post injection. **b:** Rounding of intra-vascular cancer cells on day 3. **c:** Cancer cell on day 3 breaking through the vessel wall during extravasation. **d:** Extravasated cancer cell on day 3. **e-g:** Extra-vascular cancer cells on day 7. Bars: 50 µm (a-d), 25 µm (e-g). **(B)** Percentage of cancer cells located inside versus outside blood vessels. The quantification was performed for 3 different cells lines: MDA-MB-

435, MDA-MB-231/brain, and 4T1. **(C)** Analysis of early cell location by confocal microscopy. Cancer cells were stained for human CD44 (green) and blood vessels for CD31 (red). An intravascular cell (left), a cell in the process of extravasation (middle), and extravascular cells (right) are shown. **(D)** Association of intravascular 4T1 cancer cells with fibrin and platelets ($GPIb_{\alpha}$ staining) on day 3. Bar: 25 µm. **(E)** Day 50: Long-term fate of MDA-MB-435 cells was monitored by IHC (a,b) and immunofluorescence (c,d). **a:** Intra-parenchymal macrometastases grew preferentially around co-opted blood vessels. **b,c:** solitary tumor cells outside blood vessels on day 50, detected by anti human CD44 (mab 29.7) are mostly negative for Ki67. **d:** In contrast, most cells within lesions as shown in (a) are Ki67 positive. Bars: 200 µm (a), 50 µm (b-d). **(F)** Quantification of Ki67-positive cells within the solitary cancer cell population and within the macrometastatic lesions for MDA-MB-435 and MDA-MB-231/brain cells 30 to 50 days post-injection.

Figure 3. Blood vessel types involved in cancer cell extravazation and growth.
Blood vessel types were analyzed by immunofluorescence. Representative images for MDA-MB-435 cells are shown. **(A)** Day 7: In the brain parenchyma, cancer cells (white, see arrows) arrest and extravasate exclusively from capillaries or post capillary venules positive for CD34 and lacking smooth-muscle cells (no smooth muscle actin (SMA) signal). Bars: 100 µm. **(B)** Day 7: Blood vessels from which cancer cells (gray) extravasate are surrounded by PDGFRβ-positive pericytes. **Top:** BS-1 lectin; **middle:** anti-PDGFRβ; **bottom:** merge. Bar: 20 µm. **(C)** Day 50: intra-parenchymal metastases grow around co-opted capillaries lacking smooth-muscle cells. Leptomeningeal metastases contain capillaries as well as larger, smooth-muscle cell-positive vessels. Bars: 100 µm.

Figure 4. Microglial cell responses to invading cancer cells are heterogeneous. Microglial activation in response to cancer cell invasion varies at early as well as late stages, as detected by immunofluorescence analysis. **(A)** MDA-MB-435 cells in immunosuppressed mice; **a:** Diverse microglial responses (green) to incoming cancer cells (red) on day 7. Responses include **b:** absence of microglial cells, **c:** presence of hypertrophic stellate activated, or **d:** amoeboid reactive microglial cells. Similarly, on day 50, **e:** some macrometastases show no microglial involvement, or **f:** contain stellate or **g:** amoeboid microglia. Bars: 100 µm (a), 50 µm (b-g). **(B)** 4T1 cells in immunocompetent mice; **a:** Distribution of activated microglia (red) in the mouse brain 7 days after carotid artery injection of cancer cells (left) or medium alone (right). White arrowheads mark the GFP-labeled cancer cells (green). Diverse microglial responses to cancer cells include **b:** absence of microglial cells, **c:** presence of hypertrophic stellate, or **d:** reactive amoeboid microglial cells. Bar: 50 µm.

Figure 5. Cancer cell invasion induces strong astrocytic responses. Astrocytes were investigated by immunofluorescence staining. **(A) Left:** On day 3 after cancer cell injection into the left carotid artery, GFAP in astrocytes is already up-regulated strongly in the vicinity of intravascular arrested cancer cells (MDA-MB-435, red arrows). Astrocyte activation can be detected in the left hemisphere in brain overview sections, while the corresponding area of the contralateral hemisphere is devoid of GFAP reactivity. **Right:** Also, no GFAP activity was found in the brain of control animals injected with medium alone. **(B)** Number of reactive astrocytes 3 days after carotid artery injection of cancer cells, quantified within the 150 µm distance from cancer cells (cancer cell associated) and within the corresponding region of the contralateral hemisphere that lacks cancer cells (normal control). **(C)** Activated astrocytes with thick processes and up-regulated expression of GFAP are detected next to MDA-MB-435 cancer cells that are still intravascular. Note the cytoplasmic protrusions of cancer cells on day 3 post-inoculation that apparently cause stretching of the vessel wall (blue arrowheads) (day 3, upper left). GFAP positive astrocytes stay close to extravasated tumor cells (day 7, lower left). Reactive astrocytes persist close to cancer cells throughout their development into macrometastases (day 50, right). Bars: 20 µm. **(D)** Activated astrocytes are also present in the vicinity of 4T1 breast cancer cells injected into the carotid artery of syngeneic BALB/c mice. Bars: 20 µm. **(E)** In addition to GFAP up-regulation, some reactive astrocytes simultaneously express nestin. Merged images are shown on the left. Human vimentin or GFP (light blue), nestin (green), GFAP (red), Dapi (dark blue).Bar: 20 µm. **(F)** Strong up-regulation of MMP-9 is detected in reactive astrocytes located in the immediate vicinity of extravasated MDA-MB-435 tumor cell. Bar: 20 µm.

Figure S1. Cancer cell extravasation: 4T1 and MDA-MB-231/brain breast cancer cell lines. (A) Localization of 4T1 cells inside and outside the cerebral microvasculature on day 3 and 7 post carotid artery injection. Bar: 20 µm. **(B)** Localization of MDA-MB-231/brain breast cancer cells inside and outside the vasculature on day 3 and 7 post carotid artery injection. Note a cell in the process of extravasation extending green protrusions (day 3, third image from the top). Bar: 20 µm.

Figure S2. Localization of nestin expression in the vicinity of extravascular MDA-MB-435 cell. Upper panel: In addition to astrocytes, blood vessels also express nestin, but can be clearly distinguished from the astrocytes due to their morphology and CD31-positivity. Lower panel: Microglia (F4/80 staining) do not express nestin. Merged images are shown on the left. Bar: 20 µm.

References

1. Santarelli JG, Sarkissian V, Hou LC, Veeravagu A, Tse V: Molecular events of brain metastasis, Neurosurg Focus 2007, 22:E1
2. Al-Shamy G, Sawaya R: Management of brain metastases: the indispensable role of surgery, J Neurooncol 2009, 92:275-282
3. Albini A, Sporn MB: The tumour microenvironment as a target for chemoprevention, Nat Rev Cancer 2007, 7:139-147
4. Joyce JA, Pollard JW: Microenvironmental regulation of metastasis, Nat Rev Cancer 2009, 9:239-252
5. Witkiewicz AK, Casimiro MC, Dasgupta A, Mercier I, Wang C, Bonuccelli G, Jasmin JF, Frank PG, Pestell RG, Kleer CG, Sotgia F, Lisanti MP: Towards a new "stromal-based" classification system for human breast cancer prognosis and therapy, Cell Cycle 2009, 8:1654-1658
6. Nicolson GL, Menter DG, Herrmann JL, Yun Z, Cavanaugh P, Marchetti D: Brain metastasis: role of trophic, autocrine, and paracrine factors in tumor invasion and colonization of the central nervous system, Curr Top Microbiol Immunol 1996, 213 (Pt 2):89-115
7. Zhang C, Zhang F, Tsan R, Fidler IJ: Transforming growth factor-beta2 is a molecular determinant for site-specific melanoma metastasis in the brain, Cancer Res 2009, 69:828-835
8. Calabrese C, Poppleton H, Kocak M, Hogg TL, Fuller C, Hamner B, Oh EY, Gaber MW, Finklestein D, Allen M, Frank A, Bayazitov IT, Zakharenko SS, Gajjar A, Davidoff A, Gilbertson RJ: A perivascular niche for brain tumor stem cells, Cancer Cell 2007, 11:69-82
9. Carbonell WS, Ansorge O, Sibson N, Muschel R: The vascular basement membrane as "soil" in brain metastasis, PLoS One 2009, 4:e5857
10. Veeravagu A, Bababeygy SR, Kalani MY, Hou LC, Tse V: The cancer stem cell-vascular niche complex in brain tumor formation, Stem Cells Dev 2008, 17:859-867
11. Ballinger WE, Jr., Schimpff RD: An experimental model for cerebral metastasis: preliminary light and ultrastructural studies, J Neuropathol Exp Neurol 1979, 38:19-34
12. Kawaguchi T, Tobai S, Nakamura K: Extravascular migration of tumor cells in the brain: an electron microscopic study, Invasion Metastasis 1982, 2:40-50
13. Paku S, Dome B, Toth R, Timar J: Organ-specificity of the extravasation process: an ultrastructural study, Clin Exp Metastasis 2000, 18:481-492
14. Daginakatte GC, Gutmann DH: Neurofibromatosis-1 (Nf1) heterozygous brain microglia elaborate paracrine factors that promote Nf1-deficient astrocyte and glioma growth, Hum Mol Genet 2007, 16:1098-1112
15. Fitzgerald DP, Palmieri D, Hua E, Hargrave E, Herring JM, Qian Y, Vega-Valle E, Weil RJ, Stark AM, Vortmeyer AO, Steeg PS: Reactive glia are recruited by highly proliferative brain metastases of breast cancer and promote tumor cell colonization, Clin Exp Metastasis 2008, 25:799-810

16. He BP, Wang JJ, Zhang X, Wu Y, Wang M, Bay BH, Chang AY: Differential reactions of microglia to brain metastasis of lung cancer, Mol Med 2006, 12:161-170
17. Hoelzinger DB, Demuth T, Berens ME: Autocrine factors that sustain glioma invasion and paracrine biology in the brain microenvironment, J Natl Cancer Inst 2007, 99:1583-1593
18. Roggendorf W, Strupp S, Paulus W: Distribution and characterization of microglia/macrophages in human brain tumors, Acta Neuropathol 1996, 92:288-293
19. Markovic DS, Glass R, Synowitz M, Rooijen N, Kettenmann H: Microglia stimulate the invasiveness of glioma cells by increasing the activity of metalloprotease-2, J Neuropathol Exp Neurol 2005, 64:754-762
20. Markovic DS, Vinnakota K, Chirasani S, Synowitz M, Raguet H, Stock K, Sliwa M, Lehmann S, Kalin R, van Rooijen N, Holmbeck K, Heppner FL, Kiwit J, Matyash V, Lehnardt S, Kaminska B, Glass R, Kettenmann H: Gliomas induce and exploit microglial MT1-MMP expression for tumor expansion, Proc Natl Acad Sci U S A 2009,
21. Murata J, Ricciardi-Castagnoli P, Dessous L'Eglise Mange P, Martin F, Juillerat-Jeanneret L: Microglial cells induce cytotoxic effects toward colon carcinoma cells: measurement of tumor cytotoxicity with a gamma-glutamyl transpeptidase assay, Int J Cancer 1997, 70:169-174
22. Zhang M, Olsson Y: Hematogenous metastases of the human brain--characteristics of peritumoral brain changes: a review, J Neurooncol 1997, 35:81-89
23. Marchetti D, Aucoin R, Blust J, Murry B, Greiter-Wilke A: p75 neurotrophin receptor functions as a survival receptor in brain-metastatic melanoma cells, J Cell Biochem 2004, 91:206-215
24. Marchetti D, Li J, Shen R: Astrocytes contribute to the brain-metastatic specificity of melanoma cells by producing heparanase, Cancer Res 2000, 60:4767-4770
25. Sierra A, Price JE, Garcia-Ramirez M, Mendez O, Lopez L, Fabra A: Astrocyte-derived cytokines contribute to the metastatic brain specificity of breast cancer cells, Lab Invest 1997, 77:357-368
26. Langley RR, Fan D, Guo L, Zhang C, Lin Q, Brantley EC, McCarty JH, Fidler IJ: Generation of an immortalized astrocyte cell line from H-2Kb-tsA58 mice to study the role of astrocytes in brain metastasis, Int J Oncol 2009, 35:665-672
27. JuanYin J, Tracy K, Zhang L, Munasinghe J, Shapiro E, Koretsky A, Kelly K: Noninvasive imaging of the functional effects of anti-VEGF therapy on tumor cell extravasation and regional blood volume in an experimental brain metastasis model, Clin Exp Metastasis 2009, 26:403-414
28. Yoneda T, Williams PJ, Hiraga T, Niewolna M, Nishimura R: A bone-seeking clone exhibits different biological properties from the MDA-MB-231 parental human breast cancer cells and a brain-seeking clone in vivo and in vitro, J Bone Miner Res 2001, 16:1486-1495
29. Lorger M, Krueger JS, O'Neal M, Staflin K, Felding-Habermann B: Activation of tumor cell integrin alphavbeta3 controls angiogenesis and metastatic growth in the brain, Proc Natl Acad Sci U S A 2009, 106:10666-10671
30. Deryugina EI, Quigley JP: Chick embryo chorioallantoic membrane model systems to study and visualize human tumor cell metastasis, Histochem Cell Biol 2008, 130:1119-1130
31. Lu W, Bucana CD, Schroit AJ: Pathogenesis and vascular integrity of breast cancer brain metastasis, Int J Cancer 2007, 120:1023-1026
32. Chambers AF: MDA-MB-435 and M14 cell lines: identical but not M14 melanoma?, Cancer Res 2009, 69:5292-5293
33. Hollestelle A, Schutte M: Comment Re: MDA-MB-435 and M14 cell lines: identical but not M14 Melanoma?, Cancer Res 2009, 69:7893
34. Du R, Lu KV, Petritsch C, Liu P, Ganss R, Passegue E, Song H, Vandenberg S, Johnson RS, Werb Z, Bergers G: HIF1alpha induces the recruitment of bone marrow-derived vascular modulatory cells to regulate tumor angiogenesis and invasion, Cancer Cell 2008, 13:206-220
35. Fidler IJ, Schackert G, Zhang RD, Radinsky R, Fujimaki T: The biology of melanoma brain metastasis, Cancer Metastasis Rev 1999, 18:387-400
36. Puduvalli VK: Brain metastases: biology and the role of the brain microenvironment, Curr Oncol Rep 2001, 3:467-475
37. Davis EJ, Foster TD, Thomas WE: Cellular forms and functions of brain microglia, Brain Res Bull 1994, 34:73-78
38. Hayashi Y, Nomura M, Yamagishi S, Harada S, Yamashita J, Yamamoto H: Induction of various blood-brain barrier properties in non-neural endothelial cells by close apposition to co-cultured astrocytes, Glia 1997, 19:13-26
39. Hurwitz AA, Berman JW, Rashbaum WK, Lyman WD: Human fetal astrocytes induce the expression of blood-brain barrier specific proteins by autologous endothelial cells, Brain Res 1993, 625:238-243
40. Megard I, Garrigues A, Orlowski S, Jorajuria S, Clayette P, Ezan E, Mabondzo A: A co-culture-based model of human blood-brain barrier: application to active transport of indinavir and in vivo-in vitro correlation, Brain Res 2002, 927:153-167
41. Tamagno I, Schiffer D: Nestin expression in reactive astrocytes of human pathology, J Neurooncol 2006, 80:227-233
42. Hlobilkova A, Ehrmann J, Knizetova P, Krejci V, Kalita O, Kolar Z: Analysis of VEGF, Flt-1, Flk-1, nestin and MMP-9 in relation to astrocytoma pathogenesis and progression, Neoplasma 2009, 56:284-290
43. Wang HH, Hsieh HL, Wu CY, Yang CM: Oxidized Low-Density Lipoprotein-Induced Matrix Metalloproteinase-9 Expression via PKC-delta/p42/p44 MAPK/Elk-1 Cascade in Brain Astrocytes, Neurotox Res 2009,
44. Bonavia R, Bajetto A, Barbero S, Pirani P, Florio T, Schettini G: Chemokines and their receptors in the CNS: expression of CXCL12/SDF-1 and CXCR4 and their role in astrocyte proliferation, Toxicol Lett 2003, 139:181-189
45. Cui X, Chen J, Zacharek A, Li Y, Roberts C, Kapke A, Savant-Bhonsale S, Chopp M: Nitric oxide donor upregulation of stromal cell-derived factor-1/chemokine (CXC motif) receptor 4 enhances bone marrow stromal cell migration into ischemic brain after stroke, Stem Cells 2007, 25:2777-2785
46. Peng H, Erdmann N, Whitney N, Dou H, Gorantla S, Gendelman HE, Ghorpade A, Zheng J: HIV-1-infected and/or immune activated macrophages regulate astrocyte SDF-1 production through IL-1beta, Glia 2006, 54:619-629
47. Xu Q, Wang S, Jiang X, Zhao Y, Gao M, Zhang Y, Wang X, Tano K, Kanehara M, Zhang W, Ishida T: Hypoxia-induced astrocytes promote the migration of neural progenitor cells via vascular endothelial factor, stem cell factor, stromal-derived factor-1alpha and monocyte chemoattractant protein-1 upregulation in vitro, Clin Exp Pharmacol Physiol 2007, 34:624-631
48. Nieswandt B, Hafner M, Echtenacher B, Mannel DN: Lysis of tumor cells by natural killer cells in mice is impeded by platelets, Cancer Res 1999, 59:1295-1300
49. Bos PD, Zhang XH, Nadal C, Shu W, Gomis RR, Nguyen DX, Minn AJ, van de Vijver MJ, Gerald WL, Foekens JA, Massague J: Genes that mediate breast cancer metastasis to the brain, Nature 2009, 459:1005-1009
50. Al-Mehdi AB, Tozawa K, Fisher AB, Shientag L, Lee A, Muschel RJ: Intravascular origin of metastasis from the proliferation of endothelium-attached tumor cells: a new model for metastasis, Nat Med 2000, 6:100-102
51. Chambers AF, MacDonald IC, Schmidt EE, Koop S, Morris VL, Khokha R, Groom AC: Steps in tumor metastasis: new concepts from intravital videomicroscopy, Cancer Metastasis Rev 1995, 14:279-301
52. Chambers AF, MacDonald IC, Schmidt EE, Morris VL, Groom AC: Clinical targets for anti-metastasis therapy, Adv Cancer Res 2000, 79:91-121
53. Chambers AF, Schmidt EE, MacDonald IC, Morris VL, Groom AC: Early steps in hematogenous metastasis of B16F1 melanoma cells in chick embryos studied by high-resolution intravital videomicroscopy, J Natl Cancer Inst 1992, 84:797-803
54. Kosir MA, Wang W, Zukowski KL, Tromp G, Barber J: Degradation of basement membrane by prostate tumor heparanase, J Surg Res 1999, 81:42-47
55. Kawaguchi T, Kawaguchi M, Miner KM, Lembo TM, Nicolson GL: Brain meninges tumor formation by in vivo-selected metastatic B16 melanoma variants in mice, Clin Exp Metastasis 1983, 1:247-259

56. Bachelder RE, Crago A, Chung J, Wendt MA, Shaw LM, Robinson G, Mercurio AM: Vascular endothelial growth factor is an autocrine survival factor for neuropilin-expressing breast carcinoma cells, Cancer Res 2001, 61:5736-5740
57. Buffo A, Rite I, Tripathi P, Lepier A, Colak D, Horn AP, Mori T, Gotz M: Origin and progeny of reactive gliosis: A source of multipotent cells in the injured brain, Proc Natl Acad Sci U S A 2008, 105:3581-3586
58. Itoh T, Satou T, Hashimoto S, Ito H: Isolation of neural stem cells from damaged rat cerebral cortex after traumatic brain injury, Neuroreport 2005, 16:1687-1691
59. Sofroniew MV: Reactive astrocytes in neural repair and protection, Neuroscientist 2005, 11:400-407
60. Alvarez-Buylla A, Herrera DG, Wichterle H: The subventricular zone: source of neuronal precursors for brain repair, Prog Brain Res 2000, 127:1-11
61. Faiz M, Acarin L, Villapol S, Schulz S, Castellano B, Gonzalez B: Substantial migration of SVZ cells to the cortex results in the generation of new neurons in the excitotoxically damaged immature rat brain, Mol Cell Neurosci 2008, 38:170-182
62. Ghashghaei HT, Weimer JM, Schmid RS, Yokota Y, McCarthy KD, Popko B, Anton ES: Reinduction of ErbB2 in astrocytes promotes radial glial progenitor identity in adult cerebral cortex, Genes Dev 2007, 21:3258-3271
63. Heyn C, Ronald JA, Ramadan SS, Snir JA, Barry AM, MacKenzie LT, Mikulis DJ, Palmieri D, Bronder JL, Steeg PS, Yoneda T, MacDonald IC, Chambers AF, Rutt BK, Foster PJ: In vivo MRI of cancer cell fate at the single-cell level in a mouse model of breast cancer metastasis to the brain, Magn Reson Med 2006, 56:1001-1010
64. Luzzi KJ, MacDonald IC, Schmidt EE, Kerkvliet N, Morris VL, Chambers AF, Groom AC: Multistep nature of metastatic inefficiency: dormancy of solitary cells after successful extravasation and limited survival of early micrometastases, Am J Pathol 1998, 153:865-873
65. Bachoo RM, Kim RS, Ligon KL, Maher EA, Brennan C, Billings N, Chan S, Li C, Rowitch DH, Wong WH, DePinho RA: Molecular diversity of astrocytes with implications for neurological disorders, Proc Natl Acad Sci U S A 2004, 101:8384-8389
66. Wilkin GP, Marriott DR, Cholewinski AJ: Astrocyte heterogeneity, Trends Neurosci 1990, 13:43-46
67. Mori T, Buffo A, Gotz M: The novel roles of glial cells revisited: the contribution of radial glia and astrocytes to neurogenesis, Curr Top Dev Biol 2005, 69:67-99
68. Chmielnicki E, Benraiss A, Economides AN, Goldman SA: Adenovirally expressed noggin and brain-derived neurotrophic factor cooperate to induce new medium spiny neurons from resident progenitor cells in the adult striatal ventricular zone, J Neurosci 2004, 24:2133-2142

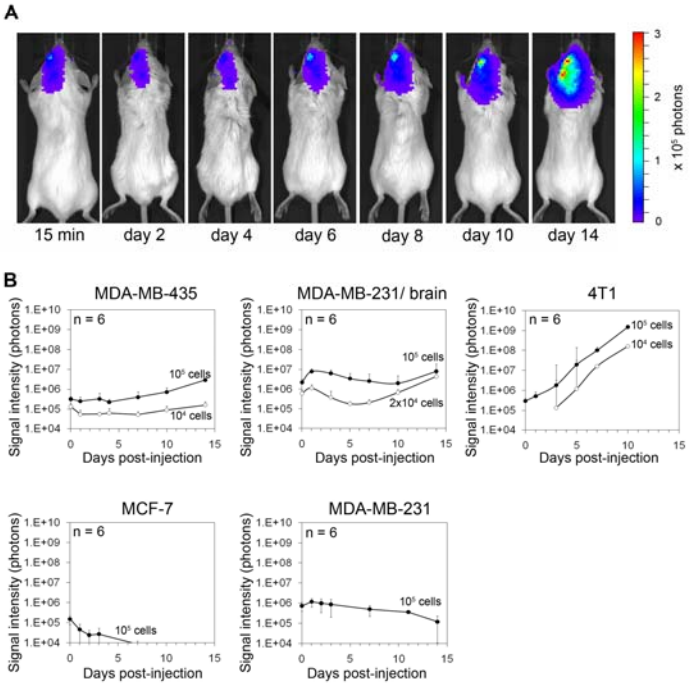

Figure 1

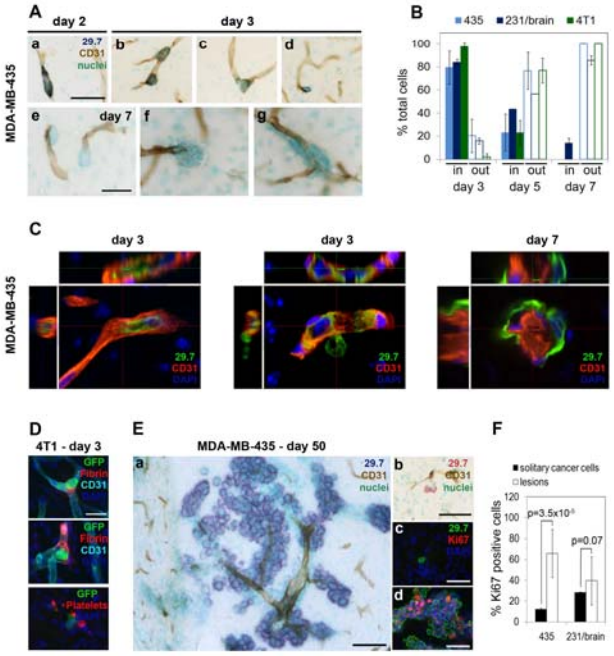

Figure 2

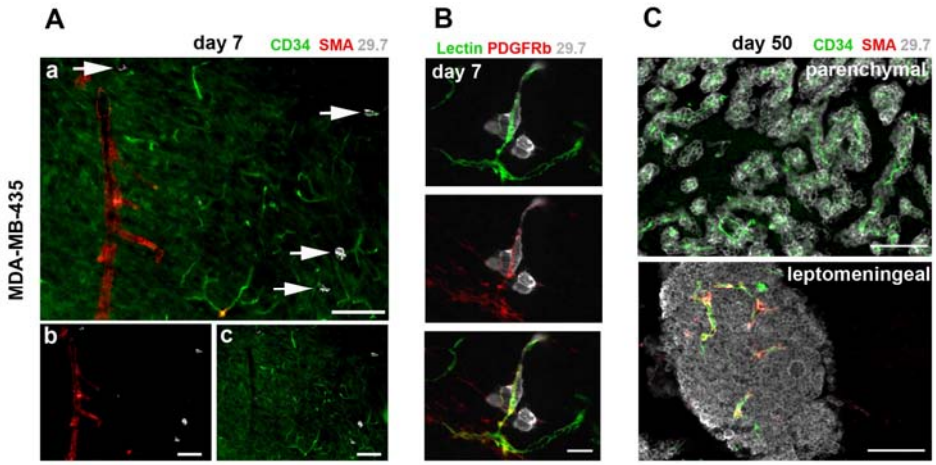

Figure 3

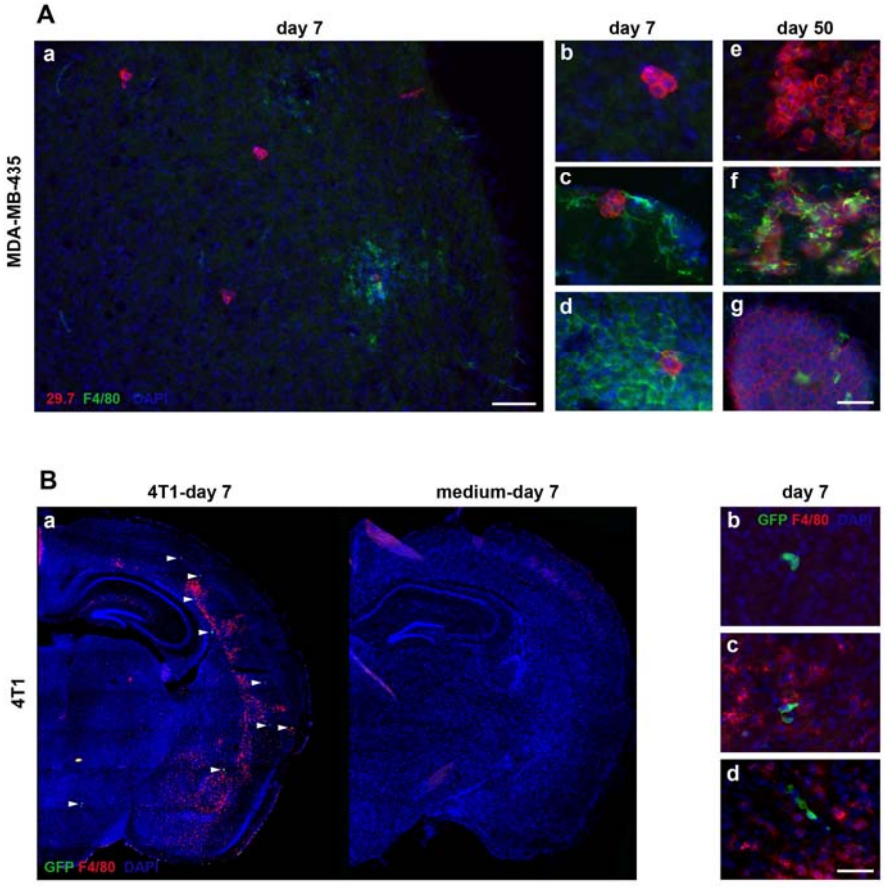

Figure 4

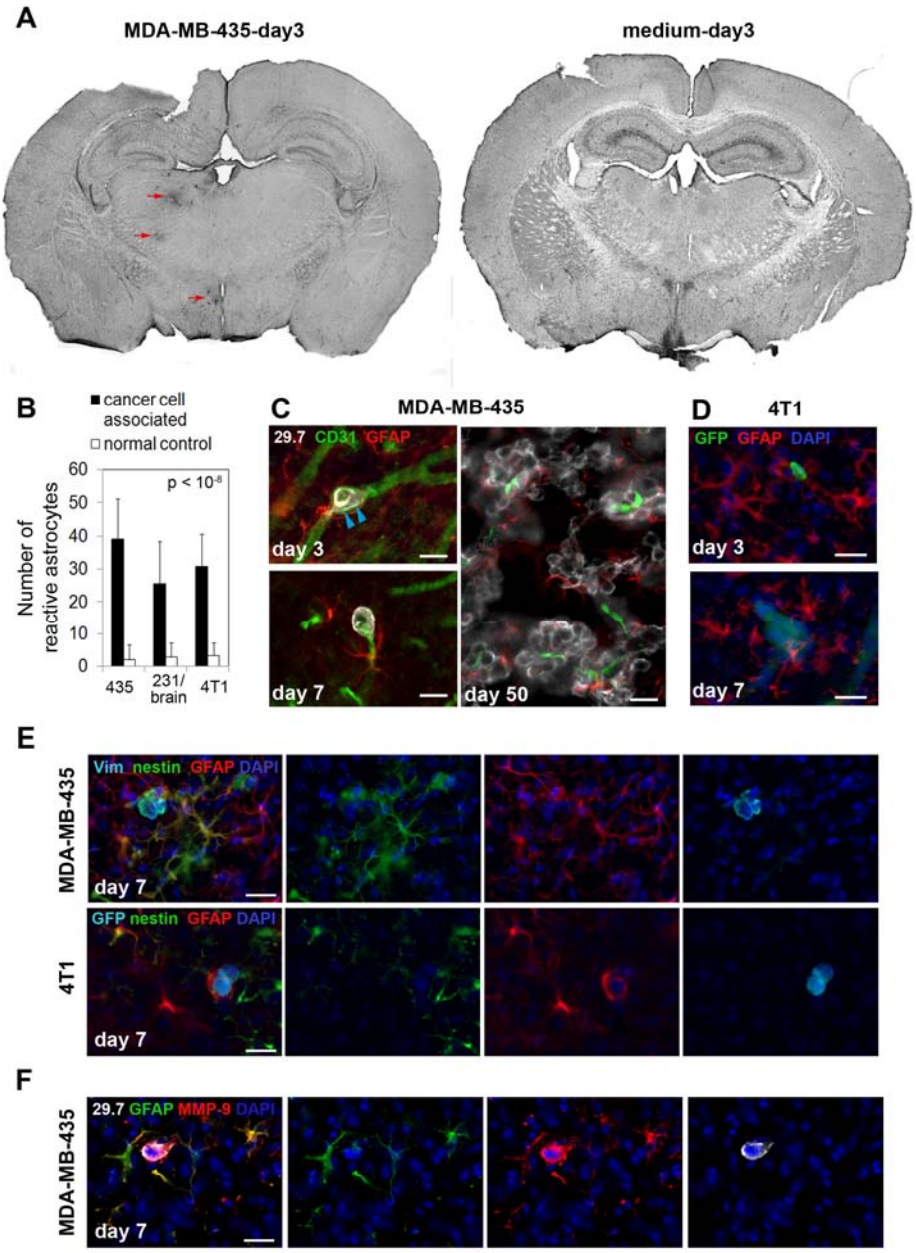
A
MDA-MB-435-day3
medium-day3
B
cancer cell associated
normal control
p < 10-8
Number of reactive astrocytes
60
50
40
30
20
10
0
435
231/ brain
4T1
C
MDA-MB-435
29.7 CD31 GFAP
day 3
day 7
day 50
D
4T1
GFP GFAP DAPI
day 3
day 7
E
MDA-MB-435
Vim nestin GFAP DAPI
day 7
4T1
GFP nestin GFAP DAPI
day 7
F
MDA-MB-435
29.7 GFAP MMP-9 DAPI
day 7

Figure 5

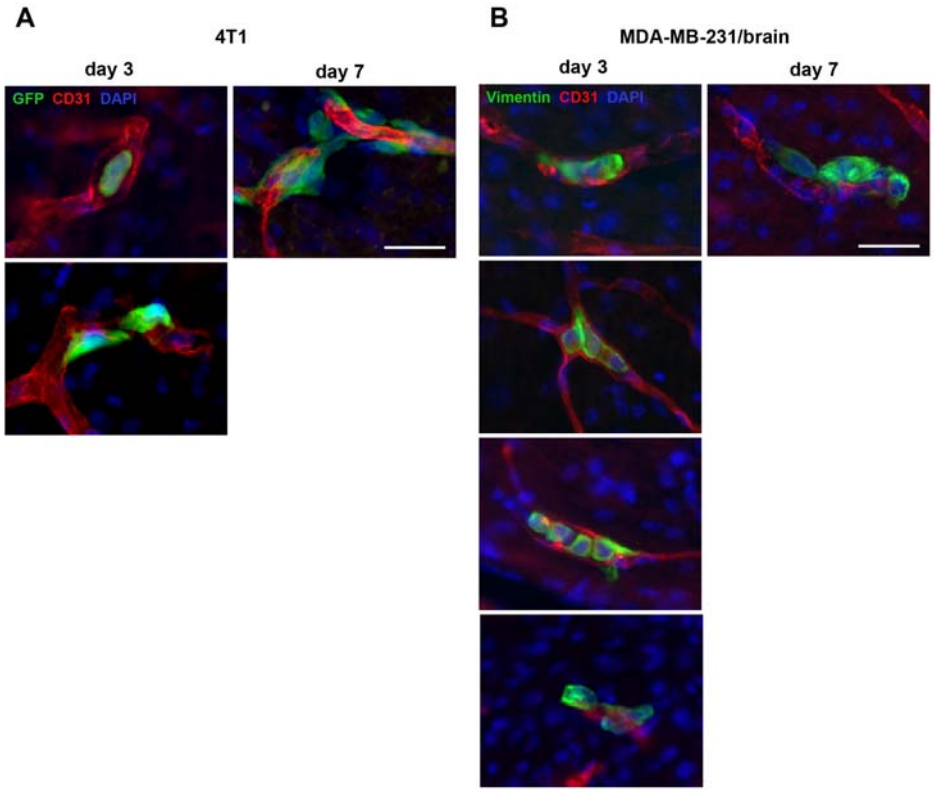

Figure S1

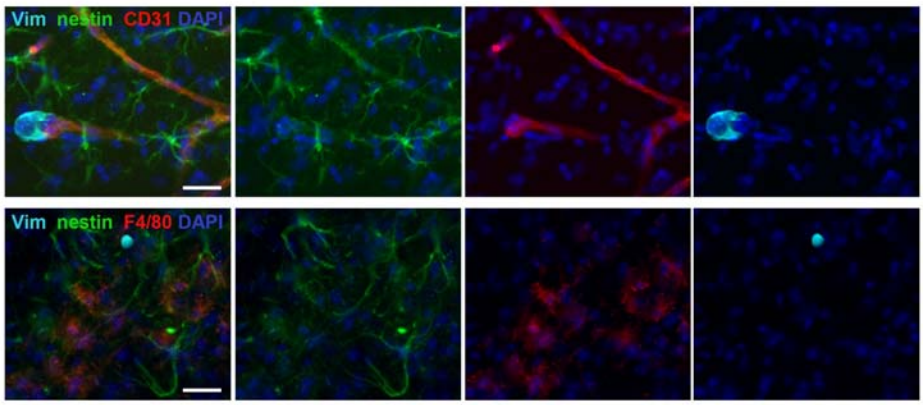

Figure S2

Targeting activated integrin αvβ3 with patient-derived antibodies impacts late-stage multiorgan metastasis

Karin Staflin[1], Joseph S Krueger[1], Janna Hachmann[1], Jane S Forsyth[1], Mihaela Lorger[1], Sebastian CJ Steiniger[2], Jenny Mee[2], Cristina Pop[3], Guy S Salvesen[3], Kim D Janda[2], and Brunhilde Felding-Habermann[1]

[1]Department of Experimental Medicine, [2] Department of Chemistry, The Scripps Research Institute, La Jolla, CA 92037, USA

[3] Program in Cell Death and Apoptosis Research, The Burnham Institute, La Jolla, CA 92037, USA

Running title: Patient-derived antibodies impact late stage metastasis

Keywords: advanced metastasis, treatment, activated integrin, patient antibodies

Correspondence: B. Felding-Habermann, The Scripps Research Institute, MEM 150, 10550 North Torrey Pines Road, La Jolla, CA 92037, brunie@scripps.edu

Grant support: NIH grants CA095458, CA112287 to BFH, CBCRP grants 12NB0176 and 13NB0180 to BFH and DOD grant W81XWH-08-1-0468 to BFH, and fellowships from the Swedish Research Council to KS, and from SG Komen to JSK and ML

Acknowledgement: We thank Dr. J. Koziol of The Scripps Research Institute for statistical analyses

All animal work was performed in accordance with NIH guidelines and approved by the Institutional Animal Care and Use Committee of The Scripps Research Institute Animal Resources (AAALAC accredited)

ABSTRACT

Advanced metastatic disease is difficult to manage and specific therapeutic targets are rare. We showed earlier that metastatic breast cancer cells use the activated conformer of adhesion receptor integrin αvβ3 for dissemination. We now investigated if targeting this form of the receptor can impact advanced metastatic disease, and we analyzed the mechanisms involved. Treatment of advanced multi-organ metastasis in SCID mice with patient-derived scFv antibodies specific for activated integrin αvβ3 caused stagnation and regression of metastatic growth. The antibodies specifically localized to tumor lesions *in vivo* and inhibited αvβ3 ligand binding at nanomolar levels *in vitro*. At the cellular level, the scFs associated rapidly with high affinity αvβ3 and dissociated extremely slowly. Thus, the scFvs occupy the receptor on metastatic tumor cells for prolonged periods of time, allowing for inhibition of established cell interaction with natural αvβ3 ligands. Potential apoptosis inducing effects of the antibodies through interaction with caspase-3 were studied as potential additional mechanism of treatment response. However, in contrast to a previous concept, neither the RGD-containing ligand mimetic scFvs nor RGD peptides bound or activated caspase-3 at the cellular or molecular level. This indicates that the treatment effects seen in the animal model are primarily due to antibody interference with αvβ3 ligation. Inhibition of advanced metastatic disease by treatment with cancer patient derived single chain antibodies against the activated conformer of integrin αvβ3 identifies this form of the receptor as a suitable target for therapy.

INTRODUCTION

Advanced multi-organ metastasis is difficult to manage, and therapies could be improved if new functional targets on tumor cells were identified (1). A potential target for inhibition of metastatic growth is the high affinity conformer of adhesion receptor integrin αvβ3. αvβ3 is an important player in tumor angiogenesis, but it also promotes tumor cell adhesion, invasive migration and survival (2-6). The expression of αvβ3 in tumors and the tumor associated vasculature correlates with tumor grade and progression in several tumor types, most prominently in melanoma, glioma, and breast cancer (4;7-10). αvβ3 antagonists, including antibodies, can disrupt tumor-induced angiogenesis in animal models (11-13) and interfere with metastasis promoting tumor cell functions (14-16). We previously documented that the activation state of αvβ3 is critical for supporting metastatic progression and that the high affinity form of αvβ3 identifies a metastatic subset of tumor cells (5). Interestingly, we also found that the immune repertoire of cancer patients can contain anti-tumor antibodies, which specifically react with the activated form of αvβ3. These antibodies are ligand-mimetics of the αvβ3 integrin and carry an Arg-Gly-Asp (RGD) sequence within their CDR-H3 regions (17).

In the present study, we investigated whether targeting the high affinity conformer of integrin αvβ3 with the ligand mimetic antibodies can interfere with advanced metastatic disease. This was examined in immune deficient mice after inducing progressive metastatic burden with human tumor cells expressing high affinity αvβ3. Response to treatment was followed with non-invasive bioluminescence imaging. The observed anti-metastatic properties of the scFv antibodies are due to their ability to specifically and nearly irreversibly bind and inhibit the activated conformer of αvβ3. Thus, activated αvβ3 appears as a suitable target for the inhibition of widespread metastatic disease. The fully human antibodies used in this study and their derivatives, or compounds with similar specific properties, might provide a basis for powerful therapeutic intervention of advanced metastasis.

RESULTS

The main goal of this study was to investigate if the high affinity conformer of tumor cell integrin αvβ3 is a suitable target for inhibition of advanced and widespread metastatic disease. We used human tumor cell models expressing activated αvβ3 in immune deficient mice, and analyzed the ability of patient derived scFv antibodies against this form of the receptor to interfere with advanced metastatic progression.

Antibody binding validation and routes of administration

To test in principle whether targeting activated αvβ3 with the ligand mimetic scFvs interfere with advanced metastatic disease, we chose a phage-displayed format of the antibodies for treatment. By using this format, we took advantage of the tissue penetrating properties of phage and their ability for multivalent antibody display (18). To verify the cell binding characteristics of the phage antibodies, we analyzed each scFv-phage batch for tumor cell binding before using the material for animal treatment. ScFv phage binding was examined on two different tumor cell models, each expressing the activated form of integrin αvβ3, namely M21 human melanoma cells (high αvβ3 expression) and MDA-MB-435 $\beta3_{D723R}$ human breast cancer cells (5) (intermediate αvβ3 expression). Binding of αvβ3 directed scFv1- and scFv5-phage was compared to wild type phage as a control (Fig. 1A). Appropriate routes of administration and *in vivo* distribution of scFv phage were examined in non-tumor bearing mice to assess if and to what extent the antibodies were able to reach major target organs of metastasis, without the bias of tumor burden there. Inoculation of $5x10^{10}$ scFv1 or scFv5 phage intranasally, intravenously or intraperitoneally lead to efficient phage recovery from the lungs, brain, liver, and kidneys of SCID mice 24 hours after scFv injection (Fig. 1B shows scFv5). Intravenous and intraperitoneal routes produced the highest phage titers in the examined organs (>$1x10^8$ phages per gram of tissue). The lowest titer was found in the brain. Having established that scFv phage can reach sites that are most frequently involved in metastasis, we chose the intraperitoneal route for scFv phage treatment of tumor bearing animals, as this route lead to high phage tissue recovery and can be used repeatedly for treatment.

Treatment of metastatic disease with scFv antibodies targeting activated integrin αvβ3

Metastasis was induced in SCID mice by injecting variants of the MDA-MB-435 human metastatic cancer cell line (19;20) into the venous circulation. The tumor cells were stably tagged with Firefly luciferase to follow their growth and response to treatment based on non-invasive longitudinal

measurements by bioluminescence signal of whole body imaging.

Treatment response measurements initially focused on lung lesions because these represented the strongest burden and were consistently found. For the treatment studies, scFv phage purification was optimized to remove endotoxin, and it was verified that phage injection had no adverse side effects. Metastatic lesions were allowed to develop for 56 days before starting i.p. treatment with scFv1 or scFv 5 phage ($5x10^{10}$), given every 48 h (Fig.2A-C) or every 24h (Fig.2D) for a total of 7 days. Lung burden was monitored in each animal over time and measured based on photon flux ($p/s/cm^2$). The fold-change in lesion growth under treatment was calculated by comparing lesion growth during 7 days before treatment and during the 7 days of treatment. After four doses of scFv given every 48h, regression or stabilization of lung lesion growth was seen in 57% of the animals in the scFv1 treatment group, and in 60% of the scFv5 treatment group, while all controls showed continued progression. Representative mice of the Wt phage and scFv1 treatment groups are shown in Figure 2A before, at the beginning, and after treatment. The results indicate that only 4 doses of the ligand mimetic antibodies, given at an advanced disease stage, could impact extensive metastatic burden in the lung and reduce its *in vivo* growth rate. Treatment given every 24h for 7 days (8 doses) and starting with an even heavier lung lesion burden reduced progression of lung burden or stabilized its growth in 75% of mice in the scFv1 group, and in 25% in the scFv5 group (Fig. 2D). All control animals showed continuous lesion progression. The results indicate that targeting the high affinity form of integrin $\alpha v\beta 3$ can impact advanced metastatic burden and slow its growth.

To emulate a clinical situation where patients may present with widespread advanced metastatic disease to multiple organs, and to monitor treatment response of lesions at individual target sites, we injected SCID mice i.v. with a subline of MDA-MD 435 (MDA-MB 435 met) that we selected *in vivo*. This subline expresses intrinsically activated integrin $\alpha v\beta 3$ and consistently causes multiorgan metastasis in SCID mice. All injected mice developed metastatic lesions in multiple target organs, including the brain, lymph nodes, liver, spleen, bone, kidneys and lungs. We selected the animals with the highest tumor burden and the most widespread metastasis for therapy with scFv1 or scFv 5 phage. The animals were treated every 24h for 7 days, and lesion growth was monitored by bioluminescence imaging (Fig. 3). Individual animals had metastases in up to three different organs. In all cases, these included the lung. Interestingly, metastatic lesions in different organs within the same animal showed distinct responses to treatment in several cases (Fig.3A). For example in one animal, burden in the lungs and lymph node did not respond to treatment, but a soft tissue metastasis formed under the lower spine regressed in response to scFv1. Reduced progression or stabilization of lesion growth in the lung and soft tissue

was observed in several animals after only 4 days of treatment (not shown). There was no apparent correlation between lesion size at the beginning of treatment and the ability to respond. In fact, lesions with 1000-fold differences in photon flux intensity were seen to respond in all experiments. Overall, scFv1 treatment reduced progression or lead to stabilization of the highest metastatic burden in 60% of the animals, and scFv5 treatment in 40%. All animals treated with control phage showed continuous progression in individual lesions and overall tumor burden. In some of these cases, scFv treatment substantially reduced (by 80%) or actually eliminated individual lesions after only 3 daily doses (Fig. 3B). For example, treatment with scFv1 caused a dramatic regression of renal metastases together with a decrease or stabilization in lung burden (Fig. 3B). In one case, an adrenal lesion clearly documented before treatment, disappeared and was no longer detectable by non-invasive whole body imaging (Fig. 3B lower panel) or by *ex vivo* imaging of the excised organ. Control treatment with wild-type phage had no effect, and spontaneous regression of established metastases was never observed in mice bearing MDA-MB 435 human breast cancer or other human metastatic cancer cells expressing the activated form of integrin $\alpha v\beta 3$.

An overview of treatment responsiveness and response types is given in Table 1. The results indicate that scFv1 or scFv5 treatment interfered with *in vivo* growth of advanced metastatic lesions in a significant number of animals compared to treatment controls ($p=0.0164$ by Fisher exact test).

In vivo localization of scFv to metastatic lesions and in situ treatment response

Having evidence that scFv1 or scFv 5 treatment directed against the high affinity conformer of integrin $\alpha v\beta 3$ can interfere with advanced metastatic growth, we investigated whether the antibodies actually reached the tumor cells within metastatic lesions to assess whether the tumor cells are direct targets of this treatment. To track the antibodies in lesion bearing animals that had received scFv1 or scFv5, the animals were terminally perfused 24 hours after the last antibody dose and cryosections prepared of control and tumor bearing organs. Tumor cells were identified by staining for human CD44 (21) (dark blue in Fig. 4A), and scFv phage was detected with anti-M13 (brown in Fig. 4A or red fluorescence in 4B). ScFv1 and scFv 5 phage specifically accumulated at metastatic lesions and in their immediate proximity. This was observed in different organs with metastatic burden, but not in non-tumor bearing tissues. Wild type phage, used as a control, did not accumulate at tumor lesions. Non-tumor bearing tissues sporadically showed a faint signal for wild type phage, but not associated with any specific cell type. Figure 4 documents that scFv1 and scFv5 phage localized to lung or lymph node metastases. In some cases, scFv signal was found directly associated with the tumor cells. An example of a lung lesion is shown by deconvolution microscopy in Fig. 4B (bottom row). These results indicate that the ligand mimetic antibodies, directed against the activated conformer of integrin $\alpha v\beta 3$, localized

to advanced metastatic lesions in the mouse model in a therapeutic setting. Integrin αvβ3 is known to be a key player in angiogenesis, and the activated form of the receptor is expressed by sprouting endothelial cells (22). We found that the patient derived antibodies, scFv1 and scFv5, react with the murine antigen (by flow cytometry on proliferating murine endothelial cells and the Bend3 endothelial cell line, not shown). However, there was no difference in micro vessel density within lung tumor lesions in control versus antibody treated animals. This was measured on anti- CD34 stained step sections covering 600-800 μm depth of lung tissue (data not shown). There was a tendency for fewer lesions in the lungs of animals responding to treatment (1-9 lesions) compared to controls (10-25 lesions).

To investigate how scFv treatment targeting the activated conformer of integrin αvβ3 affects lesion development *in vivo*, we studied cell cycle marker expression in lung metastases that responded to scFv treatment. Compared to controls, the number of proliferating Ki67-positive cells was reduced in lesions responding to treatment (Fig. 5A). In addition, the responding lesions showed enhanced infiltration by activated macrophages (F4/80 signal) (Fig. 5B). The results indicate that scFv treatment affected the growth rate of metastatic lesions at the cellular level and involved host cell responses. These responses may have potentially helped to clear apoptotic or dead tumor cells, which were only rarely detected (not shown).

Inhibition of receptor-ligand binding at the molecular level

To investigate mechanisms involved in the observed treatment responses, we studied the interactions of the ligand-mimetic antibodies and αvβ3 at the molecular and cellular levels.

To assess molecular interactions between integrin αvβ3 and the scFv antibodies, we analyzed their ability to interfere with ligand binding to the purified receptor. Vitronectin, fibronectin and fibrinogen are natural ligands of αvβ3 in extracellular matrices and plasma. A hallmark characteristic of the activated conformer of αvβ3 is that the receptor can recognize these ligands as soluble proteins. Incubation of the biotinylated proteins with immobilized αvβ3 in the presence of cations and increasing concentrations of the antibodies showed that scFv 1 and scFv 5 efficiently interfered with αvβ3 ligand binding (Fig. 6A). The half maximal inhibitory concentrations (IC_{50}) for scFv 1 were 1.25 nM for vitronectin, 0.71 nM for fibronectin, and 0.35 nM for fibrinogen. For scFv 5, the IC_{50} values were 25 nM for vitronectin, 12.5 nM for fibronectin, and 10.7 nM for fibrinogen. ScFv20 used as a control antibody failed to inhibit. While patient derived scFv antibodies scFv 1 and scFv 5 contain the RGD integrin binding motif within their CDR-H3 regions and are specific for αvβ3, scFv 20 lacks the RGD motif, does

not block function and detects αv integrins regardless of their β subunit association (17). The results demonstrate that scFv1 and scFv 5 have a high affinity for αvβ3 and compete very effectively with ligands binding to this receptor.

Characteristics of scFv binding to human tumor cells expressing activated integrin αvβ3

To understand inhibitory activities of scFv1 and scFv5 on tumor cell functions that rely on integrin αvβ3 and might promote metastasis, we analyzed interaction between the scFvs and tumor cell expressed αvβ3. Integrin binding of natural ligands in their soluble form requires the high affinity state of the receptor (23). Furthermore, tumor cells within target tissues interact dynamically with components of the extracellular matrix and derive signals from their matrix environment for survival and growth. To investigate the binding characteristics of tumor cell expressed high affinity αvβ3 and the ligand mimetic scFvs, we analyzed cellular association and dissociation. All scFv cell binding experiments were carried out at 0°C to prevent internalization. Flow cytometry binding analysis of fluorescinated scFv5 protein and MDA-MB 435 human breast cancer cells, expressing either activated high-affinity $\alpha v\beta 3_{D723R}$ or non-activated $\alpha v\beta 3_{WT}$, indicated that the ligand-mimetic antibody depended on αvβ3 activation for efficient binding. Binding was experimentally maximized in the presence of Mn^{2+} (Fig. 6B, left panel), a cation known to induce a high affinity state in integrin heterodimers (24-26). Using a Mn^{2+} concentration (25 μM) that supports suboptimal (75%) scFv5 binding to tumor cells expressing the intrinsically activated receptor ($\beta 3_{D723R}$ mutant), we titrated the antibody to determine binding saturation. Saturable binding in the presence of divalent cations indicated specificity and cation dependence (Fig. 6B, right panel). These findings underscore the ligand mimetic nature of the scFv antibodies and define conditions suitable to determine cellular association and dissociation of the antibodies. The association and dissociation characteristics are important for understanding the therapeutic potential of the antibodies and their ability to interfere with established αvβ3 ligand interactions. Such interactions support tumor cell integration and growth within target tissues of metastasis.

Using tumor cells expressing intrinsically activated $\alpha v\beta 3_{D723R}$ and 25μM Mn^{2+}, we found that the ligand mimetic antibodies scFv1 and scFv5 exhibit a fast cellular association rate, with half maximal binding observed after 5 min, the earliest measured time point (shown for scFv 5 in Fig. 6C, left panel). In contrast, scFv dissociation after binding saturation was exceedingly slow, with only 22% binding loss after 160 min, whereas binding of fibrinogen, a natural ligand of αvβ3, was reduced by 50% after 60 min, and 88% after 120 min (Fig. 6C, right panel). These results indicate that the ligand mimetic antibodies can occupy the receptor efficiently and stay bound for prolonged periods of time. Thereby

the antibodies may displace natural ligands that dissociate off the receptor. Based on these properties, the antibodies efficiently interfere with dynamic αvβ3 mediated cell adhesive functions during cell migration and invasion as previously seen *in vitro* (17). Importantly, the observed scFv cell binding characteristics likely enable the antibodies to interfere with tumor cell behavior *in vivo* and to disrupt established tumor cell adhesion mediated by integrin αvβ3.

Analysis of caspase-3 activation by the RGD-containing scFv antibodies

The *in vivo* responses to treatment with the αvβ3 ligand-mimetic scFv antibodies may have diverse underlying reasons. The antibodies could exert their therapeutic effects primarily through their ligand-mimetic nature interfering with αvβ3 ligand binding. However, additional mechanisms may also be involved. We previously showed that scFv 1 and scFv 5 are internalized by tumor cells expressing activated integrin αvβ3 and induce apoptosis (17). We therefore reasoned that the internalized RGD-containing scFvs might interact with intracellular proteins, such as the apoptosis inducing caspase-3. Caspase-3 contains a putative RGD binding site, close to its Asp^{175} cleavage site (Asp-Asp-Met, DDM) (27;28). Intriguing results suggested that cell internalized RGD peptides might induce apoptosis by directly binding and activating caspase-3 (27;29;30). To explore if such a mechanism might be involved in the observed anti-metastatic properties of the RGD containing scFv antibodies, we verified that the tumor cells used in our treatment study expressed caspase-3, and analyzed if the scFvs could interact with caspase-3 and activate the enzyme.

We confirmed caspase-3 expression in MDA-MB-435 human tumor cells used in our *in vivo* treatment study express (Fig. 7A). MCF7 cells lacking caspase-3 (31) were used as negative control, and SKBr3 (32) as positive control. To investigate if RGD containing scFv 1 and scFv 5 can directly bind caspase-3, we analyzed whether the scFvs immuno-precipitate caspase-3 from tumor cell lysates, or if the scFvs - added to tumor cell lysates - could be co-immunoprecipitated with anti-caspase-3. We found no evidence of scFvs caspase-3 interaction (not shown). Furthermore, we found no interaction between recombinant caspase-3 and RGD-containing scFv1 or scFv5 by ELISA under various cation conditions known to affect RGD binding (Fig. 7B).

Once internalized by cells, RGD-containing proteins might transiently interact with caspase-3 in a biologically relevant but difficult to detect manner. Considering the therapeutic effects on metastatic growth by the RGD-containing scFvs in our animal model, we therefore investigated whether the scFvs could contribute to caspase-3 activation in cell lysates and by using recombinant human caspase-3 protein. Hypotonic lysates of 293A cells, deprived of mitochondria and containing caspase-3, were

readily activated by addition of cytochrome c and dATP to form apoptosomes that can activate caspase-3 (Fig. 7C,D). Cofactors in these gently generated lysates promote the stability of procaspase-3 and support its activation. In contrast, RGD-containing scFv 5, or RGD peptides, showed no induction of caspase-3 activity over RGE-containing scFv Mut5, or RAD, as negative controls. Similar results were obtained despite increasing scFv concentrations, and after investigating the kinetics of caspase-3 activation by continuous measurement of substrate cleavage over time (Fig. 7D). Likewise, reducing the complexity of the assay system further and using recombinant caspase-3 to ensure that the reaction and potential interaction between caspase-3 and scFv antibody was not influenced by components present in cells or cell lysates, did not reveal RGD induced caspase-3 activation (Fig.7D right). Thus, these results make it very unlikely that the internalized RGD-containing antibodies scFv1 or scFv5 induce apoptosis by direct activation of caspase-3. We therefore conclude that the inhibitory properties and *in vivo* treatment effects, that the antibodies exerted on tumor cells expressing the activated conformer of integrin $\alpha v\beta 3$ and their metastatic lesions, are most likely based on the ability of the antibodies to interfere efficiently with ligand binding to the target integrin.

DISCUSSION

Metastatic disease is mainly treated with chemotherapy to halt tumor growth or with specific inhibitors of receptors and pathways to interfere with tumor cell viability. Development of effective combinations of such therapies and discovery of new targets are urgently needed to improve therapeutic responses.

Our study explored the high affinity, activated conformer of integrin αvβ3 on metastatic tumor cells as a functional target for therapy with human antibodies that specifically recognize and block this form of the receptor. We showed earlier that a metastatic subset of human tumor cells expresses the activated integrin and uses this form of the receptor for successful early steps of dissemination to distant organs (5). Interestingly, the immune repertoire of cancer patients contains antibodies that recognize the high affinity form of αvβ3. These antibodies mimic natural ligands of the receptor through expression of an RGD integrin-binding motif within CDR-H3 of the antigen recognition site. This feature is combined with specificity for αvβ3 (17).

Integrin αvβ3 is expressed by certain invasive tumor types, such as metastatic melanoma, glioma, and breast cancer (7-10;13). The receptor is also present on angiogenic blood vessels (3) and serves as an important mediator to secure blood supply for tumor growth. As on metastatic tumor cells, αvβ3 is activated on angiogenic blood vessels (33) and potentially fulfills similar growth promoting and invasive functions of the sprouting endothelial cells. Integrin αvβ3 antagonists, targeting the receptor regardless of its functional activation state, have been used in animal models and recently in cancer patients, to curb angiogenesis and slow tumor growth (34). In the clinic, antibodies against αvβ3 and a cyclic peptide-based inhibitor of αvβ3 and αvβ5 have shown varying effects (14). MEDI-522, a second generation humanized anti-αvβ3 mAb showed low toxicity and induced stable disease in some patients with renal metastasis (35).

Generally, integrin ligation supports signal transduction that promotes cell survival, migration and proliferation (36). Transient expression of the high affinity form of certain integrins in normal cells is tightly regulated and necessary for specific functions. These include leukocyte and platelet interaction with the vessel wall during immune reactions and hemostasis (37). Expression of activated αvβ3 and the constitutive presence of the high affinity receptor on disseminating tumor cells may be key for metastatic progression. Thus, therapeutic targeting of the high-affinity conformer of αvβ3 could offer a focused strategy for interfering with metastatic growth and angiogenic support. Here, we show that treatment of experimental mice with advanced metastatic disease induced by human tumor cells expressing activated αvβ3, can stabilize lesion growth and block progression. We applied scFv fragments of patient derived antibodies against the high affinity form of αvβ3 displayed on phage. This

approach increases scFv valency and *in vivo* half-life. It also takes advantage of the phage tissue penetration properties. In the clinic, this format may not be not preferred but could be replaced with multivalent scFvs, Fab fragments or whole IgG, possibly coupled to toxins or effector molecules (38). The scFv format could be helpful for diagnosis and tumor cell tracing to report metastatic disease because of the low molecular weight of the scFvs (27 kDa) and their rapid clearance from the circulation and tissues (18;39).

Characterizing mechanisms involved in the observed therapeutic response of advanced metastasis to treatment with scFvs against high affinity integrin $\alpha v\beta 3$, we found that the antibodies specifically localize to metastatic lesions and inhibit $\alpha v\beta 3$ ligand binding in the nanomolar range. The scFvs associate rapidly with $\alpha v\beta 3$ on tumor cells and, in contrast to natural ligand, dissociate extremely slowly. This finding supports the concept that the scFvs may displace natural ligand from the receptor and block the integrin efficiently. This is relevant during adhesion and migration when $\alpha v\beta 3$ temporarily dissociates from its natural ligands. Through this mechanism, the scFvs likely exert long-term inhibitory functions and may effectively impact tumor cell survival and growth mediated by high affinity $\alpha v\beta 3$. In addition to inhibiting activated $\alpha v\beta 3$ on tumor cells, the scFvs might interfere with tumor angiogenesis. We found that the ligand mimetic scFvs react with the murine receptor. However, we did not see differences in microvessel density in lesions of control versus antibody treated animals.

It is well known that RGD-containing peptides can induce apoptosis by binding to integrins and blocking their functions. Several intriguing reports suggested an additional mechanism through which RGD-containing molecules might impact tumor cell survival (27;29;30). Upon cell internalization, RGD peptides were proposed to interact with an RGD-binding site within procaspase-3 (27;28). It was claimed that interactions between the RGD-binding site and RGD-peptides could induce auto-activation of caspase-3. In fact, we showed earlier that tumor cells expressing activated $\alpha v\beta 3$ can internalize the ligand mimetic scFvs used in this study and respond with apoptosis (17). However, here we did not detect any interaction between caspase-3 and the scFvs or RGD-peptides. In addition, we found no evidence for procaspase-3 activation in cell lysates or using recombinant caspase protein. It is therefore very unlikely that the RGD-containing scFv antibodies exerted their treatment effects on advanced metastatic lesions through direct induction of caspase-3 activity.

Together, our results indicate that the high affinity conformer of integrin $\alpha v\beta 3$, expressed by a metastatic subset of human tumor cells, is a promising target for inhibition of advanced and widespread metastatic disease. The activated receptor can be efficiently blocked with antibodies from the cancer patient immune repertoire which interfere with metastatic growth.

MATERIALS AND METHODS

scFv protein and phage production and preparation for *in vivo* use

ScFv antibodies directed against activated integrin $\alpha v\beta 3$, svFv1 and scFv 5, (17) were displayed as pIII fusion proteins on M13 bacteriophage and expressed in E. coli. Phage or scFv protein were purified as described (40). For *in vivo* use, endotoxin was removed from phage preparations by repeated phase separations using 1% Triton X-114 (41). Phage was further purified on protein purification spin columns (Pierce, Rockford IL) and sterile filtered. Phage titer was determined by infecting *E.coli* TG1 with serial dilutions ($1x10^4$ - $1x10^{10}$ fold) and enumerating colonies on carbenicillin containing agar plates. Phage titers were generally around 10^{11}/ml.

In vivo Phage distribution

Phage were injected i.v, i.p or applied intranasally into non-tumor bearing mice to determine phage organ distribution. For intranasal gavage, a phage volume of 10µl was administered directly into the nostrils in 2 µl increments over 5 min. The organs were harvested and weighed 24h after phage injection, homogenized in PBS, washed and serially diluted to infect bacteria before counting carbenicillin resistant colonies to calculate the number of phages per gram of tissue.

Analysis of scFv cell binding by flow cytometry

Before use in animals, each scFv phage batch was analyzed by flow cytometry for binding to tumor cells expressing high affinity integrin $\alpha v\beta 3$ in the presence of Ca^{2+} (17). Phage-ScFvs were used at a concentration of $5x10^8$ in TBS and incubated with cells on ice, followed by murine anti-M13 mAb 10µg/ml (Exalpha Biologicals, Watertown, MA) and goat FITC-anti mouse 1:50 (Zymed, San Francisco, CA).

In vivo treatment of metastatic disease

Advanced metastatic burden for analysis of treatment response was induced by tail vein injection of 6-8 week old CB.17 SCID mice with $1x10^5$ – $2.5x10^5$ luciferase tagged MDA-MB 435 or MDA-MB 435-met cells (*in vivo* selected for enhanced metastatic activity). scFv phage were prepared freshly for each experiment and binding activity validated. Mice were assigned to experimental groups based on non-invasive imaging (photon flux as p/s/cm^2) (IVIS 200, Caliper Lifesciences, Alameda, CA) so that control

and scFv treatment groups included animals with a similar range of metastatic burden. Under treatment, location and extent of lesion growth were again monitored by bioluminescence imaging, followed by histology.

Deeply anesthetized mice were terminally perfused through the ascending aorta with saline followed by 4% paraformaldehyde (PFA). The perfused organs were post-fixed in para formaldehyde for 4h before transfer into 25% sucrose in phosphate buffer. Frozen tissues were cryo sectioned (35 μm) and stored in cryoprotective solution at -20°C. For analyses of phage tissue distribution and phage titer, animals were euthanized 24h after the last phage injection (i.v., i.p., or intranasal) and organs were weighed and homogenized, followed by infection of bacteria with the extracts. The numbers of carbenicillin resistant colonies (bacteria infected with phage) were counted, and phage count was normalized to phages per gram of tissue. All animal work was performed in accordance with The Scripps Research Institute Animal Resources (AAALAC accredited).

Definition of treatment response and statistical analysis

Late stages of metastatic growth present a high level of complexity and variations in the extent and distribution of metastatic burden from experimental animal to animal. Therefore, we chose analysis criteria similar to “Response Evaluation Criteria in Solid Tumors” (42-44). These criteria are used in clinical trials for treatment of advanced metastatic disease to assess individual treatment responses. Treatment responses were evaluated based on longitudinal measurements of tumor cell signal by non-invasive bioluminescence imaging of metastatic burden, before and during treatment in each animal. If, in a given experiment, an animal was treated for 7 days, then lesion growth during the 7-day period before treatment was compared to lesion growth during the 7 days of treatment. The difference in tumor growth before and during treatment was calculated. The resulting fold-changes were defined as: Progression (>1.3 fold), Stabilization (0.7-1.3 fold), Reduced Progression (0.1-0.7 fold), or Regression (<0.1 fold). It was then determined how the animals in each group distributed between the response categories. For comparison of responses between the three treatment groups, scFv1, scFv5, and wild type phage as control, we note that the overall likelihood ratio chi-squared statistic with 6 degrees of freedom may be partitioned into two independent components, each with 3 degrees of freedom: the first component corresponds to comparison of ScFv1 vs. ScFv5, and the second component corresponds to the comparison of controls to the pooled ScFv1/ScFv5 category (45). We report Fisher exact tests for these component comparisons.

Immunohistochemistry

To detect scFv phage in tumor lesions, free floating tissue sections were quenched with 3% H_2O_2 (in case of DAB staining) and blocked with goat serum for 1h, before adding a primary antibody against human CD44 (Mab 29.7) kindly provided by Jim Quigley, TSRI (21), or M13 phage (anti-M13, Exalpha Biologicals Inc. Watertown, MA). After overnight incubation and washing, sections were incubated for 2 h with anti-mouse HRP/Alexa Fluor-594 (Invitrogen/Molecular Probes), washed again and placed onto slides for incubation with 3.3-diaminobenzidine as a chromogen for HRP (BD Biosciences). Zink fixed tissues were de-paraffinized and antigen retrieval performed in 1mM EDTA for 15 min at 100 °C followed by treatment as above. Tissues were incubated with primary antibodies anti-mouse F4/80 (Cedarlane) or anti-human Ki67 (BD Pharmingen) for 1h, followed by HRP-anti rat (Jackson Immunoresearch) or biotinylated anti-mouse (Vector Laboratories Inc.) antibodies respectively. Following the biotinylation step, tissues were treated with the vectastain ABC kit and all samples were subsequently treated with the peroxidase substrate Vector SG (Vector Laboratories Inc.). Slides were analyzed and images deconvoluted using an AxioImager M1m microscope and AxioVision 4.6 software (Zeiss, Thornwood, NY).

ScFv and ligand binding to purified αvβ3 receptor protein

Biotinylated natural ligands of αvβ3: vitronectin (VN), fibronectin (FN) or fibrinogen (Fg) (10µg/ml) were incubated with purified immobilized αvβ3 receptor protein in TBS containing Ca^{2+}, Mg^{2+}, and Mn^{2+} (1mM each), in the presence of increasing concentrations of purified scFv protein. A non-function blocking scFv directed against the integrin αv subunit, scFv 20, was used as a control. Ligand binding was measured after 1 h at 30˚C using alkaline phosphatase-conjugated goat-anti-biotin antibody, followed by a colorimetric substrate reaction.

Antibody cell binding kinetics

To define conditions for half maximal scFv binding, MDA-MB-$435_{\beta3D723R}$ cells were incubated with purified FLAG-tagged scFv protein in increasing concentrations of Mn^{2+} (3.75 µM-100 µM). Binding was measured by flow cytometry with murine M2 anti-FLAG antibody (Sigma, St. Louis, MO) followed by FITC anti-mouse (Pierce). Using the Mn^{2+} concentration (25 μM) that yielded half maximal scFv binding, scFv binding saturation was then measured by incubating MDA-MB-$435_{\beta3D723R}$ cells for 1h with increasing concentrations of directly FITC-labeled scFv 5 protein (2.34µg/ml-150µg/ml). The kinetics of scFv cell association and dissociation were analyzed by flow cytometry with directly FITC-

labeled scFv protein at half maximal Mn^{2+} concentration and saturating scFv concentration, using MDA-MB-$435_{\beta 3D723R}$ cells. Association time was measured after removing unbound ligand in 10 min intervals. To determine dissociation, cells were first allowed to bind scFv for 1 h to reach binding saturation, after which unbound ligand was removed and the cells washed, before measuring remaining bound scFv in 10 min intervals. FITC-labeled fibrinogen (Fg) was used as a natural ligand for comparison. All incubations were done on ice using ice-cold buffers to prevent scFv or ligand internalization.

Western blot analysis and Immunoprecipitation

To study scFv caspase-3 interaction, tumor cells were lysed in RIPA buffer and equal amounts of protein separated, blotted, and detected with rabbit-anti-caspase-3 antibody Sc7148 (Santa Cruz) followed by goat-anti-rabbit-IgG/HRP conjugate (Zymed, San Fransisco, CA). Caspase-3 was immunoprecipitated from cell lysates in the presence of protease inhibitors (Roche complete Mini tablet, EDTA-free and 2 mM PMSF) using goat-anti-caspase-3 antibody Sc1225 (Santa Cruz) and protein G sepharose beads. Control lysates were incubated with Protein G beads only. Precipitated proteins were analyzed on 4-20% SDS-PA gels, blotted and detected with rabbit-anti-caspase-3 and goat-anti-rabbit-IgG/ HRP conjugate. Interaction between scFv antibodies and caspase-3 was analyzed by co-immuno precipitation using anti-caspase-3 as above. Flag-tagged scFv 5, or scFv Mut 5 (RGE mutant of scFv 5) as control, were added to cell lysates before western blotting with mouse-anti-Flag, followed by donkey-anti-mouse-IgG. Controls included IP without scFv antibodies, addition of scFv 5 but no goat-anti-caspase-3 antibody, and a combination of beads, lysis buffer (instead of lysate) and either scFv 5 or scFv Mut 5.

ELISA-based analysis of caspase-3 and scFv interaction

To analyze binding of caspase-3 to the scFv antibodies, 96-well plates were coated with recombinant procaspase-3 (BioVision, Moutain View, CA), blocked, and incubated with Flag tagged scFv 5 or scFv Mut 5 (non RGD containing control) in the presence of 2mM $MnCl_2$. Binding was measured after incubation with mouse-anti-Flag (Sigma) and donkey-anti-mouse-IgG (Jackson Immuno Research Laboratories, West Grove, PA).

Activation of caspase-3 in hypotonic cell lysates

Activation of caspase-3 in hypotonic lysates of 293A cells or as recombinant protein was measured at

end points using the Caspase-Glo 3/7 Assay (Promega) and caspase-3/7 specific peptide sequence Asp-Glu-Val-Asp (DEVD). Hypotonic cell lysates were pepared as desribed (46). Cell lysates were combined with scFv 5 or scFvMut 5, or with RGD or RAD peptides. Cytochrome c/dATP was used as positive control and PBS as negative control. Samples were incubated for 1 h at 37˚C, before adding Glo reagent (Promega, Madison, WI) and measuring bioluminescence as relative light units (RUL). GRGDNP was used as RGD peptide and GRADSP as RAD control as reported (27). Chromogenic substrate reactions were used for continuous measurements of caspase-3 activity. Hypotonic cell lysates were combined with scFv 5 or scFv Mut 5, and DEVD-pNA was added in excess to monitior absorption at 405 nm every 20 s for 2 h at 37˚C. Cytochrome c/dATP was used as positive control. Maximum reaction velocity (V_{max}) was determined by graphing absorption versus time using the linear graph parts.

Activation of recombinant caspase-3

Recombinant procaspase-3 was expressed in *E. coli* and His-tag purified as described (47). Recombinant procaspase-3 was incubated with scFv 5, or scFv Mut 5 as control, in caspase assay buffer (50 mM HEPES, pH 7.5, 150 mM NaCl, 0.1% CHAPS, 10% sucrose, 10 mM DTT) in the presence of 1 mM Mg^{2+}. Granzyme B was used as a positive control. Activity was measured based on bioluminescence signal 30 min after adding Glo Reagent. For continuous measurement of recombinant caspase-3 activity, recombinant procaspase-3 was incubated with scFv 5, or scFv Mut 5 as negative control, in PBS with 10 mM DTT, with or without 4 mM $MgCl_2$ for 15 min at 37˚C. Ac-DEVD-AFC (100 µM final) was added as fluorgenic caspase-3 substrate and fluorescence measured continuously for 30 min. V_{max} was determined by graphing fluorescence against time.

FIGURE LEGENDS

Figure 1

Antibody binding validation and routes of administration

(A) Before use in animals, the binding properties of each scFv phage batch were analyzed by flow cytometry on tumor cells expressing high affinity integrin $\alpha v\beta 3$. scFv phage was tested in the presence of calcium on M21 human melanoma cells that carry activated αvβ3 and on MDA-MB 435 cells which express mutant $\alpha v\beta 3_{D723R}$. **(B)** scFv phage organ distribution in the mouse model. Phage were injected i.v., i.p. or applied intranasally to non-tumor bearing mice to determine phage organ distribution 24 h later.

Figure 2

Lung metastases regress in response to treatment with scFv 1 or scFv 5.

F-luc tagged MDA-MB-435 cells were injected i.v. and lesion development monitored by non-invasive bioluminescence imaging (photons/second/cm^2) over time. Treatment with scFv phage ($5x10^{10}$ per dose) started on day 56 post tumor cell injection. **(A)** Non- invasive bioluminescence imaging of representative animals before treatment on day 49, at treatment onset on day 56, and after 4 doses of treatment on day 63. Reduced progression in lung lesions is seen after treatment with scFv1 but not with Wt-phage. **(B)** Response to treatment given every 48 h (4 doses). Fold-changes of lesion growth were calculated based on growth during 7 days before treatment compared to 7 days under treatment. ScFv1-phage treatment yielded a 57% animal response rate in lung burden and one animal with stabilization of lesion growth. ScFv5-phage treatment resulted in a 60% animal response rate for lung burden. Wt-phage gave no reduction in tumor growth. **(C)** *Non*-invasive bioluminescence imaging of lung burden (photons/second/cm^2) over time before and during treatment. Animals were treated every 48h for (4 doses). Lung lesion growth was monitored pre-treatment (day 49-56) and during treatment until day 63 (the end of treatment). Dashed vertical lines indicate the start of treatment on day 56. Animals responding to treatment are colored. **(D)** Response to treatment given every 24h (8 doses) to animals with very advanced metastatic burden. Treatment with Wt-phage gave no response, whereas regression and reduced tumor progression was seen in the scFv treated animals. ScFv1-phage treatment yielded a response in 75% of the animals, and scFv5-phage in 25%. Animals responding to treatment are colored.

Figure 3

Advanced multi-organ metastases in the lung and soft tissues can regress or stabilize after treatment with scFv 1 or scFv5.

(A) *F-luc* tagged, *in vivo* selected and highly metastatic MDA-MB-435-met cells were injected i.v. to induce multiorgan metastasis. Metastatic progression was monitored by non-invasive bioluminescence imaging (photons/second/cm^2) over time. Animals with the largest tumor burden were selected for daily treatment with either scFv5-phage, or scFv1 phage for 7 days, beginning on day 41. Wt-phage was used as control. Metastases at individual sites showed reduced progression or a stabilization of lesion growth in response to scFv1 or scFv5 treatment. Fold-change in lesion growth was calculated for individual lesions during an equal number of days before treatment and under treatment. Animals responding to treatment are colored. The control group treated with Wt phage did not show tumor regression. Bars represent lung metastatic burden, except where specified otherwise. Tumor lesions originating in the same animal are denoted with an * or $^{\#}$. Lesions were frequently found in the liver, adrenal glands, lymph node, lung, brain, and within soft tissues below the spine. **(B)** Examples of animals with regression in both lung and renal metastases in response to 3 daily doses of scFv 1. Lung metastatic burden partially regressed or stabilized in the treated group and renal metastases regressed considerably. Wild type (wt)-phage treatment had no effect. Fold-change in metastatic burden shown for tumor growth before and during treatment. *In vivo* images confirm regression of renal lesion signal.

Figure 4

Localization of scFv1 or scFv 5 phage to areas in and around metastatic lesions in mice with multi-organ metastasis.

(A) Immunohistochemical detection of phage homing to metastases in the lungs and lymph node. ScFv phage, or wt control phage, were injected i.p. daily for 7 days into tumor bearing mice. 24h after the last scFv dose, the animals were terminally perfused and frozen tissue sections stained with mAb 29.7 (dark blue), specific for human CD44 indicating the tumor cells, and anti-M13 mAb to detect phage (DAB, brown). Animals treated with wt-phage did not show phage localization to tumor metastases (left panels), but lung metastasis from scFv5-phage treated animals showed phage localization in the tumor proximity as well as within the lung lesion (middle). A lymph node metastasis from an animal treated with scFv1-phage showed phage localizing to the tumor bulk as well as to the outer border of the lesion (right). Controls treated with secondary antibody and substrate did not show specific staining in or around any lesions. Scale bars indicate 100µm. **(B)** Fluorescence microscopy detecting phage (red). (Upper row) M13 phage was detected in and around lung metastases of scFv1-phage treated animals (right), as well as within the near proximity of the tumor lesions (second right), with minimal phage

signal in the unaffected lung tissue away from a tumor lesion (left). Lymph node metastasis showed scFv1-phage localization in the tumor mass and within the tumor proximity (second left, top and bottom). Animals treated with wt-phage showed no specific staining in tumor lesions. Only a weak signal was sometimes seen in non-tumor bearing parts of the tissues, comparable to that seen for scFv phage in unaffected areas of lung tissue (lower left). Using optical sectioning and deconvolution of *z*-stack images, scFv phage was specifically detected associated with tumor cells (lower second right). Scale bars indicate 100 µm.

Figure 5

Effects of scFv treatment on tumor cells in vivo and host cell infiltration

(A) Ki67 staining on lung metastases treated with wt-phage or scFv1/5-phage (top panel). Lesions in animals responding to treatment showed fewer proliferating cells. Nuclear staining with contrast green (middle), H&E staining (lower panel). **(B)** F4/80 macrophage staining of lung metastases in mice treated with wt-phage or scFv1/5-phage. An increased infiltrate was seen in lesions responding to treatment. Scale bars indicate 100 µm in all sections.

Figure 6

Inhibitory and binding properties of scFv 1 and scFv5.

(A) Biotinylated natural ligands of αvβ3: vitronectin (VN), fibronectin (FN) or fibrinogen (Fg) (10µg/ml) were incubated with purified immobilized αvβ3 receptor protein in TBS containing Ca^{2+}, Mg^{2+}, and Mn^{2+} (1mM each), in the presence of increasing concentrations of purified scFv protein. A non-function blocking scFv directed against the integrin αv subunit, scFv 20, was used as a control. **(B)** Flow cytometric binding analysis of fluorescinated scFv5 protein and MDA-MB 435 human tumor cells, expressing either activated high-affinity $\alpha v\beta 3_{D723R}$ or non-activated $\alpha v\beta 3_{WT}$. Binding was experimentally maximized in the presence of Mn^{2+}, known to induce a high affinity state in integrin heterodimers. Using a Mn^{2+} concentration (25 µM) that supports suboptimal scFv5 binding to tumor cells expressing activated $\alpha v\beta 3_{D723R}$, antibody was titrated to determine binding saturation. **(C)** Kinetics of scFv cell association and dissociation were analyzed by flow cytometry with FITC-labeled scFv protein at half maximal Mn^{2+} concentration and saturating scFv concentration, using MDA-MB-$435_{\beta 3D723R}$ cells. (Left) Association time was measured after removing unbound ligand in 10 min intervals. (Right) Dissociation was determined after allowing cells to bind scFv for 1 h to reach binding saturation, followed by removal of unbound ligand, washing and measuring scFv that remained bound in 10 min intervals. FITC-labeled fibrinogen (Fg) was used as a natural ligand for comparison. All incubations were done

on ice using ice-cold buffers to prevent scFv or ligand internalization. No binding was detected in the absence of divalent cations.

Figure 7

Caspase-3 expression in the target tumor cells and analysis of caspase-3 binding and activation by RGD-containing scFv1 and scFv5.

(A) (Top) Western blot analysis of caspase-3 expression in MDA-MB-435, MCF-7 (negative control) and SKBR-3 (positive control) cells. (Bottom) Verification for procaspase-3 by immunoprecipitation of caspase-3 from tumor cell lysates. **(B)** ELISA-based analysis of caspase-3 and scFv antibody interaction. Plates were coated with recombinant pro-caspase-3 or BSA (negative control) or scFv 5 (positive control). Addition of RGD-containing scFv 5 or RGE-containing scFv Mut 5 antibody, at concentrations as indicated showed no specific binding to caspase-3. **(C)** Analysis of caspase-3 activation by scFv antibodies. Hypotonic cell lysates, depleted of mitochondria, were combined with either scFv 5 or scFvMut 5 (4 µM), or RGD or RAD peptides (1 mM) (left panel). Cytochrome c/dATP were used as positive control and PBS as negative control in a bioluminescence assay. Cytochrome c and dATP were able to activate caspase-3 in the lysates, whereas all other samples showed only background signal. A higher scFv concentration was used to verify the lack of activation (10 µM) in the presence of Mg^{2+} (right panel). **(D)** Continuous measurement of caspase-3 activity in cell lysates based on chromogenic substrate reaction. Cleavage of colorimetric capsase 3 substrate N-acetyl-Asp-Glu-Val-Asp-*p*-nitroanilide (Ac-DEVD-*p*NA) was measured after combining hypotonic cell lysates with either scFv 5 or scFvMut 5 (2 µM). Absorption was measured continuously for 2 h at 37˚C (left panel). Activation measurement of recombinant caspase-3 by scFv 5 or scFvMut 5 in the presence of Mg^{2+} using Granzyme B as positive and PBS as negative control. After 30 min incubation at 37˚C, Glo reagent was added and bioluminescence measured after 30 min incubation at RT (right panel).

Table 1

Response categories:

Fold-changes in lesion growth, p/sec/cm^2, comparing same time span before and under treatment

Progression: $\geq$ 1.3 fold

Stabilization: 0.7 fold - 1.3 fold

Reduced progression: 0.1 fold - 0.7 fold

Regression: $\leq$ 0.1 fold

Response category	**ScFv1**	**ScFv5**	**Control**
Progression	7/19	9/15	15/16
Stabilization	4/19	1/15	1/16
Reduced Progression	4/19	3/15	0/16
Regression	4/19	2/15	0/16

Compared to controls, treatment response was seen in a significant number of animals receiving scFv1 or scFv5 ($p= 0.0164$, Fisher exact test). There was no significant difference between responses to scFv1 compared to scFv5 ($p=0.55$, Fisher exact test).

For comparison of responses between the three groups, scFv1, scFv5, and controls, we note that the overall likelihood ratio chi-squared statistic with 6 degrees of freedom may be partitioned into two independent components, each with 3 degrees of freedom: the first component corresponds to comparison of scFv1 vs scFv5, and the second component corresponds to the comparison of controls to the pooled scFv1/scFv5 category (45).

References

(1) Steeg PS (2008) Heterogeneity of drug target expression among metastatic lesions: lessons from a breast cancer autopsy program. Clin Cancer Res 14(12): 3643-3645.

(2) Cooper CR, Chay CH, Pienta KJ (2002) The Role of alpha(v)beta(3) in Prostate Cancer Progression. Neoplasia 4(3): 191-194.

(3) Brooks PC, Montgomery AM, Rosenfeld M, et al. (1994) Integrin alpha v beta 3 antagonists promote tumor regression by inducing apoptosis of angiogenic blood vessels. Cell 79(7): 1157-1164.

(4) Lim M, Guccione S, Haddix T, et al. (2005) alpha(v)beta(3) Integrin in central nervous system tumors. Hum Pathol 36(6): 665-669.

(5) Felding-Habermann B, O'Toole TE, Smith JW, et al. (2001) Integrin activation controls metastasis in human breast cancer. Proc Natl Acad Sci U S A 98(4): 1853-1858.

(6) Desgrosellier JS, Barnes LA, Shields DJ, et al. (2009) An integrin alpha(v)beta(3)-c-Src oncogenic unit promotes anchorage-independence and tumor progression. Nat Med.

(7) Albelda SM, Mette SA, Elder DE, et al. (1990) Integrin distribution in malignant melanoma: association of the beta 3 subunit with tumor progression. Cancer Res 50(20): 6757-6764.

(8) Gingras MC, Roussel E, Bruner JM, Branch CD, Moser RP (1995) Comparison of cell adhesion molecule expression between glioblastoma multiforme and autologous normal brain tissue. J Neuroimmunol 57(1-2): 143-153.

(9) Gladson CL, Hancock S, Arnold MM, Faye-Petersen OM, Castleberry RP, Kelly DR (1996) Stage-specific expression of integrin alphaVbeta3 in neuroblastic tumors. Am J Pathol 148(5): 1423-1434.

(10) Ding Q, Stewart J, Jr., Olman MA, Klobe MR, Gladson CL (2003) The pattern of enhancement of Src kinase activity on platelet-derived growth factor stimulation of glioblastoma cells is affected by the integrin engaged. J Biol Chem 278(41): 39882-39891.

(11) Brooks PC, Clark RA, Cheresh DA (1994) Requirement of vascular integrin alpha v beta 3 for angiogenesis. Science 264(5158): 569-571.

(12) Fujita Y, Abe R, Shimizu H (2008) Clinical approaches toward tumor angiogenesis: past, present and future. Curr Pharm Des 14(36): 3820-3834.

(13) Cai W, Chen X (2006) Anti-angiogenic cancer therapy based on integrin alphavbeta3 antagonism. Anticancer Agents Med Chem 6(5): 407-428.

(14) Desgrosellier JS, Cheresh DA (2010) Integrins in cancer: biological implications and therapeutic opportunities. Nat Rev Cancer 10(1): 9-22.

(15) Paolillo M, Russo MA, Serra M, Colombo L, Schinelli S (2009) Small molecule integrin antagonists in cancer therapy. Mini Rev Med Chem 9(12): 1439-1446.

(16) Schottelius M, Laufer B, Kessler H, Wester HJ (2009) Ligands for mapping alphavbeta3-integrin

expression in vivo. Acc Chem Res 42(7): 969-980.

(17) Felding-Habermann B, Lerner RA, Lillo A, et al. (2004) Combinatorial antibody libraries from cancer patients yield ligand-mimetic Arg-Gly-Asp-containing immunoglobulins that inhibit breast cancer metastasis. Proc Natl Acad Sci U S A 101(49): 17210-17215.

(18) Carter PJ (2006) Potent antibody therapeutics by design. Nat Rev Immunol 6(5): 343-357.

(19) Chambers AF (2009) MDA-MB-435 and M14 Cell Lines: Identical but not M14 Melanoma? Cancer Res 96(13): 5292-5293.

(20) Hollestelle A, Schutte M (2009) Comment Re: MDA-MB-435 and M14 cell lines: identical but not M14 Melanoma? Cancer Res 69(19): 7893.

(21) Deryugina EI, Quigley JP (2008) Chick embryo chorioallantoic membrane model systems to study and visualize human tumor cell metastasis. Histochem Cell Biol 130(6): 1119-1130.

(22) Byzova TV, Kim W, Midura RJ, Plow EF (2000) Activation of integrin alpha(V)beta(3) regulates cell adhesion and migration to bone sialoprotein. Exp Cell Res 254(2): 299-308.

(23) Luo BH, Carman CV, Springer TA (2007) Structural Basis of Integrin Regulation and Signaling. Annu Rev Immunol 25: 619-647.

(24) Ajroud K, Sugimori T, Goldmann WH, Fathallah DM, Xiong JP, Arnaout MA (2004) Binding Affinity of Metal Ions to the CD11b A-domain Is Regulated by Integrin Activation and Ligands. J Biol Chem 279(24): 25483-25488.

(25) Xiong JP, Stehle T, Goodman SL, Arnaout MA (2003) Integrins, cations and ligands: making the connection. J Thromb Haemost 1(7): 1642-1654.

(26) Xiong JP, Stehle T, Goodman SL, Arnaout MA (2003) New insights into the structural basis of integrin activation. Blood 102(4): 1155-1159.

(27) Buckley CD, Pilling D, Henriquez NV, et al. (1999) RGD peptides induce apoptosis by direct caspase-3 activation [see comments]. Nature 397(6719): 534-539.

(28) Roy S, Bayly CI, Gareau Y, et al. (2001) Maintenance of caspase-3 proenzyme dormancy by an intrinsic "safety catch" regulatory tripeptide. Proc Natl Acad Sci U S A 98(11): 6132-6137.

(29) Anuradha CD, Kanno S, Hirano S (2000) RGD peptide-induced apoptosis in human leukemia HL-60 cells requires caspase-3 activation. Cell Biol Toxicol 16(5): 275-283.

(30) Aguzzi MS, Giampietri C, De Marchis F, et al. (2004) RGDS peptide induces caspase 8 and caspase 9 activation in human endothelial cells. Blood 103(11): 4180-4187.

(31) Janicke RU, Ng P, Sprengart ML, Porter AG (1998) Caspase-3 is required for alpha-fodrin cleavage but dispensable for cleavage of other death substrates in apoptosis. J Biol Chem 273(25): 15540-15545.

(32) Devarajan E, Sahin AA, Chen JS, et al. (2002) Down-regulation of caspase 3 in breast cancer: a possible mechanism for chemoresistance. Oncogene 21(57): 8843-8851.

(33) Byzova TV, Rabbani R, D'Souza SE, Plow EF (1998) Role of integrin alpha(v)beta3 in vascular

biology. Thromb Haemost 80(5): 726-734.

(34) Stupack DG, Cheresh DA (2004) Integrins and angiogenesis. Curr Top Dev Biol 64:207-38.: 207-238.

(35) McNeel DG, Eickhoff J, Lee FT, et al. (2005) Phase I trial of a monoclonal antibody specific for alphavbeta3 integrin (MEDI-522) in patients with advanced malignancies, including an assessment of effect on tumor perfusion. Clin Cancer Res 11(21): 7851-7860.

(36) Stupack DG, Cheresh DA (2002) Get a ligand, get a life: integrins, signaling and cell survival. J Cell Sci 115(Pt;%19): 3729-3738.

(37) Takagi J, Springer TA (2002) Integrin activation and structural rearrangement. Immunol Rev 186: 141-163.

(38) Holliger P, Hudson PJ (2005) Engineered antibody fragments and the rise of single domains. Nat Biotechnol 23(9): 1126-1136.

(39) Colcher D, Pavlinkova G, Beresford G, Booth BJ, Choudhury A, Batra SK (1998) Pharmacokinetics and biodistribution of genetically-engineered antibodies. Q J Nucl Med 42(4): 225-241.

(40) Mao S, Gao C, Lo CH, Wirsching P, Wong CH, Janda KD (1999) Phage-display library selection of high-affinity human single-chain antibodies to tumor-associated carbohydrate antigens sialyl Lewisx and Lewisx. Proc Natl Acad Sci U S A 96(12): 6953-6958.

(41) Krag DN, Fuller SP, Oligino L, et al. (2002) Phage-displayed random peptide libraries in mice: toxicity after serial panning. Cancer Chemother Pharmacol 50(4): 325-332.

(42) Jaffe CC (2006) Measures of response: RECIST, WHO, and new alternatives. J Clin Oncol 24(20): 3245-3251.

(43) Therasse P, Eisenhauer EA, Verweij J (2006) RECIST revisited: a review of validation studies on tumour assessment. Eur J Cancer 42(8): 1031-1039.

(44) Eisenhauer EA, Therasse P, Bogaerts J, et al. (2009) New response evaluation criteria in solid tumours: revised RECIST guideline (version 1.1). Eur J Cancer 45(2): 228-247.

(45) Agresti A (1990) Categorical Data Analysis. Sec. 3.3.7. ed.

(46) Denault JB, Salvesen GS (2003) Expression, purification, and characterization of caspases. Curr Protoc Protein Sci Chapter 21:Unit 21.13.: Unit.

(47) Stennicke HR, Jurgensmeier JM, Shin H, et al. (1998) Pro-caspase-3 is a major physiologic target of caspase-8. J Biol Chem 273(42): 27084-27090.

Figure 1

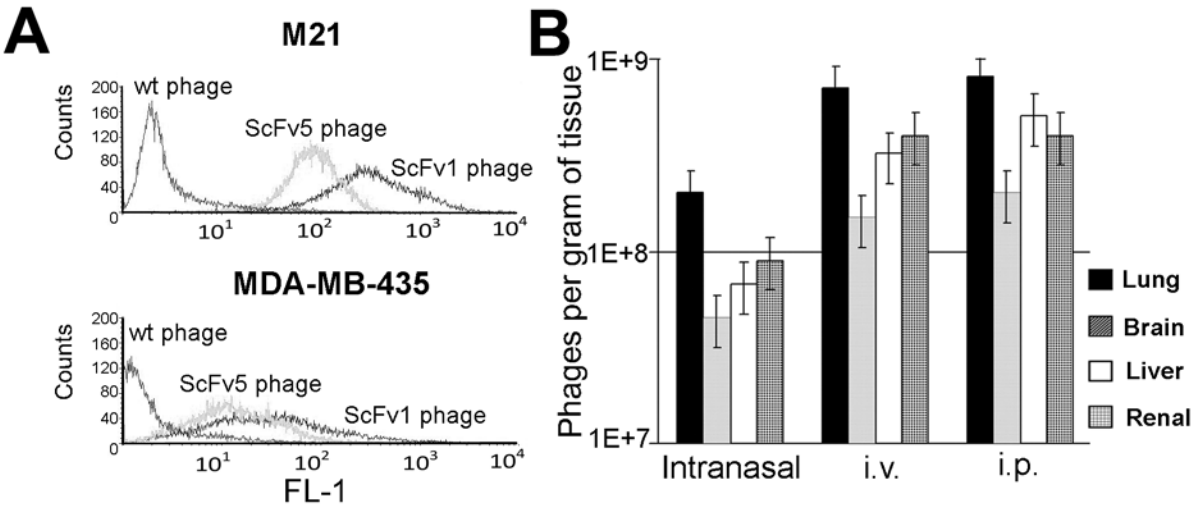
A
M21
wt phage
ScFv5 phage
ScFv1 phage
Counts
MDA-MB-435
FL-1
B
Phages per gram of tissue
1E+9
1E+8
1E+7
Intranasal
i.v.
i.p.
Lung
Brain
Liver
Renal

Figure 2

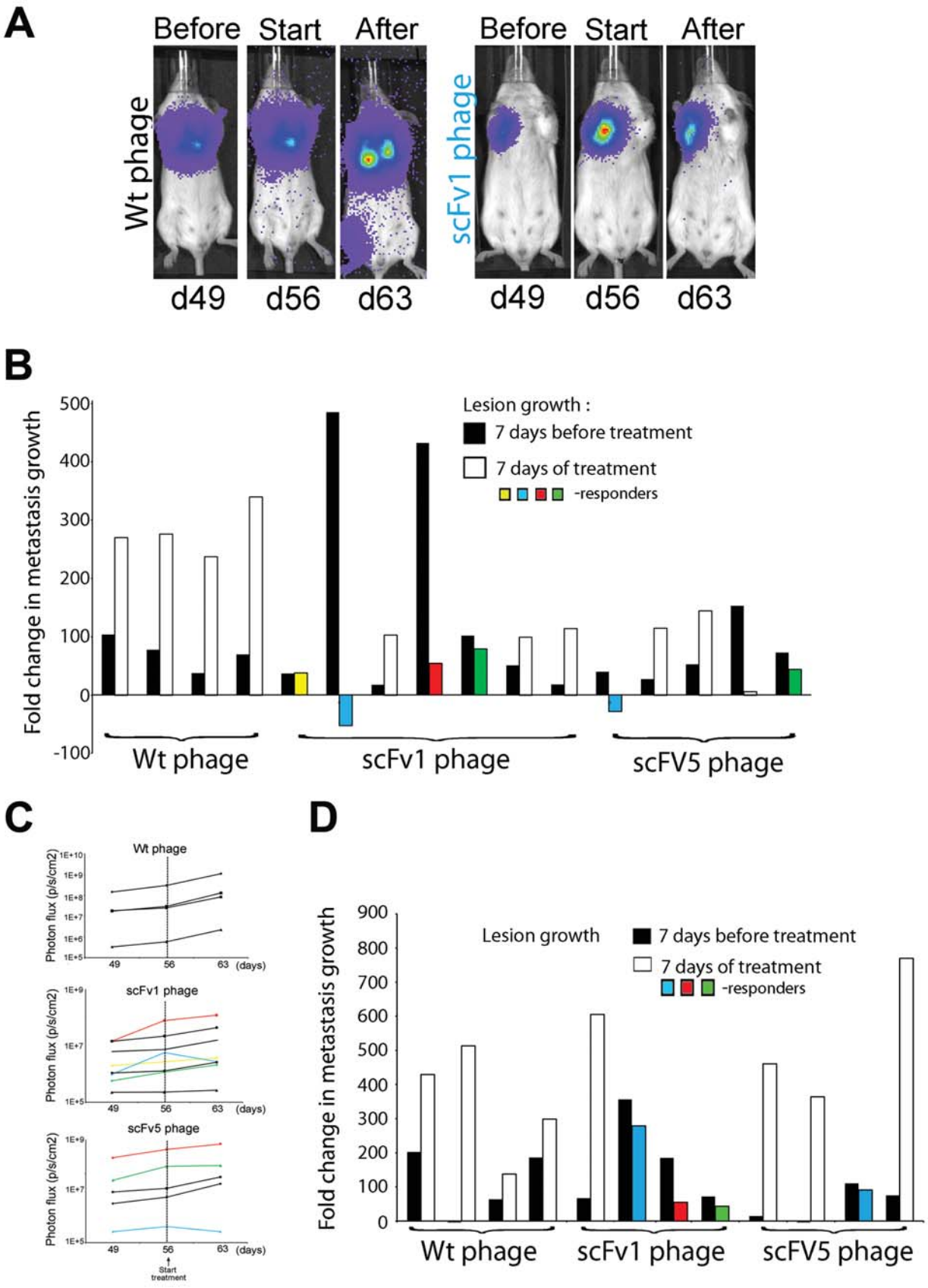
A
Before
Start
After
Wt phage
scFv1 phage
d49
d56
d63
B
Fold change in metastasis growth
Lesion growth :
7 days before treatment
7 days of treatment
-responders
Wt phage
scFv1 phage
scFV5 phage
C
Wt phage
scFv1 phage
scFv5 phage
Photon flux (p/s/cm2)
(days)
Start treatment
D
Lesion growth
7 days before treatment
7 days of treatment
-responders
Fold change in metastasis growth
Wt phage
scFv1 phage
scFV5 phage

Figure 3

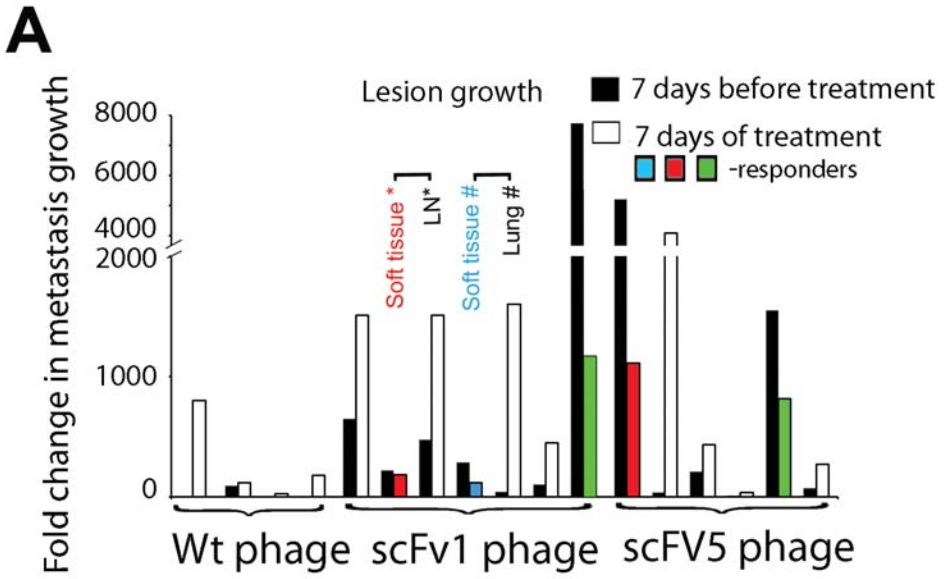
A
Lesion growth
7 days before treatment
7 days of treatment
-responders
Fold change in metastasis growth
8000
6000
4000
2000
1000
0
Soft tissue *
LN*
Soft tissue #
Lung #
Wt phage
scFv1 phage
scFV5 phage

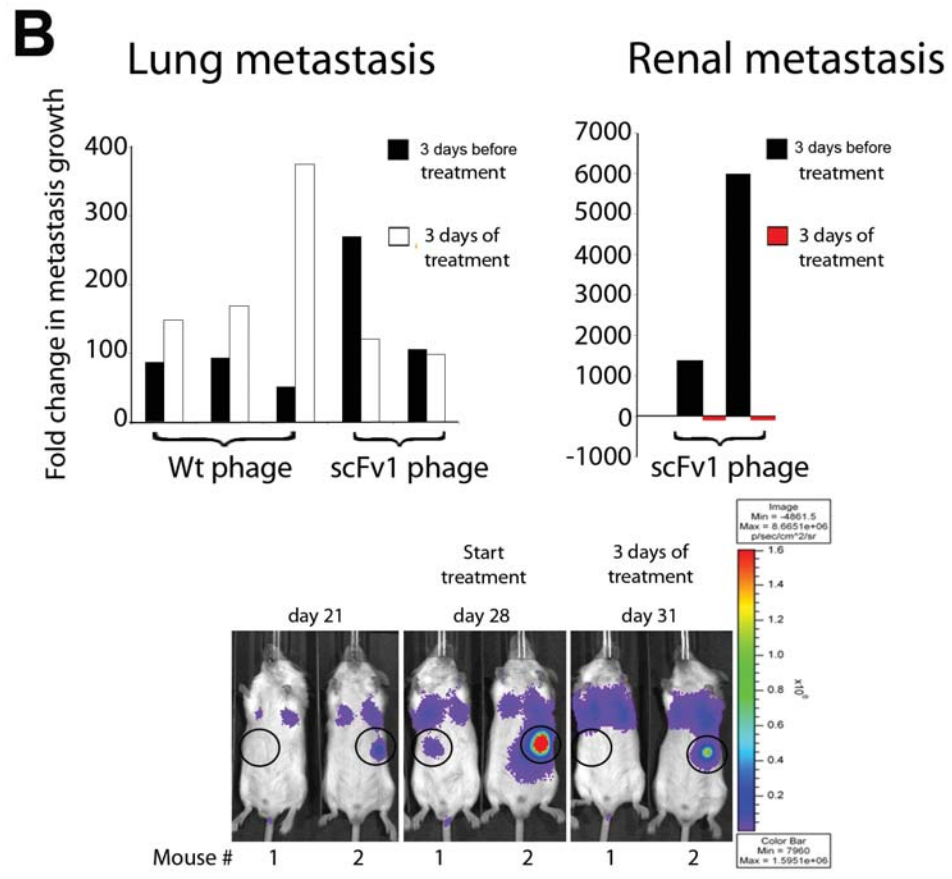
B
Lung metastasis
Renal metastasis
Fold change in metastasis growth
400
300
200
100
0
3 days before treatment
3 days of treatment
Wt phage
scFv1 phage
7000
6000
5000
4000
3000
2000
1000
0
-1000
3 days before treatment
3 days of treatment
scFv1 phage
Start treatment
3 days of treatment
day 21
day 28
day 31
Mouse #
1
2
1
2
1
2
Image
Min = -4861.5
Max = 8.6651e+06
p/sec/cm^2/sr
1.6
1.4
1.2
1.0
0.8
0.6
0.4
0.2
x10^6
Color Bar
Min = 7960
Max = 1.5951e+06

Figure 4

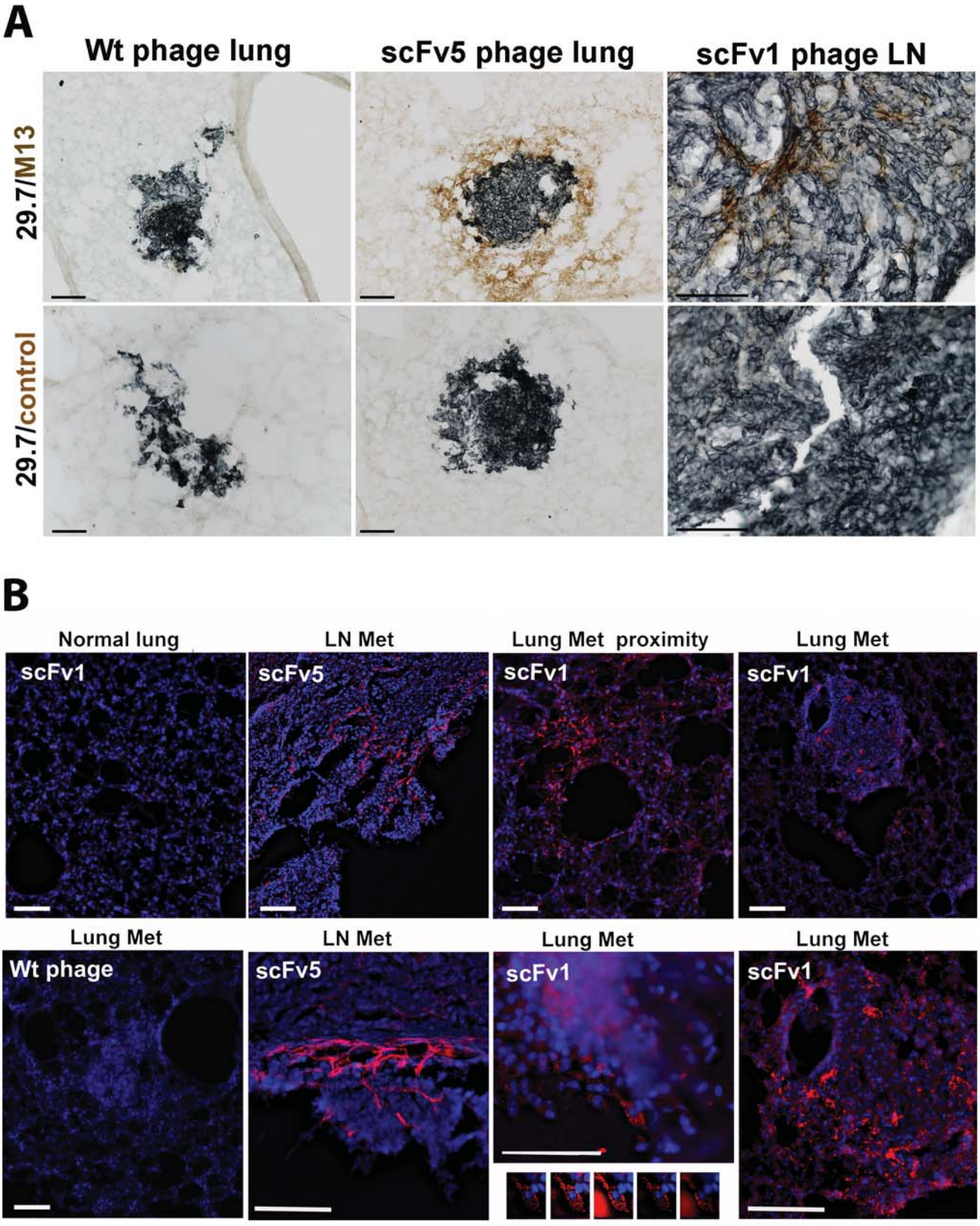
A
Wt phage lung
scFv5 phage lung
scFv1 phage LN
29.7/M13
29.7/control
B
Normal lung
scFv1
LN Met
scFv5
Lung Met proximity
scFv1
Lung Met
scFv1
Lung Met
Wt phage
LN Met
scFv5
Lung Met
scFv1
Lung Met
scFv1

Figure 5

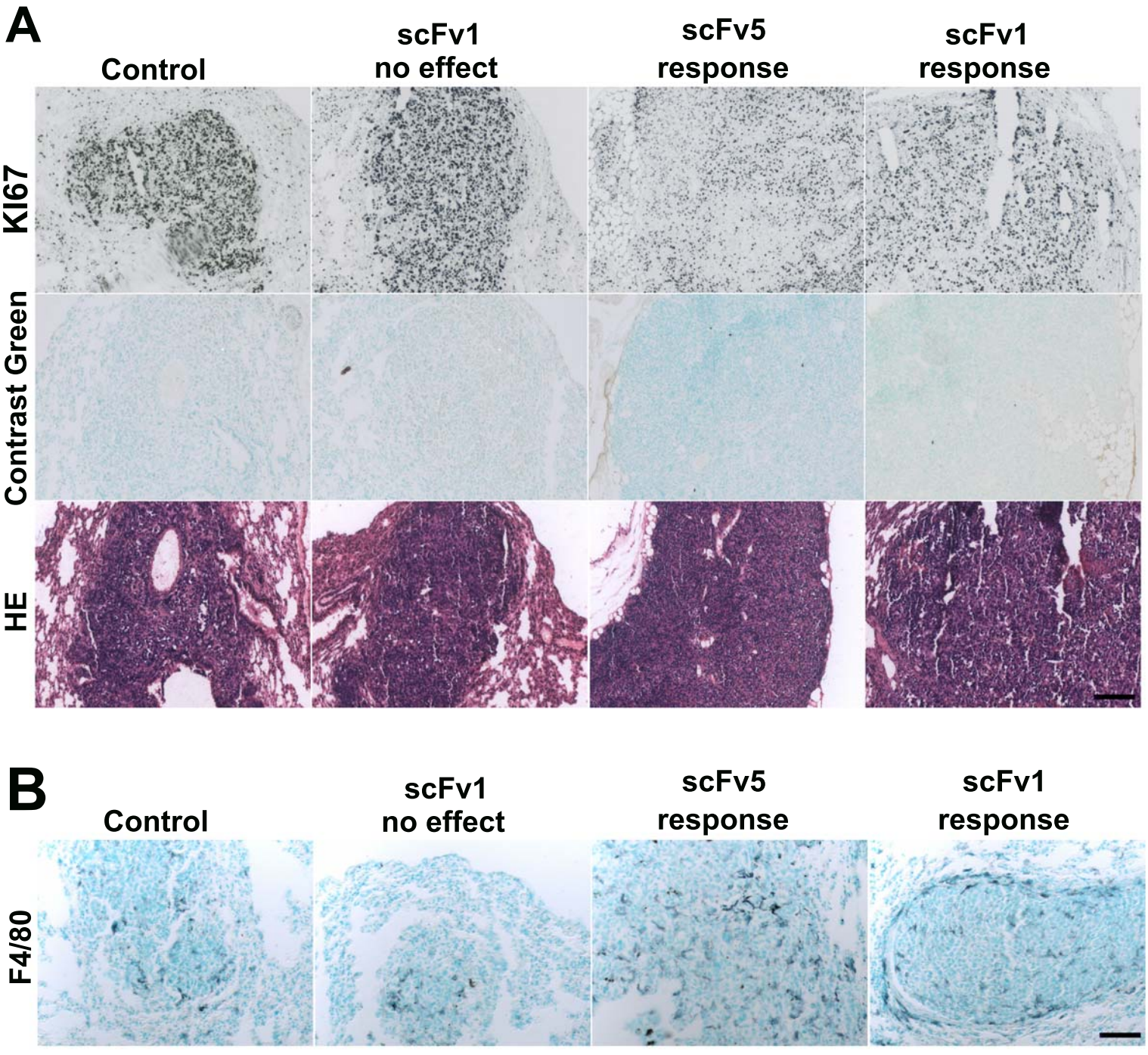
A
Control
scFv1
no effect
scFv5
response
scFv1
response
KI67
Contrast Green
HE
B
Control
scFv1
no effect
scFv5
response
scFv1
response
F4/80

Figure 6

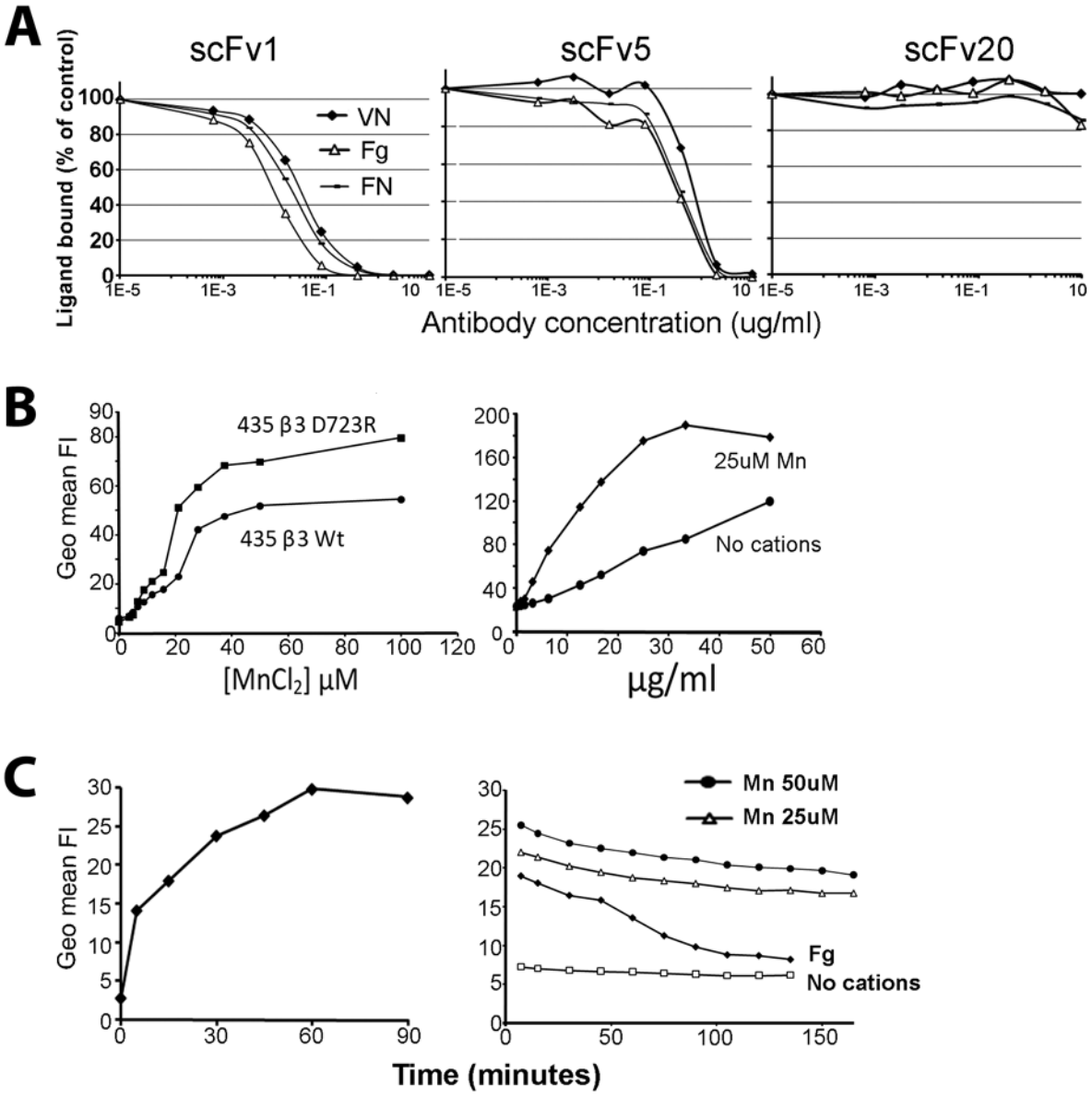
A
scFv1
scFv5
scFv20
Ligand bound (% of control)
VN
Fg
FN
Antibody concentration (ug/ml)
B
435 β3 D723R
435 β3 Wt
Geo mean FI
[MnCl2] µM
25uM Mn
No cations
µg/ml
C
Geo mean FI
Mn 50uM
Mn 25uM
Fg
No cations
Time (minutes)

Figure 7

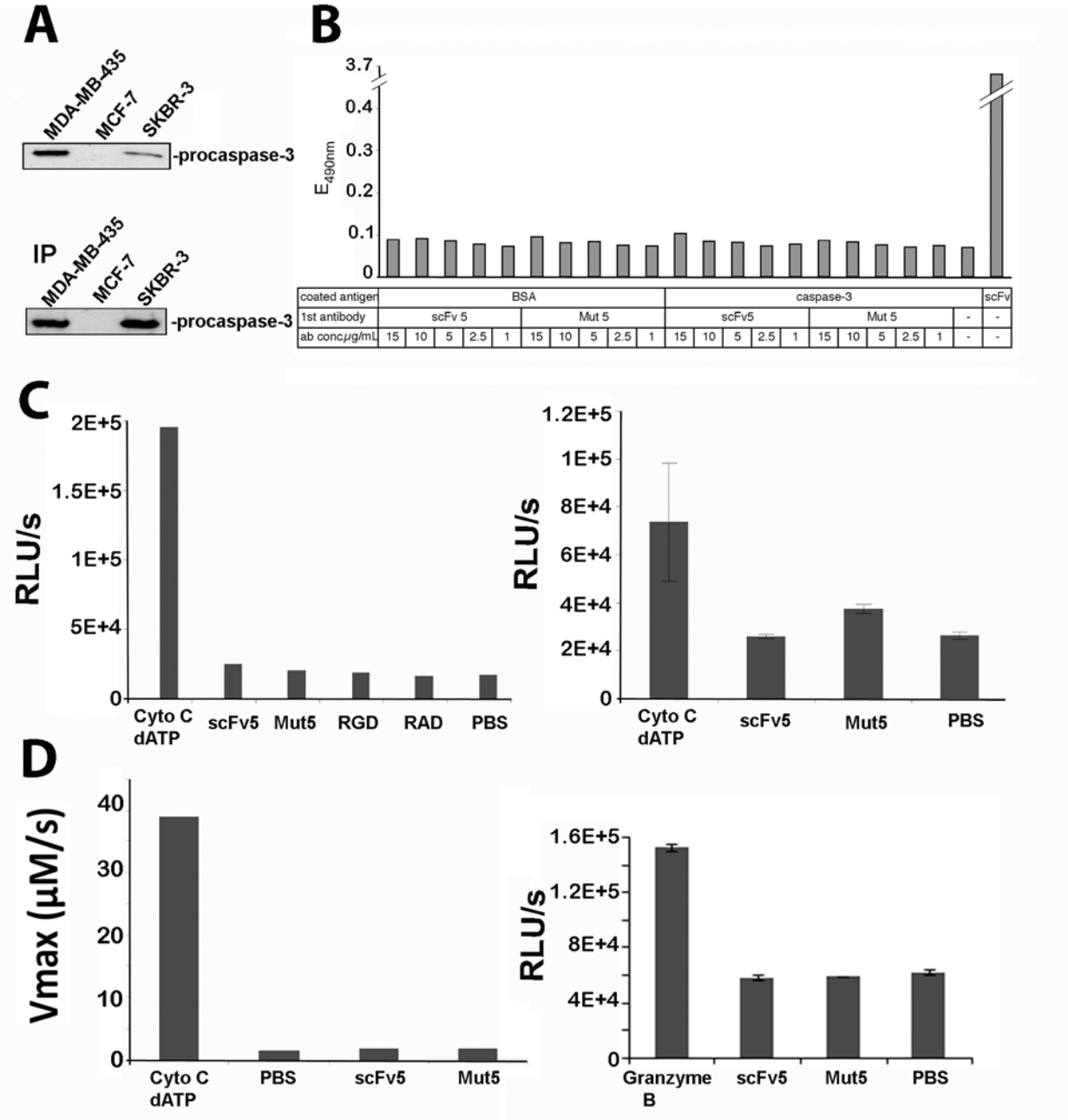
A
MDA-MB-435
MCF-7
SKBR-3
-procaspase-3
IP
MDA-MB-435
MCF-7
SKBR-3
-procaspase-3
B
3.7
0.4
0.3
0.2
0.1
0
E490nm
coated antiger
BSA
caspase-3
scFv
1st antibody
scFv 5
Mut 5
scFv5
Mut 5
-
-
ab conc.μg/mL
15 10 5 2.5 1 15 10 5 2.5 1 15 10 5 2.5 1 15 10 5 2.5 1 - -
C
RLU/s
2E+5
1.5E+5
1E+5
5E+4
0
Cyto C dATP
scFv5
Mut5
RGD
RAD
PBS
RLU/s
1.2E+5
1E+5
8E+4
6E+4
4E+4
2E+4
0
Cyto C dATP
scFv5
Mut5
PBS
D
Vmax (μM/s)
40
30
20
10
0
Cyto C dATP
PBS
scFv5
Mut5
RLU/s
1.6E+5
1.2E+5
8E+4
4E+4
0
Granzyme B
scFv5
Mut5
PBS